2016

1,1-Diamino-2,2-Dinitroethylene (Fox-7) Under High Pressure-Temperature

Matthew Marc Bishop
University of Alabama at Birmingham

1,1-DIAMINO-2,2-DINITROETHYLENE (FOX-7) UNDER HIGH PRESSURE-TEMPERATURE

by

MATTHEW M. BISHOP

YOGESH K. VOHRA, PHD, CHAIR
TRACY P. HAMILTON, PHD
AARON L. LUCIUS, PHD
NENAD VELISAVLJEVIC, PHD
SERGEY VYAZOVKIN, PHD

A DISSERTATION

Submitted to the graduate faculty of The University of Alabama at Birmingham,
in partial fulfillment of the requirements for the degree of
Doctor of Philosophy

BIRMINGHAM, ALABAMA

2016

1,1-DIAMINO-2,2-DINITROETHYLENE (FOX-7) UNDER HIGH PRESSURE-TEMPERATURE

MATTHEW M. BISHOP

CHEMISTRY

ABSTRACT

The high pressure-temperature (P-T) phase diagram of 1,1-diamino-2,2-dinitroethylene (FOX-7) was determined by *in situ* synchrotron infrared radiation spectroscopy and resistively heated diamond anvil cell (DAC) techniques. The stability of the high P-T FOX-7 polymorphs is established from ambient pressure up to 10 GPa and temperatures until decomposition. The phase diagram indicates two near isobaric phase boundaries at ~2 GPa ($\alpha \rightarrow$ I) and ~ 5 GPa (I $\rightarrow \varepsilon$) that persists from 25°C until the onset of decomposition at ~300°C. In addition, the ambient pressure, high-temperature $\alpha \rightarrow \beta$ phase transition (~111°C) lies along a steep boundary (~100°C/GPa) with an ($\alpha + \beta + \gamma$) triple point at ~1 GPa and 300°C. A 0.9 GPa isobaric temperature ramping measurement indicated a limited stability range for the γ-phase between 0.5 – 0.9 GPa and 180 – 260°C, terminating in a ($\beta + \gamma + \delta$) triple point. With increasing pressure, the δ-phase exhibited a small negative dT/dP slope (up to ~0.2 GPa) before turning over to a positive 70°C/GPa slope, at higher pressures; until ~ 2 GPa, where it appears to terminate in an ($\alpha + \delta$ + Phase-I) triple point. The decomposition boundary then exhibits an anomalous change of slope at an (a + Phase I + decomposition) triple point with a negative slope of ~180°C/GPa; which may indicate a structural modification to a higher symmetry than the α-phase ($P2_1/n$) or evidence of a potential 'island' phase. The high pressure ε-phase has a moderate positive decomposition boundary slope of ~29°C/GPa up to 10 GPa.

Additionally, the high P-T phase diagram of 2,4,6-triamino-1,3,5-trinitrobenzene (TATB) was determined from ambient pressure up to 10 GPa and decomposition. TATB appeared to remain triclinic (P1) and has a very moderate ~4°C/GPa decomposition boundary slope up to 10 GPa. The similarities between the decomposition boundaries of the ε-phase of FOX-7 and TATB are remarkable: both phases have triclinic symmetry and planar molecular/layering structures with moderate positive slopes extending over a broad range of pressure. These results provide the first recorded evidence of high P-T stability of two similar high explosives and the potential mechanisms behind sensitivity and performance.

Keywords: High Explosive, Low Sensitivity, Insensitive, FOX-7, TATB, Phase Diagram

ACKNOWLEDGEMENTS

Los Alamos National Laboratory LANL is operated by LANS, LLC for the DOE/NNSA. This work was, in part, supported by the U.S. DOE under contract #DE-AC52-06NA25396 and Science Campaign 2 Program. MB is supported by the DOE/NNSA under award number DE-NA0002014, and the Science Campaign 2 under the HE Science Program. We thank the Swedish Defense Research Agency (FOI) for the synthesis of the sample. Use of the National Synchrotron Light Source is supported by DOE Office of Science, Office of Basic Energy Science, under Contract No. DE-AC02-98CH10886. Beamline U2A is supported by the Consortium for Materials Properties Research in Earth Science (COMPRES), under NSF Cooperative Agreement Grant No. EAR01-35554 and the U.S. DOE (CDAC, Contract No. DEFC03-03N00144).

I would also like to thank my thesis committee members Drs. Yogesh K. Vohra, Tracy Hamilton, Aaron Lucius, and Sergey Vyazovkin for their suggestions and guidance throughout my dissertation research.

I thank family and friends for their support and patience during my graduate school career. I could not have done it without you!

TABLE OF CONTENTS

Page

LIST OF FIGURES

LIST OF TABLES

Table *Page*

LIST OF ABBREVIATIONS

APS	Advanced Photon Source
BNL	Brookhaven National Laboratory
CJ	Chapman-Jouguet
COMPRES	Consortium for Materials Properties Research
DAC	Diamond Anvil Cell
DADNE	1,1-diamino-2,2-dinitroethylene
DOE	Department of Energy
DSC	Differential Scanning Calorimetry
FIR	Far-Infrared
FOI	Swedish Defense Research Agency
FOX-7	1,1-diamino-2,2-dinitroethylene
GPa	Gigapascal
HE	High Explosive
HMX	1,3,5,7-tetranitro-1,3,5,7-tetrazocine
IR	Infrared

KBr	potassium bromide
LANL	Los Alamos National Laboratory
MIR	Mid-Infrared
NG	Nitroglycerine
NNSA	National Nuclear Security Administration
NSLS	National Synchrotron Light Source
NSLS II	National Synchrotron Light Source II
P	Pressure
P-T	Pressure-Temperature
RDX	1,3,5-trinitroperhydro-1,3,5-triazine
T	Temperature
TATB	2,4,6-triamino-1,3,5-trinitroethylene
TNT	trinitrotoluene
VUV	Vacuum Ultraviolet
WWII	World War II

CHAPTER 1

INTRODUCTION

1.1 Explosives

BOOM! POP, CRACK – the distinct sounds we equate with 'explosions', but what are the underlying physical drivers of an explosion? Whether it is the popping of a balloon, the firing of a gun, or the detonating of a bomb, an explosion occurs when energy previously confined is suddenly released to affect the surroundings [1]. However, a balloon and a bomb have drastically different orders of magnitude with respect to the energy released. Beyond just the different orders of magnitudes; the mechanisms, types of energy, and fundamental properties are drastically different. When such divisions in the fundamental properties of physical events, like an explosions occur we tend to classify them, but we will get to that soon enough. For now, let's take a quick glance at the history of explosives; so that we can understand the reasons behind the classification system that we use today.

The accidental discovery of blackpowder in China around 200 BC sparked a revolution in entertainment; however the true importance of that discovery would remain dormant until the 13th and 14th centuries, when the English monk Roger Backon (1249) and the German monk Berthold Schwarz (1320) started to research the poperties of blackpoweder.[2] In 1425, their research inspired the development of a process known as, "corning." Which the process of pelletizing blackpowder, that allowed for the development of one of the first propellant charges for small and later on, large caliber guns.[3]

Perhaps the most famous milestone in the study of explosives, is that of Italian chemist Ascanio Sobrero (1846), and Imanual (1863) and Alfred Nobel with the first small-

scale synthesis of nitroglycerine (NG). Imanual's son, Alfred would go on to fully commercialize the process in a small factory near Stockholm; tragically though, in 1864 that same factory was destroyed by an explosion due to the high sensitivity of NG – killing Alfred's brother Emil.[2]

Explosive accidents would plague chemist for decades, and with the close succession of two world wars, research intensified to find explosives that had more insensitive properties. Researchers soon discovered that blending explosives could yield a mixture of preferable properties depending on the intended application. In 1920, there was a massive breakthrough in explosives research with the refined development of 1,3,5-trinitroperhydro-1,3,5-triazine (RDX: Research Department eXplosive).[2] An immensely powerful explosive during it's time and still to this day. It takes the common military and civilian name of Composition A when blended with plastic binders, and when blended with trinitrotoluene (TNT) it becomes Composition B – perhaps the most commonly used explosives today. As military advancements continued (the rise of a nuclear capable world) – so did explosives research. While many novel explosives have been developed since the rapid expansion of research during WWII, the fundamental mechanisms behind why certain explosives are more insensitive to external stimuli or perform better than others – remains to be solved.

1.1.1 Explosive Classification

Explosives can be grouped into two main categories: low explosives (propellants) and high explosives (primary and secondary). Low explosives are combustible materials, containing within themselves all the oxygen needed for their combustion, which burn but

do not explode, and function by developing gases that produce explosions. Under normal conditions, low explosives undergo deflagration (subsonic combustion that usually propagates through thermal conductivity) at rates from a few centimeters per second to ~400 meters per second.[4] Propellants are mixtures of one or more explosives with plasticizers to improve processing characteristics, stabilizers to increase storage life, and inorganic additives to facilitate handling, improve ignitability and decrease muzzle flash. Common examples of low explosives (propellants) are black, smokeless, and flash powders for uses ranging from launching projectiles from guns, rockets, and missile systems.[5]

High explosives undergo a rapid release of chemical energy that is propagated, not by heat transfer, but by a supersonic shockwave traveling through the material – detonation. The release of chemical energy maintains the shockwave as it propagates through the material until nearly all the matter is exhausted. Due to the wide range of characteristics found in high explosives, they are further classified into primary and secondary explosives. Primary explosives are typically styphnates, azides, or fulminates, organic diazo compounds (diazodinitrophenol), or organic peroxides; which are all highly susceptible to shock, flame, and friction to which they will respond by burning rapidly or detonating.[6] Secondary explosives cannot be initiated simply through heat or shock. In order to initiate, primary explosives have to be used; whereby the shockwave of the primary explosive initiates the secondary. In addition, secondary explosives tend to be higher performing the primary explosives. Common used secondary explosives include: TNT, RDX, HMX, and TATB. Furthermore, secondary explosives can be further classified, into low sensitivity and insensitive high explosives. In general, the definition is not clearly defined in the area of high explosives research; perhaps this is due to the lack finely detailed information of

the fundamental characteristics that define sensitivity. However, in general the impact sensitivity, molecular layering, and peak decomposition temperature can be loosely used a defining factor. For the scope of this paper, we will define a lower sensitivity high explosive is having an impact sensitivity, peak decomposition temperature, and non-graphitic like layering structure similar to that of RDX, and an insensitive high explosive having similar characteristics to TATB. For the main purpose of this manuscript, FOX-7 is currently accepted as a lower sensitivity high explosive by the explosives community, and will be discussed with respect to its current classification.

1.1.2 Sensitivity and Performance

Sensitivity of an explosive substance may be defined as the ease with which detonation or deflagration is initiated by physical stimuli such as; friction (thermal and kinetic energy), impact (kinetic energy), electrostatic discharge (electrical energy), and thermal shock (thermal energy).[7] Whereas, the performance of an explosive substance may also be quantified by these same type of physical attributes, many are difficult to assess experimentally due to safety or diagnostic constraints. However, some of the primary performance metrics include the detonation pressure (detonation shockwave front), detonation velocity (rate of propagation), heat of detonation (thermal energy released during detonation at constant pressure), detonation temperature (detonation products temperature), and the volume of gas produced by the detonation. In assessing the individual explosives on a more granular level, the chemical composition or the percent nitrogen/oxygen balance, molecular structure and layering, decomposition products, and behavior under high pressure-temperature conditions can be used to assess the explosive on a more fundamental level.

1.1.3 Applications of Explosives

High explosives have a long history of being used in non-military applications: including use in oil and space exploration, manufacturing, mining, and even in the pharmaceutical industry. In fact, during the 1960's a pharmaceutical firm based in Alabama was using a blend of TATB and sugar as a heart medication. For the scope of this work however, higher performing secondary explosives can be used for destructive work (blast effect), for metal acceleration (welding), and for shape charges; while lower sensitivity secondary explosives are used for missiles with multiple shape charges due to their higher thermal stability and lower mechanical sensitivity (i.e. bullet impact).[2]

1.2 Fundamental Properties of 1,3,5-Triamino-2,4,6-Trinitrobenzene (TATB)

The search for a high explosive (HE) with improved performance and at the same time a strong resistance to external stimuli (insensitivity) is an ongoing effort. Chemists have focused considerable efforts trying to emulate the insensitivity properties of one explosive in particular – 2,4,6-triamino-1,3,5-trinitrobenzene (TATB). In addition to being insensitive (i.e. exceptionally resistant to shock, friction, and impact) [8], TATB has moderate performance with a Chapman-Jouguet (CJ) pressure of ~26 GPa and detonation velocity of ~7.66 km/s. [9, 10] At ambient and extreme conditions, TATB presences in a near graphitic layer structure dominated by strong hydrogen bonding in a triclinic (P1) symmetry. [11] Efforts into studying TATB have been plagued by a variety of issues, such as the difficulties associated with resolving the low symmetry crystal structure by X-ray diffraction [9], radiation induced chemistry [9], as well as synthesis particle morphology, and

purity[12]. Due to the multitude of experimental difficulties, the mechanisms behind TATB's insensitivity characteristics still remain a mystery. While many efforts to gain insight into the fundamental properties of TATB have been conducted using X-ray[9] and spectroscopic techniques[8, 12-20], experimental difficulties have precluded an in-depth analysis into the pressure-temperature phase behavior of TATB.

It was though that, due to TATB's high ambient pressure exothermic decomposition temperature of 360-390°C [12], that the slope of the decomposition boundary would exceed the PT-regions obtainable by conventional diamond anvil cell technology. That is partially why, until this study, no PT-phase diagram on TATB existed. For many years, the explosives community has chosen to focus on HEs similar to that of TATB in order to gain insights into the potential mechanisms behind sensitivity and performance.

1.3 Fundamental Properties of 1,1-Diamino-2,2-Dinitroethylene (FOX-7)

1,1-diamino-2,2-dinitroethylene ($C_2H_4N_4O_4$), commonly referred to as FOX-7 or DADNE, is among the less sensitive high explosives.[21] While being more sensitive than 1,3,5-triamino-2,4,6-trinitrobenzene (TATB), it has comparable performance to related secondary high explosives hexahydro-1,3,5-trinitro-1,3,5-triazine (RDX) and octahydro-1,3,5,7-tetranitro-1,3,5,7-tetrazocine (HMX). [22,23,24] In order to better understand the mechanisms behind high explosive (HE) performance and sensitivity, it is important to explore the structural phase stability across a broad range of pressure (P) and temperature (T) conditions. Due to the high cost and complexity of preforming experiments on HE, computational models are relied upon to help expand our understanding of the mechanisms

behind performance, sensitivity, and safety. However, accurate models of the complex behavior of HEs require experiments to be performed from ambient P-T up to detonation conditions.

FOX-7 is a relatively small and simple molecule making it an ideal energetic material to investigate both experimentally and theoretically. Ambient-P thermal measurements on FOX-7 indicate multiple phase transitions with increasing T; $\alpha \rightarrow \beta$ at ~111°C[25-27]; $\beta \rightarrow \gamma$ at ~160°C[28]; $\gamma \rightarrow \delta$ ~210°C [28, 29]; followed by decomposition at ~250°C[28]. Evers *et al.* [30] have shown through single crystal X-ray diffraction (XRD) that the α-($P2_1/n$) to β-($P2_12_12_1$) high temperature phase transition is primarily displacive in nature and reversible. Additionally, Crawford *et al* [31] found that γ-phase can be quenched following heating: subsequent XRD experiments concluded that this structural phase could be indexed to the space group $P2_1/n$. We have previously confirmed [28, 29] the presence of the δ-phase, at ~210°C using differential scanning calorimetry and infrared spectroscopy, with the crystallographic structure and space-group that is yet to be determined. The δ-phase appears to be a partial decomposition of FOX-7, and differential thermal analysis by Chemagina *et* al. [29] indicate a ~20% mass loss after the transition is complete.

For HE's exhibiting high-T polymorphism, it is important to examine the effects of pressure on the stability of these polymorphs to gain insights into mechanisms that influence HE sensitivity and decomposition events. In order to establish the stability of HE polymorphs at high P-T, a resistively heated DAC technique is employed in conjunction with a variety of optical, spectroscopic and x-ray probes. Numerous investigations have established that under compression at room-T, FOX-7 undergoes a phase transition at ~2 and ~5 GPa, evident from Raman [7, 32, 33], Infrared (IR)[34], and XRD[35] measurements. These

phase transitions in FOX-7 have been observed in both quasi-hydrostatic (KBr media) compacted powder (IR)[34] and hydrostatic single crystalline Raman [32, 33] experiments. While, IR spectroscopy[34] measurements on polycrystalline FOX-7 powder point to a possible phase transition at ~10 GPa, no additional phase transitions in the 10-40 GPa regime was observed in IR and Raman spectroscopy studies on single crystal samples.[33]

1.4 Motivation and Goals of this Study

We have focused our efforts over the years in developing a very detailed picture of the phase behavior of 1,1-diaminio-2,2-dinitroethylene (FOX-7) at high-PT. In part our focus on FOX-7 was due to the similarities between FOX-7 and TATB. TATB is considered the benchmark for sensitivity and performance in nearly all explosives application fields. Both TATB and FOX-7 have similar critical chemical bonds[36], packing[23, 37], molecular structures and the absence of a melt point[38]. However, FOX-7 is designated as a low-sensitivity HE due impart to its lower peak decomposition temperature 210 – 254°C[28, 39] in comparison to TATB, but at the same time, having a higher CJ (36 GPa) and detonation velocity (8.8 km/s)[39] – higher performance. FOX-7 also differs from TATB in phase complexity – FOX-7 has multiple low-pressure phases all terminating before 2 GPa[24, 39, 40]. Furthermore, our previous work[39,24, 40] indicates two higher pressure phases: phase-I (~ 2 GPa) and phase-II (~5 GPa) that form near isobaric phase boundaries up to decomposition. Recent studies have shown similar evidence of both phase I and II [41, 42] but attempts to resolve the structure of these phases proved unsuccessful until recently. Single crystal X-ray diffraction experiments by Dreger, *et al.*[42] was used to resolve the structure of phase-II to triclinic (P1), and indicated no evidence of a structural modification

or phase transition into the region defined as phase-I. The comparison of FOX-7 to the previously unknown pressure-temperature phase behavior of TATB, allows for the first proposal of the key drivers behind detonation insensitivity and performance; which is the ultimate motivation for studying FOX-7 and TATB at high pressure-temperature. The primary goal was to find patterns in energetic materials structure, moieties, phase behavior, hydrogen bonding environments, layering and crystal structures – to aid in the future development of insensitive high explosives with the superior sensitivity properties and the highest performance. The secondary goal of this study was to provide insights into the fundamental properties of high explosives for modeling efforts, and the final goal was to investigate the potential of FOX-7 to replace TATB.

1.5 Diamond Anvil Cell Technology

1.5.1 Basic diamond anvil cells

A diamond anvil cell (DAC) is one of the main experimental apparatus' of a high pressure chemist. A DAC is comprised of two diamonds (~1/3 caret) with flatten tips placed tip-to-tip. Between the diamonds there is a metal gasket with a small hole drilled in it where the sample resides. The diamonds are mounted using high-temperature epoxy to metallic backing plates that have conical holes' drill in them for the transmission of radiation. One of the backing plates is mounted to a sliding piston. The piston has a metal membrane that resides on top of the piston; which is held in place by a metallic ring that is screwed over the membrane. All of these components reside in a solid metal cylinder that makes up the core of a DAC. When a high pressure experiment is being performed, inert

gas is pumped into the metallic membrane which causes it to expand. The expansion of the membrane forces the piston down causing the diamonds to compress the sample: pressure is equal to force (membrane compressed piston) over area (diamond tips; ~ 300 μm). By varying the volume of inert gas into the membrane, the pressure can be fine-tuned over a broad range of experimental conditions. The use of diamonds is essential due to their immense strength, but also the use of type-IIa diamonds (low nitrogen impurities) is critical to IR experiments. Figure 1.1 is a simple diagram depicting the core components of a DAC.

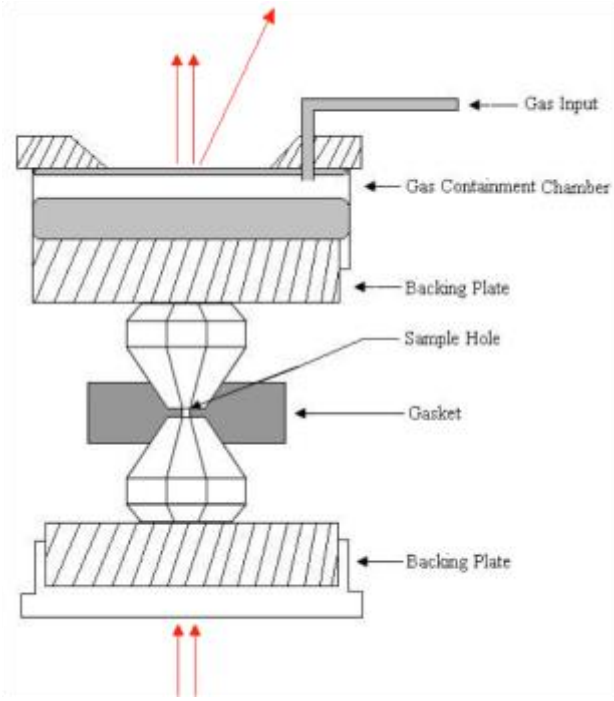

Figure 1.1. Cut-away schematics of a conventional diamond anvil cell.

The following figure is the view of a DAC with a gasketed sample loaded (Figure 1.2). The visual inspection of the loaded DAC is critical to make sure that the sample and pressure marker are positioned correctly within the sample hole. The pressure marker

should be placed near to the sample to get the most accurate reading, but not so close, such that the pressure marker interferes with the sample signal.

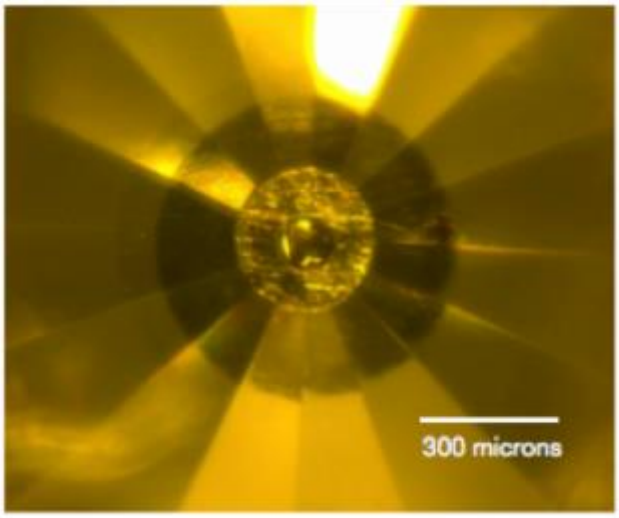

Figure 1.2. The top view in reflection of a gasketed sample between two diamond anvils.

An example of a properly loaded DAC is highlighted in Figure 1.3. The sample is placed near the center of the DAC, and the ruby (pressure marker) is placed near the sample, but not so close that it will interfere with the IR measurements.

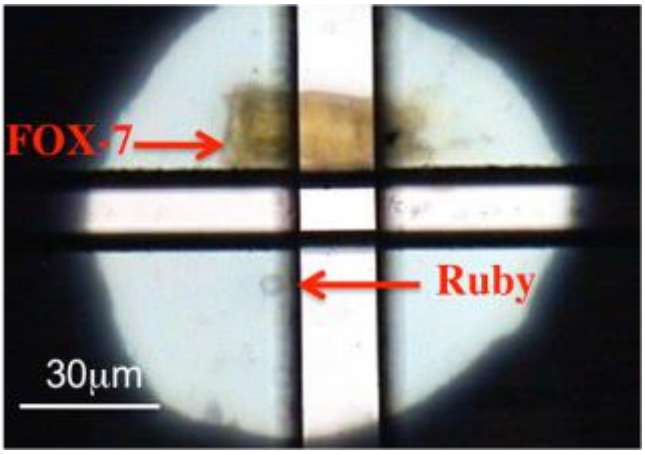

Figure 1.3. The view of a FOX-7 sample loaded into a DAC with ruby as a pressure marker and KBr (transparent surroundings) as a pressure medium.

1.5.2 Internal resistive heating systems

In order to obtain both high pressure and temperature conditions, specialized DACs have been developed with internal resistive heating coils that surround the sample entirely. An example of an internal resistive heating coil is indicated in Figure 1.4.

Figure 1.4. HeliosDAC internal resistive ceramic heater.[43]

The internal heater is placed inside the specialized HeliosDac (Figure 1.5). The value of using an internal resistive heating DAC is that it employees localized full sample heating. This is allowing for the temperature to be finely tuned on a much shorter time scale than full DAC heating blocks. With thermal kinetics playing a larger role in the decomposition of high explosives, the need for a shorter-time scale heating apparatus is paramount for conducting high pressure-temperature isobaric experiments. However, one

of the largest draw-backs of using a HeliosDAC is that the apparatus is highly expensive, and the multitude of small, proprietary, parts hinders the overall function of the DAC.

Figure 1.5. High pressure-temperature internal resistive heating HeliosDAC.[44]

1.5.3 Full cell heating blocks

The more cost effective alternative to the HeliosDAC is 'block heaters,' or full diamond anvil cell resistive heating bands (Figure 1.6).

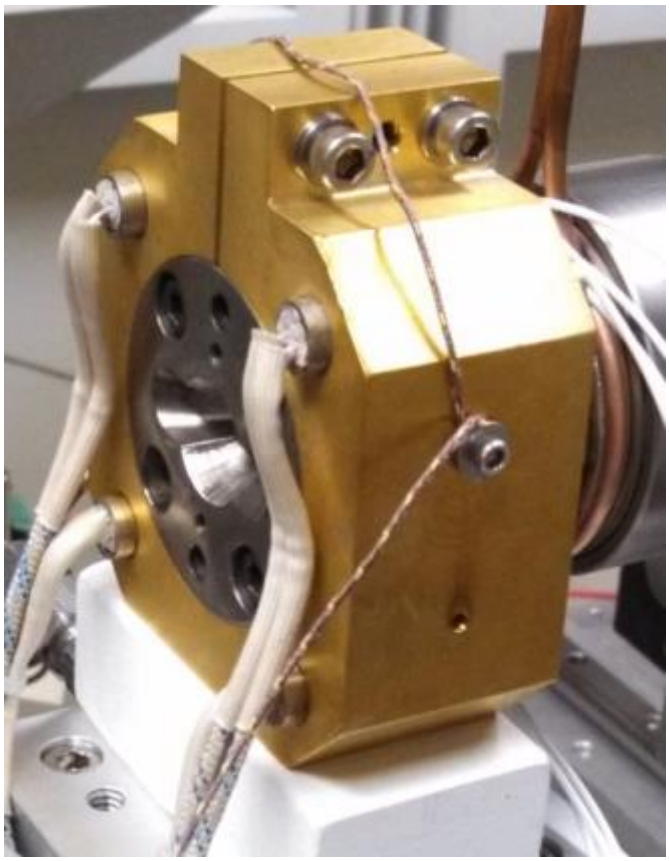

Figure 1.6. A DAC placed inside a brass heating block for a high pressure isothermal compression experiment.

Block heaters have excellent temperature stability, but because it requires heating the entire DAC, the temperature gradient from the outer-block heater to the sample can be quite large. The temperature is measured by placing multiple K-type thermocouples around the top and bottom diamond anvil; as well as, multiple K-type thermocouples on the heating block. For isothermal compression experiments, the heating block can take upwards of an hour to stabilized around the target experimental temperature (<450^{o}C; upper temperature limit). It is for this reason that block heaters are only used for isothermal compression experiments, and for temperature regimes below 450^{o}C.

CHAPTER 2

EXPERIMENTAL PROCEDURES

2.1 Differential Scanning Calorimetry

2.1.1 Ambient-pressure DSC experiment

DSC measurements were carried out on a TA Instruments model DSC Q2000 with a 1.51 mg sample of FOX-7 in a hermetic aluminum pan. The DSC was run at atmospheric pressure with a 50 ml/min nitrogen flow at a 10 ^{o}C/min heating rate up to decomposition.

2.1.2 DSC heat treatment experiment

DSC measurements were carried out on a TA Instruments model DSC Q2000 with a 0.943 mg sample of FOX-7 in a hermetic aluminum pan. The DSC was run at atmospheric pressure with a 50 ml/min nitrogen flow at a 10 ^{o}C/min heating rate up to 220 ^{o}C. Temperature was then held for 30 minutes at 220 ^{o}C, followed by a decrease at a rate of 10 ^{o}C/min all the way down to room-T. Upon cooling, the sample was held at room-T for 480 minutes, before it was once again heated at a rate of 10 ^{o}C/min up to decomposition.

2.2 Infrared Synchrotron Radiation Facility

2.2.1 National Synchrotron Light Source

The National Synchrotron Light Source (NSLS) is a second-generation synchrotron facility located in the heart of Brookhaven National Laboratory (BNL) in Upton, New York. NSLS comprised two electron storage rings: X-ray and Vacuum Ultraviolet (VUV); which provide bright focused light spanning the spectrum from the IR through X-ray. In

2014, the Department of Energy (DOE) national user facility NSLS closed after over 30 years of operation, and is being replaced by NSLS-II, which is designed to be 10,000 times brighter. Unfortunately, the IR beamlines are not scheduled to become operational until late 2017.

2.2.2 Beamline U2A capabilities

The VUV ring is where the U2A beamline resides. The brightness of the IR beamline is such that it bleeds through to the visible – making alignment much easier. A nitrogen-purged Bruker IRscope II is utilized for mid-IR measurements with a frequency range of 600 – 100000 cm^{-1}. The aperture of the beam that incidents on the sample has a limit of ~50 x 50 μm^2; which allows for highly accurate measurements of not only the sample but an internal background as well.

2.2.3 High pressure-temperature experimental setup at U2A

The U2A beamline at NSLS was used for all high pressure-temperature IR experiments – Figure 2.1.

Figure 2.1. The high pressure-temperature IR experimental setup at U2A beamline at NSLS.

As shown in the following Figure 2.2, the heating block contains the DAC and sample. The IR beam is bent off the IR section of the synchrotron, and piped into the U2A beamline where it passes through the condenser lenses, transmits through the sample and media, and incidents on the detector – Figure 2.3. The sample is positioned in line with the detector by an optical microscope with an IR filter (indicated in yellow).

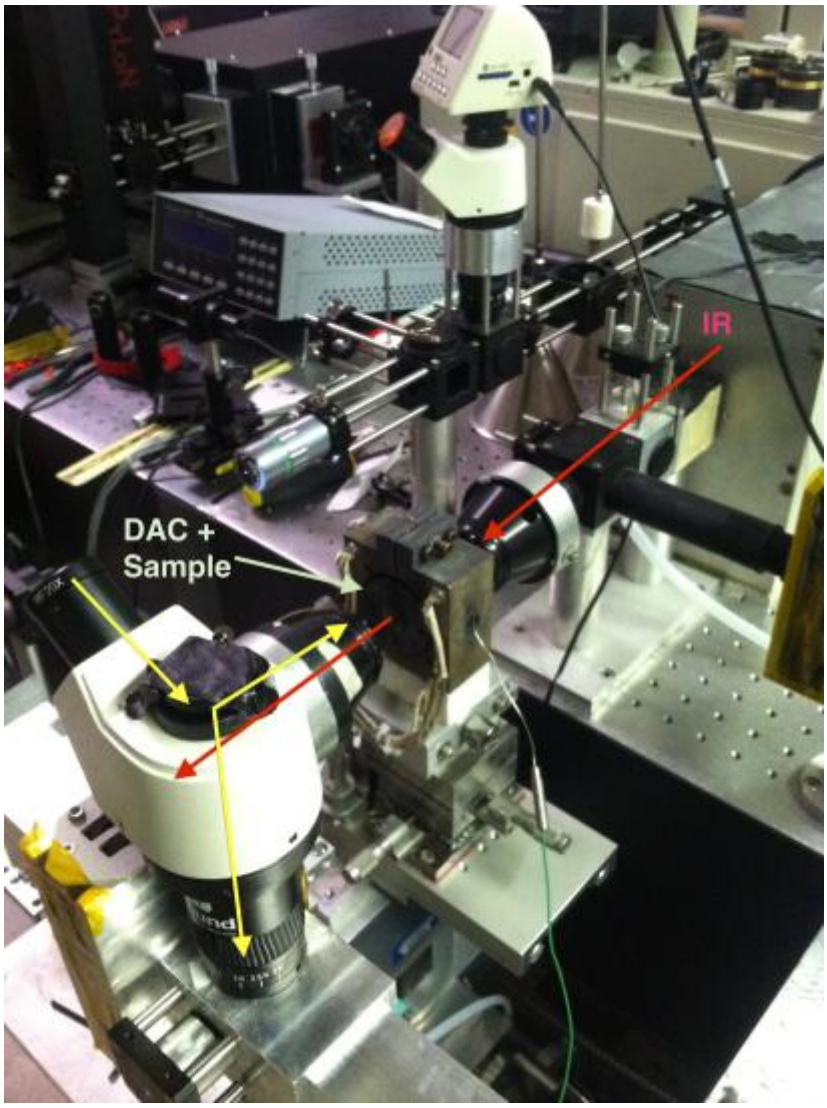

Figure 2.2. IR beam (red arrows) passing through DAC and sample (green arrow), and the sample is aligned with the detector via an optical microscope with IR filter (yellow arrow).

Figure 2.3. The IR detector at U2A beamline – NSLS.

Prior to applying pressure, the sample is thinned out between the two diamond anvils, and the transmission is optimized. Once the transmittance is optimized, the DAC is loaded with KBr and ruby (pressure marker). The pressure is then checked with ruby fluorescence by incidenting a green laser on the ruby sphere embedded in the sample + DAC using the system indicated in Figure 2.4.

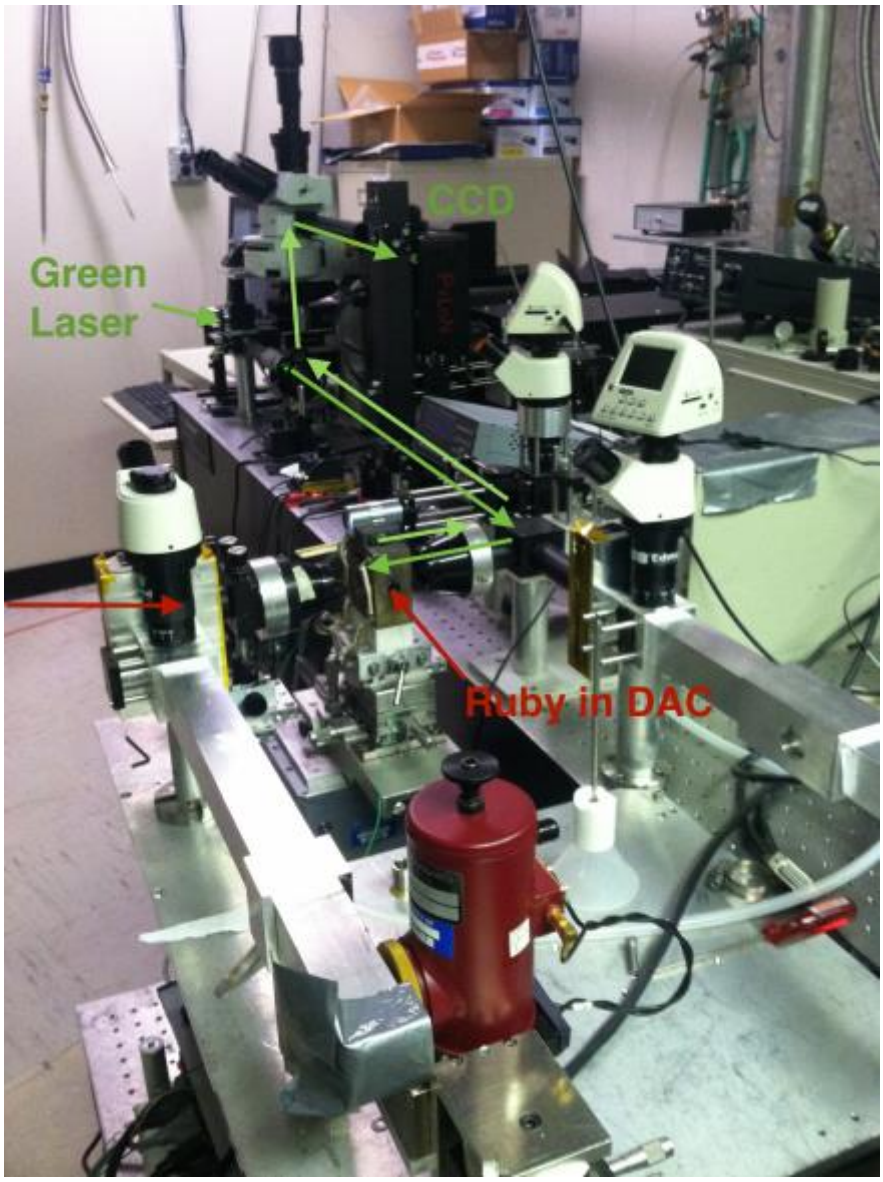

Figure 2.4. Ruby fluorescence system at U2A.

The fluorescence signal is then sent to a computer, and the pressure is calculated by fitting Gaussians to R1 and R2 fluorescence peaks of ruby using the published pressure dependency of ruby shifts at ambient temperature[45, 46] and elevated temperature[47]. Once the initial pressure and sample spectra are collected, the experiment may commence. The power of using the U2A beamline is that an internal background spectrum may be taken,

and then the beam moved to the sample (Figure 2.5). This allows for the highest quality IR spectra that can be obtained with a sample under extreme conditions. Additional details why this capability is so vital to explosives research under extreme conditions is highlighted in the next section.

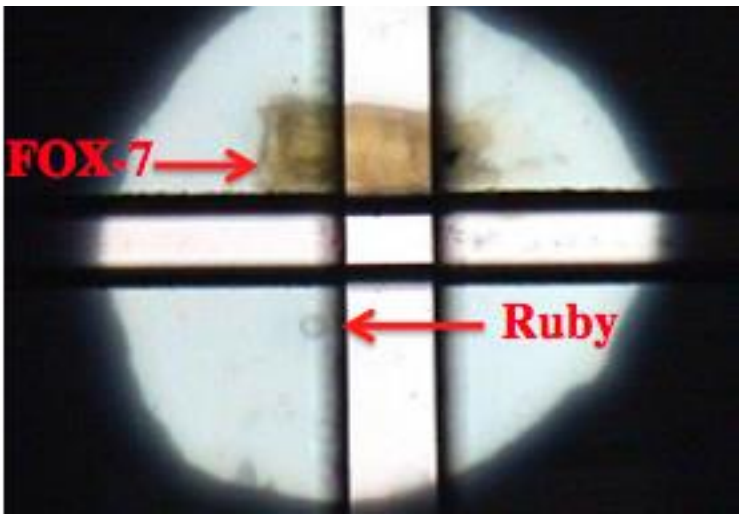

Figure 2.5. A view through the DAC during a high pressure-temperature experiment. The sample and ruby are indicated with the rest of the sample view being KBr (transparent).

2.3 Infrared Synchrotron Radiation Experiments on FOX-7

2.3.1 Overview: Systematic investigation of FOX-7 at high pressure-temperature

In our previous work, we conducted differential scanning calorimetry (DSC) [28] on FOX-7 to identify the ambient-P high-T phase transition temperatures. We then conducted a 1 atm isobaric heating experiment using synchrotron IR radiation. Analysis of the 1 atm isobaric heating experiment indicated that our IR measurements agree within ±10°C with the known transition temperatures identified in DSC. Using the identified characteristic

mode behavior of each high-T phase, we were able to then apply this phase transition schematic to all other isobaric heating experiments. By using this systematic approach to the analysis of all of our isobaric heating experiments, we were able to clearly define curvatures and slopes of each high-temperature phase. It is important to note, that while our temperature measurements are within ±10°C, the error bar for each phase boundary is indicated as the last data point along the respective PT-path. In addition, high-PT experiments are notoriously difficult because thermal expansion causes the pressure to float when temperature is increased. It is important to note that our experiments are no exception. We kept near isobaric conditions by regularly checking and slightly tuning the pressure as the temperature was increased. Our results are reported as near isobaric with pressure-temperature values indicated on spectrum stacks if deviations occurred from the reported isobaric heating pressure.

The use of high flux synchrotron IR radiation at U2A allows for the beam to be fine-tuned to a spot that allows for a background to be taken at each PT-point. The internal background, collected from KBr region where there is no sample, is then subtracted from sample spectrum to yield the most accurate sampling of FOX-7 at a given PT-point. This capability provides ultra-high-quality data that can be used for detection of subtle changes within FOX-7, that otherwise maybe difficult to detect when using in-house spectroscopic systems. Given that the change of the molecular orientation (and therefore, interaction between molecules) is likely to be reflected in the vibrational spectra, which may manifest in discontinuous frequency shifts, loss of intensity, or broadening (narrowing) of lines in the spectra,[25] we define a phase transition or structural distortion as the presence of new vibrational modes and/or discontinuities in $d\nu/dT$ ($d\nu/dP$). [24]

In addition to the ability to detect subtle structural changes in FOX-7, the ability to take a background within the DAC allows for confident detection of characteristic decomposition products. We define decomposition as the complete loss of sample vibrational modes, and the development of characteristic decomposition products. Because the δ-phase is a partial decomposition of FOX-7, we apply an additional criterion to this phase transition. The presence of CO_2 is also used in conjunction with the known mode characteristics when transitioning into δ-phase.

In addition, the literature disagreements [32] in the existence (or the lack thereof) of phase transitions have been partly attributed to the nature of starting sample (polycrystalline powder or single crystal) as well as the type of pressure media. While single crystal data is essential to indexing crystal structures, we believe that in the context of HE, powder crystalline high-PT experiments are important, as they are more representative of the bulk compacts utilized in shock initiation studies and typical applications. Additionally, the need for liquid or gas media for single crystal experiments can also be problematic for studying HE because of the large intermolecular spacing; the media can intercalate between layers, yielding lattice distortions. It is noted that the use of KBr as a solid media for high-P synchrotron IR spectroscopy provides a transparent, quasi-hydrostatic environment that is advantageous for trapping melt or decomposition products for further characterization.

2.3.1 Ambient-pressure isobaric heating experiment

The powder crystalline sample was obtained through a cooperative agreement with the Totalförsvarets forskningsinstitut (FOI, Swedish Defense Research Agency). The high-PT mid-IR (MIR) spectroscopy studies were conducted at the U2A beamline of the National Synchrotron Light Source at Brookhaven National Laboratory. An internal resistive heating DAC was used to induce high-PT conditions in this study. The 300 μm culet type-IIa diamonds were mounted in the DAC, sample of FOX-7 (~40 μm x ~10 μm) was then thinned to optimal IR transmission signal thickness of ~5 μm. This experiment did not utilize a gasket, pressure medium, or pressure marker; we choose to leave the sample between the anvils, ungasketed but not compressed to get an ambient pressure IR baseline for our future isobaric heating experiments.

2.3.2 Isobaric heating experiments (0.4, 0.9, and 2.0 GPa)

The powder crystalline sample was obtained through a cooperative agreement with the Totalförsvarets forskningsinstitut (FOI, Swedish Defense Research Agency). The high-PT mid-IR (MIR) spectroscopy studies were conducted at the U2A beamline of the National Synchrotron Light Source at Brookhaven National Laboratory. An internal resistive heating DAC was used to induce high-PT conditions in this study. The 300 μm culet type-IIa diamonds were mounted in the DAC, separated by an Inconel alloy gasket that had been pre-indented to ~30 μm thickness. For each isobaric heating experiment, a sample of FOX-7 (~40 μm x ~10 μm), along with 20 μm diameter ruby spheres (pressure marker; accurate to +/- 0.1 GPa), and KBr (pressure medium), were loaded into a ~150 μm

diameter hole that had been drilled into the gasket to allow for IR transmission measurements.

2.3.3 Isobaric heating experiments near 3.0 GPa

The high-PT mid-IR (MIR) spectroscopy experiments were conducted on the U2A beamline at the National Synchrotron Light Source at Brookhaven National Laboratory. Only internal resistive heating DACs were used to induce high-PT conditions in this study. While multiple experiments were performed, only two are indicated. The quality of the spectra for the other experiments was too poor to discern anything more than a possible decomposition. However, for two experiments, the spectra quality was usable. For the first experiment, the temperature was increase at an incremental rate of ~20°C per spectra, and for the other, larger ~100°C per spectra steps were taken up to 200°C. After 200°C the temperature steps were ~50°C increments up to decomposition. Additionally, the conventional type-IIa diamonds ~300 μm was mounted in the DACs, separated by Inconel alloy gaskets that all had been preindented. Holes were then drilled into the gaskets to allow for IR transmission measurements. The pressure medium (KBr) was used to fill the gasket hole along with an ~20 μm diameter ruby sphere (pressure marker; accurate to ± 0.1 GPa). Analysis of the vibrational spectra was performed by fitting Gaussians to each mode using Peakfit Pro in OriginPro (version 8.5.1).

2.3.4 Isobaric heating experiments near 6 and 8 GPa

The high-PT mid-IR (MIR) spectroscopy experiments were conducted on the U2A beamline at the National Synchrotron Light Source at Brookhaven National Laboratory. Both internal resistive heating DACs and full DAC resistive heating blocks were used to

induce high-PT conditions in this study. Type-IIa ~300 μm diamonds were mounted in the DACs, separated by Inconel alloy gaskets that all had been preindented. Holes were then drilled into the gaskets to allow for IR transmission measurements. The pressure medium (KBr) was used to fill the gasket hole along with an ~20 μm diameter ruby sphere (pressure marker; accurate to ± 0.1 GPa). Analysis of the vibrational spectra was performed by fitting Gaussians to each mode using Peakfit Pro in OriginPro (version 8.5.1).

2.3.5 Ambient-pressure isothermal compression

The sample of FOX-7 was synthesized by a Professor Chulsung Bae at the University of Nevada Las Vegas.[34] The 300 μm culet type-IIa diamonds were mounted in the DAC, separated by an Inconel alloy gasket that had been pre-indented to ~30 μm thickness. For each isobaric heating experiment, a sample of FOX-7 (~30 μm x ~10 μm), along with 20 μm diameter ruby spheres (pressure marker; accurate to +/- 0.1 GPa), and KBr (pressure medium), were loaded into a ~100 μm diameter hole that had been drilled into the gasket to allow for IR transmission measurements. Analysis of the vibrational spectra was performed by fitting Gaussians to each mode using Peakfit Pro in OriginPro (version 8.5.1).

2.3.6 Isothermal compression experiments on FOX-7 at 100 and 200°C; 1.1 GPa isobaric heating

The high-PT, mid- and far-IR micro-spectroscopy studies were conducted at the U2A beamline of the National Synchrotron Light Source at Brookhaven National Laboratory. A diamond anvil cell (DAC), equipped with an internal heater, was employed to induce high pressure-temperature conditions in this study. The 300 μm culet type-IIa

diamonds were mounted in the DAC, separated by an inconel alloy gasket that had been pre-indented to 30 μm thickness. The sample (~30 μm x 10 μm), along with two 20 μm diameter ruby spheres (pressure marker; accurate to ±0.1GPa), and KBr (pressure medium), were loaded into a 60 μm diameter hole that had been drilled into the gasket to allow for IR transmission measurements. The same sample was employed for 100°C and 200°C isothermal compression experiments in the mid-IR. For the 200°C far-IR isothermal compression, a new sample was loaded in the same manner as mid-IR sample. In addition, a 1.07 GPa isobar was measured using a (~30μm x 10μm), along with two 20 μm ruby spheres, and KBr that were loaded into a 60 μm hole that had been drilled into the gasket. Type-Ia diamonds were used during isobaric decomposition experiment. The type-Ia anvils contain nitrogen impurities that masked the majority of the sample vibrations, but did not diminish the capacity to resolve the decomposition phase boundary. Analysis of the vibrational spectra was performed by fitting Gaussians using Peakfit Pro in OriginPro (version 8.5.1).

2.3.7 Isothermal compression experiment at 300°C

The same procedure indicated in *2.3.6* was employed; however, the 300°C isothermal compression experiment utilized 300 μm culet type-IIa diamond anvils mounted in a DAC, separated by an Inconel alloy gasket that had been pre-indented to ~30 μm. The sample of FOX-7 (~30 μm x 10 μm), along with 20 μm diameter ruby spheres and KBr were loaded into a ~60 μm diameter hole. A heating block, which heats the whole DAC, was used in order to obtain a 300°C isotherm to within ±5°C for the duration of the experiment.

2.4 Infrared Synchrotron Radiation Experiments on TATB

2.4.1 Isobaric heating experiments at ~4, 9, and 11 GPa

The high-PT mid-IR (MIR) spectroscopy experiments were conducted on the U2A beamline at the National Synchrotron Light Source at Brookhaven National Laboratory. Type-IIa diamonds ~300 μm was mounted in the DACs, separated by Inconel alloy gaskets that all had been preindented. Holes were then drilled into the gaskets to allow for IR transmission measurements. The pressure medium (KBr) was used to fill the gasket hole along with an ~20 μm diameter ruby sphere (pressure marker; accurate to ± 0.1 GPa). While the ~4.0 GPa isobaric heating experiment had only minor (± 0.2 GPa) changes in pressure where observed, the ~9 and ~10 GPa isobaric heating experiments observed more apparent shifts in pressure due to thermal expansion of the internally resistive heating DAC. Analysis of the vibrational spectra was performed by fitting Gaussians to each mode using Peakfit Pro in OriginPro (version 8.5.1).

2.4.2 Isothermal compression experiments at 25, 50, 100, and 150°C

The high-PT mid-IR (MIR) spectroscopy experiments were conducted on the U2A beamline at the National Synchrotron Light Source at Brookhaven National Laboratory. Full DAC resistive heating blocks were used to induce high-PT conditions in this study; which indicated an extremely stable temperature across the entire PT-region investigated. Type-IIa ~300 μm diamonds were mounted in the DACs, separated by Inconel alloy gaskets that all had been preindented. Holes were then drilled into the gaskets to allow for

IR transmission measurements. The pressure medium (KBr) was used to fill the gasket hole along with an ~20 μm diameter ruby sphere (pressure marker; accurate to ± 0.1 GPa). Analysis of the vibrational spectra was performed by fitting Gaussians to each mode using Peakfit Pro in OriginPro (version 8.5.1).

2.5 Vibrational Mode Assignments

2.5.1 FOX-7 mode assignments

The room temperature far-IR and mid-IR spectra of FOX-7 (a phase) 0.2 and 0.3 GPa, respectfully, are shown in figure 2.6. We have provided a tentative assignment of the IR spectra based on established spectral signatures of $[NH_2]^-$ and $[NO_2]^-$ moieties [48-51], as well as published calculations conducted by Sorescu et al. [52]

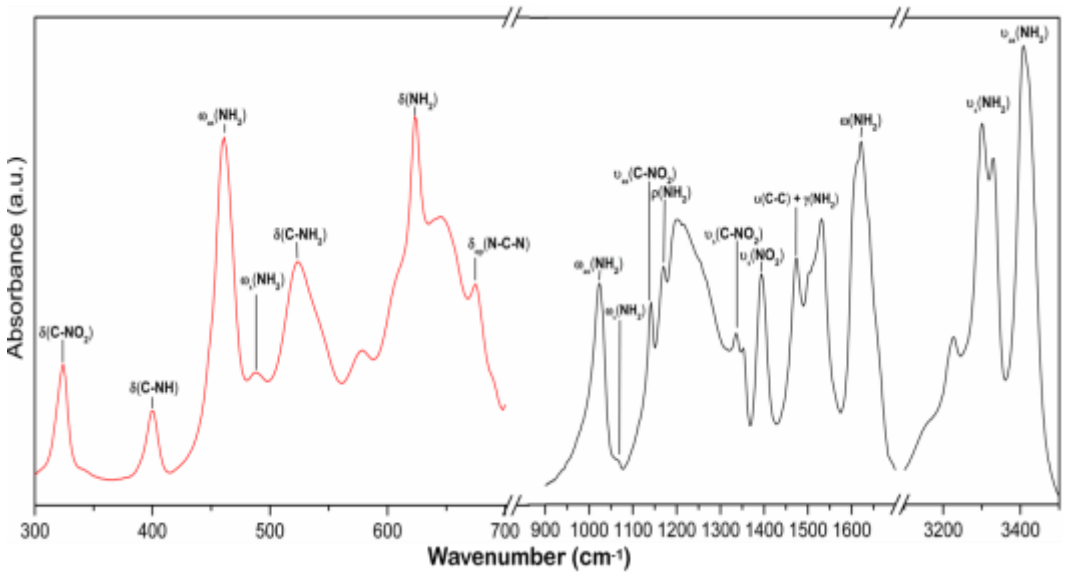

Figure 2.6. Mode Assignment of a phase of FOX-7 at 298 K. Note that the spectra from 300-600 cm^{-1} is the download spectra at 0.2 GPa from the far-IR experiment, and the 600-

3600 cm^{-1} is the download spectra at 0.3 GPa from the mid-IR 100°C experiment. Only commenced a phase modes are assigned. A complete table of the infrared vibrational mode assignments can be found in Table 1.

2.5.2 TATB mode assignments

TATB mode assignments came from a combination of literature values.[13, 14, 17, 19] The specific mode assignments may be found in the results and discussion section under the TATB section.

CHAPTER 3

RESULTS AND DISCUSSION

3.1 Differential Scanning Calorimetry on FOX-7

In order to establish a baseline for the high-temperature polymorphism of FOX-7, we conducted an ambient pressure differential scanning calorimetry (DSC) study[28]. Our investigation indicated three elevated temperature phase transitions identified as: $\alpha \rightarrow$ ß at ~112°C, ß $\rightarrow \gamma$ at ~180°C, and the onset of decomposition at ~211°C[31] with a peak decomposition temperature of ~270°C. However, the onset of decomposition is in conflict with Chemagina et al.[29], whose differential thermal analysis (DTA) experiments show that heating FOX-7 slightly above 210°C results in an irreversible phase transition to the δ-phase. The recovered δ-phase is then stable upon reheating from ~20 – 270°C, and further DTA measurements also show a single exothermal peak which coincides with the second exothermal peak of the initial FOX-7 at ~270°C. These findings suggest that not only is the onset of decomposition higher than previously reported, but that FOX-7 undergoes a polymorphic transition to the δ-phase, an intermediate phase which has the same energetic profile as the initial FOX-7, just prior to complete decomposition.

3.1.1 DSC heat treatment of FOX-7

To investigate this discrepancy, an additional DSC heat-treated experiment was conducted to compare with Chemagina *et al.*'s study. Our results indicated that indeed the δ-phase is retained at ambient conditions following heat treatment shown in Figure 3.1.a. Furthermore, based on DSC data, it also appears that FOX-7 undergoes a partial decomposition, as indicated by change in heat flow measured over a 30 minute period at constant 220 °C. When compared to a conventional DSC on FOX-7 (1.51 mg with a 10

°C/min heat rate during a continuous 50 ml/min nitrogen flow up to decomposition), the heat-treated sample indicated no elevated temperature polymorphism and an onset of decomposition starting slightly above 250 °C (Figure 3.1.b).

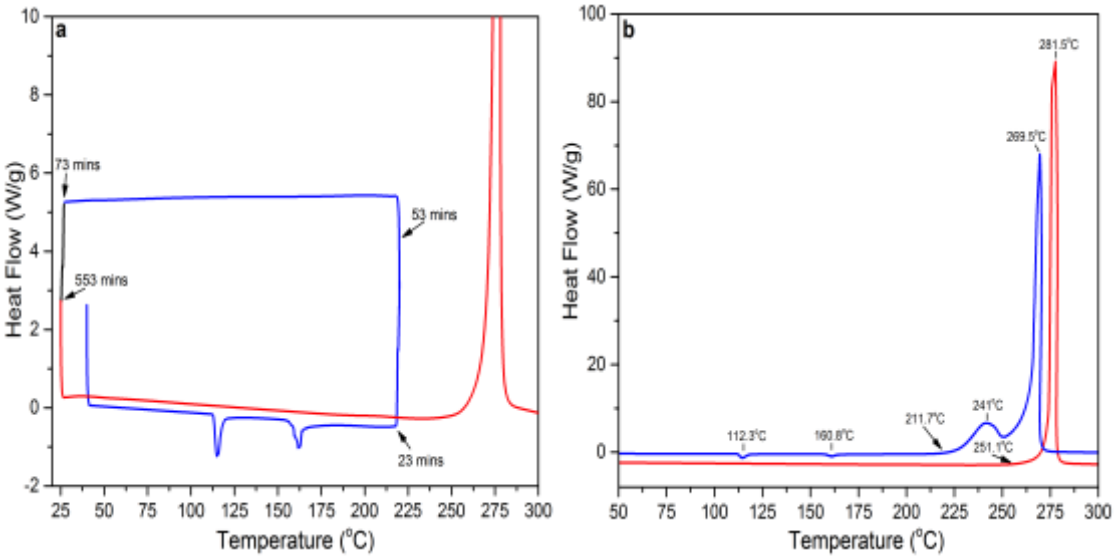

Figure 3.1. (a) The experimental path taken for heat treating FOX-7 as described in the experimental details. (b) A comparison of a normal DSC run (blue, top curve) and heat treated run (red, bottom curve) on FOX-7.

3.2 Infrared Synchrotron Radiation Isobaric Heating Experiments on FOX-7

3.2.1 Ambient-pressure isobaric heating experiment

In order to understand the characteristic vibrational behavior of the high-T polymorphs of FOX-7, a room-P isobaric heating experiment was performed on FOX-7 (Figure 3.2). The vibrational behavior of the amines is of particular importance to understanding the evolution of the hydrogen bonding network within FOX-7 and was used as a strong indication of the strength of the network over the investigated PT-space. The

α-phase of FOX-7 is a wave-shaped layered structure were both nitro groups are involved in two hydrogen bonds, resulting in eight hydrogen-accepting bonds of this type: six are intermolecular, and two are intramolecular. [30] For each individual FOX-7 molecule in the α-phase, there are 14 hydrogen bonds. [31]

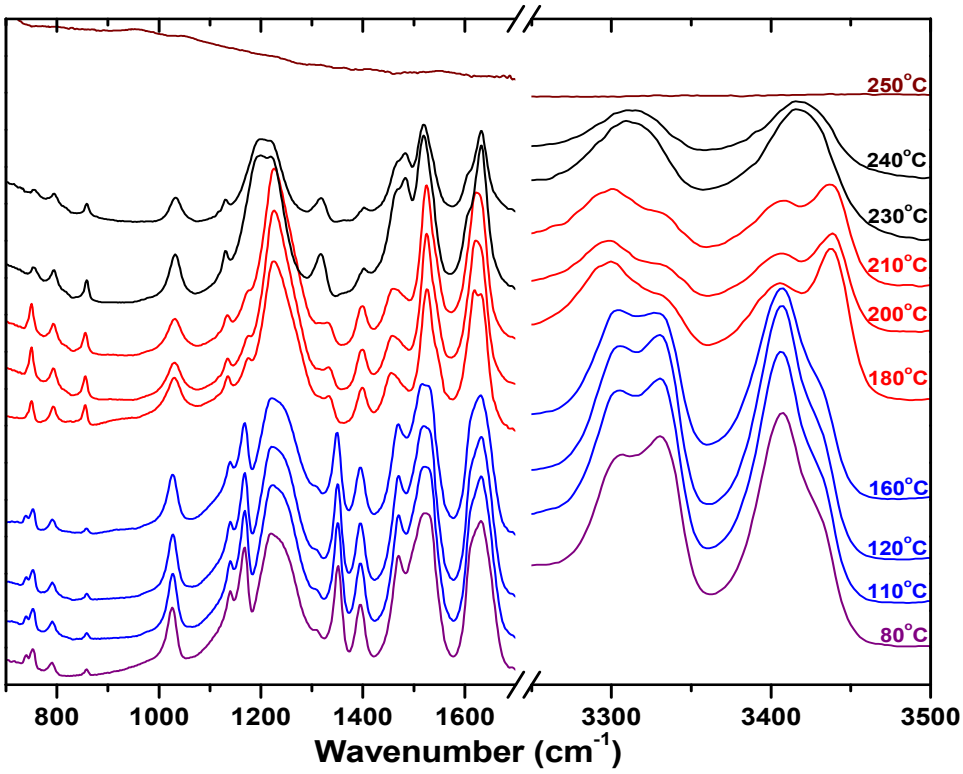

Figure 3.2. MIR spectra taken at increment temperature increase along a 1 atm isobar. The temperature of each spectrum is indicated on the right side of the figure. Approximate structural phase transitions are indicted with a change in color of the spectra at the respective pressure and temperature: α-phase (purple), β-phase (blue), γ-phase (red), δ-phase (black), and decomposition (wine).

During initial heating from 60 – 110°C, we observed slight softening in both asymmetric amine stretching modes [$\nu_{as}(NH_2)$] at ~3432 and 3407 cm^{-1}: followed by slight

hardening in both modes from 120 – 160°C (Figure 3.3). In addition, we observe a mode at ~ 3228 cm^{-1} remain at approximately the same frequency up to 110°C. Then at 120°C, we observed this mode continually soften up to 160°C. The change in the dν/dP slope about the ~110°C region, while subtle, is evidence of an α → β phase that was determined initially by both XRD and DSC. It is important to note that the α → β transition has been described as displacive in nature [7] with minor distortions that are difficult to resolve spectroscopically (Raman or IR). [28] Our data indicates that the hydrogen bonding (H-bond) network increases slightly with heating up to ~110°C; where we see a small but noticeable decrease in the strength of the H-bond network when transitioning into β-phase. Our observations are in good agreement with Evers *et al.* [30] X-ray investigation to the β-phase nitro groups which comprises 10 hydrogen acceptor bonds: eight intermolecular, and two are intramolecular. While there appears to be a net increase in hydrogen bonding, the bonds are weaker because the wave-shaped layering becomes more planer with heating. In particular, only one oxygen atom per nitro group is involved in two hydrogen bonds, while the other is involved in three. [30] With a shift in the donor network, we would expect to see a response in vibrational modes associated with the nitro group when transitioning from α → β. In fact, over the same 60 – 110°C range, we observe anti-symmetric C-NO_2 stretching mode [ν_{as} (C-NO_2)] at 1139 cm^{-1} remains approximately the same frequency, but the symmetric C-NO_2 stretching mode [(C-NO_2)] at 1351 cm^{-1} softens slightly. In addition, we observe C-C stretching and amine scissoring [ν (C-C) + γ (NH_2)] at 1469 cm^{-1} harden slightly up to 110°C. From 110 – 120°C, we observe ν_{as} (C-NO_2) harden slightly while ν_s (C-NO_2) softens slightly, and the ν (C-C) + γ (NH_2) mode softens. The strengthening in the asymmetric nitro behavior and subsequent decrease in symmetric nitro stretching

makes sense in the context alterations to donor network when transitioning into β-phase. Additionally, the flattening of the wave-shaped structure would also manifest in the ν (C-C) + γ (NH_2) as the intermolecular hydrogen bonds increase in length. From 120 – 160°C, we observe the ν_s (C-NO_2)], ν_{as} (C-NO_2), and ν (C-C) + γ (NH_2) remain at approximately the same frequency. While the amine wagging mode [ω(NH_2)] at 1608 cm^{-1} and the amine deformation mode [δ (NH_2)] at 1631 cm^{-1} both harden up to 160°C. Overall, we see a slight strengthening in the hydrogen bonding network over the 120 – 160°C temperature range.

Continued heating from 160 – 180°C revealed noticeable visual change in the amine stretching modes from ~3250 – 3450 cm^{-1} (Figure 3.3). In addition, we observed hardening by ~7 cm^{-1} in the ~3432 cm^{-1} ν_{as}(NH_2) mode; after which, the mode remained at approximately the same frequency up to 210°C. We observed slight softening in the ~3407 cm^{-1} ν_{as} (NH_2) mode from 160 – 180°C: followed by a slight softening at 190°C, then hardening by ~6 cm^{-1} from 190 – 210°C. A softening of ~13 cm^{-1} in the mode at ~3228 cm^{-1} is seen from 160 – 180°C. The mode then remains approximately the same frequency up to 210°C. The ν_s(NH_2) mode at 3306 cm^{-1} softened by ~6 cm^{-1} from 160 – 180°C, and then the mode remained approximately at the same frequency up to 210°C. With the drastic visual change in the spectrum, the marked discontinuities dν/dP, and the agreement with thermal measurements, we believe the β → γ phase transition occurs at ~180°C. It is important to note that the β → γ has a clear and very distinct infrared signature; which was expected due to the highly energetic behavior detected by DSC. [28] Interestingly though, both β- and γ-phase have a total of 18 hydrogen bonds per molecule. Analysis of the amine vibrational modes indicates that the hydrogen bonding network remains approximately the

same or slightly increases. However, the transition appears to be very energetic with a "thermosalient effect" (crystal jumping) in the DSC. [7] Single crystal XRD analysis indicated that the $\beta - \gamma$ phase transition is first order and reconstructive with an approximate two-fold increase in the unit cell volume in comparison to $\alpha-$ and β-phase. [31] The $\beta \rightarrow \gamma$ phase transition also eliminates the three dimensional rigidity of the structure, resulting in the formation of planar layer that have increase translation motion that optimizes the efficiency of the planar layer packing. [7] Like before in the $\alpha \rightarrow \beta$ transition, the shift to a more planar layering structure should have significant effects on the nitro vibrational modes. Further analysis indicates just that, from 160 – 180°C we observe the ν_{as} (C-NO_2) at 1142 cm^{-1} soften by ~7 cm^{-1} and ν_s (C-NO_2) at 1349 cm^{-1} soften by ~13 cm^{-1}. Additionally, we observe an ~11 cm^{-1} softening in ν (C-C) + γ (NH_2) at 1469 cm^{-1}, and a hardening in both ω (NH_2) at 1610 cm^{-1} and δ (NH_2) at 1635 cm^{-1}. The additional hardening in the amine modes suggest that there was indeed a net increase in hydrogen bonding when transitioning into the γ-phase. Interestingly, by 210°C nearly all modes have hardened to frequencies close too or higher than the ambient-PT α-phase frequencies with the exception of the ν (C-NO_2) modes: which are at significantly lower frequencies. This suggests that the γ-phase hydrogen bonding network strength maybe close to that of α-phase, which might explain the tendency of γ-phase being recoverable when quenched to ambient conditions. However, the γ-phase does have lower frequency C-NO_2 modes, which is a product of transitioning to a more planar layering structure. It has been proposed that cleavage of the C-NO_2 bond is a possible detonation trigger [53] for FOX-7, and appears to be consistent with our observations.

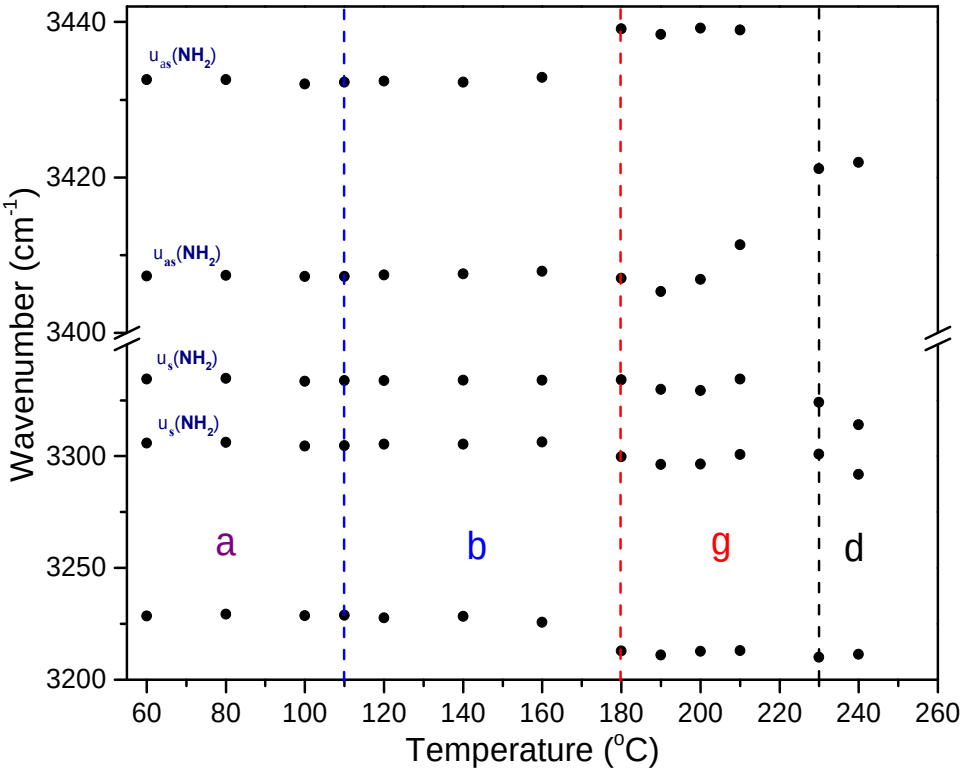

Figure 3.3. Pressure dependence of select modes during a 1 atm isobaric heating experiment about the range of 3200-3450 cm^{-1}. The dashed lines indicate approximate temperatures for the onset of the indicated structural phase transitions.

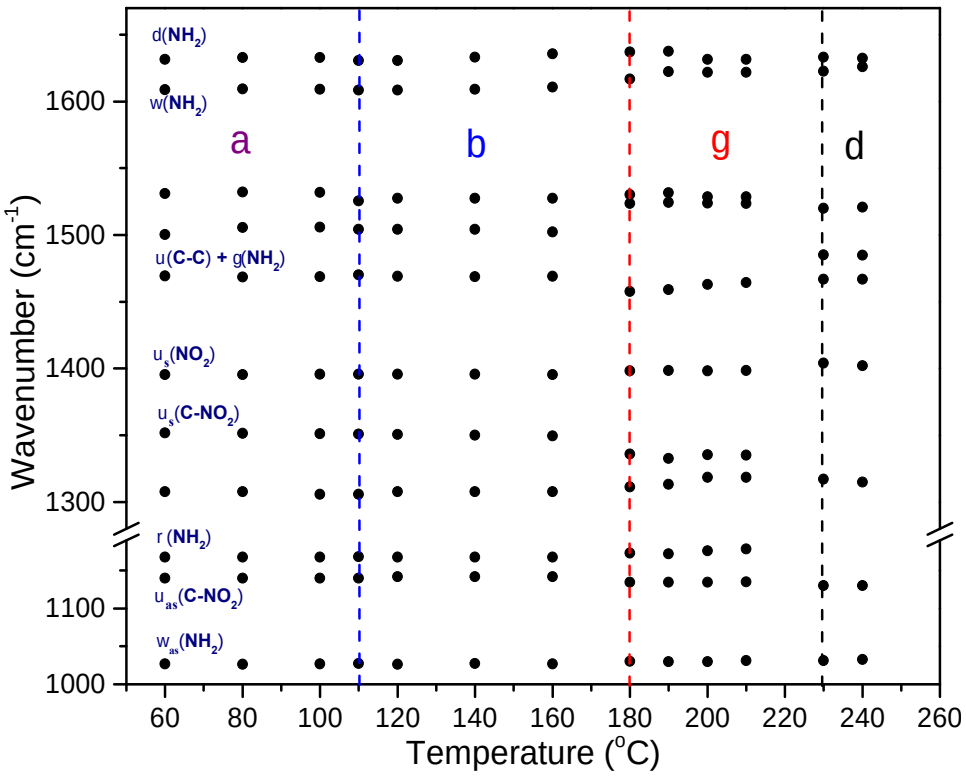

Figure 3.4. Pressure dependence of select modes during a 1 atm isobaric heating experiment about the range of 1000-1670 cm^{-1}. The dashed lines indicate approximate temperatures for the onset of the indicated structural phase transitions.

Based on our previously reported DSC results [28], we also expect that γ → δ should have a very unique infrared signature: however, the actual time scale of partial decomposition and transitioning into the δ-phase points to a highly kinetically driven effect. [28] Increasing the temperature from 210 – 230°C, we observed a drastic shift in the spectra to a unique δ-phase signature (Figure 3.2). We observed an extreme softening of the amine vibrational modes and weakening of the hydrogen bonding network (Figure 3.3). From 210 – 230°C the $\nu_s(NH_2)$ mode at 3334 cm^{-1} softened by ~10 cm^{-1}, and the $\nu_{as}(NH_2)$ modes at 3411 and 3439 cm^{-1} soften by 27 and 18 cm^{-1}, respectively. In addition, we

observed a strong hardening in ν (C-C) + γ (NH_2) at 1464 cm^{-1} by ~19 cm^{-1} and an additional mode appear at 1467 cm^{-1}. This suggest yet another restructuring of the layering structure of FOX-7. It is important to note that there is strong evidence that the $\gamma \rightarrow \delta$ phase transition is a partial decomposition characterized by formation of NO_2 gas [31] as the first step observed in non-explosive thermal decomposition of FOX-7. While we could not contain the decomposition gases in the 1 atm isobaric heating experiment, we did observe the loss of ν_s (C-NO_2) mode at 1335 cm^{-1}, and softening in ν_{as} (C-NO_2) at 1130 cm^{-1}. Which is consistent with the proposed decomposition pathway, and in fact, we observe uniform softening in all modes up to decomposition at ~250°C.

3.2.2 Near 0.4 GPa isobaric heating experiment

In order to better understand how pressure affects the high-T phase behavior of FOX-7, a near 0.4 GPa isobaric heating experiment was preformed up to decomposition. It is important to note that keeping exact pressures during heating is very difficult with diamond anvil cells due to thermal expansion. While we tried to maintain an experimental path very close to 0.4 GPa, the pressure decreased slightly throughout this experiment (Figure 3.5).

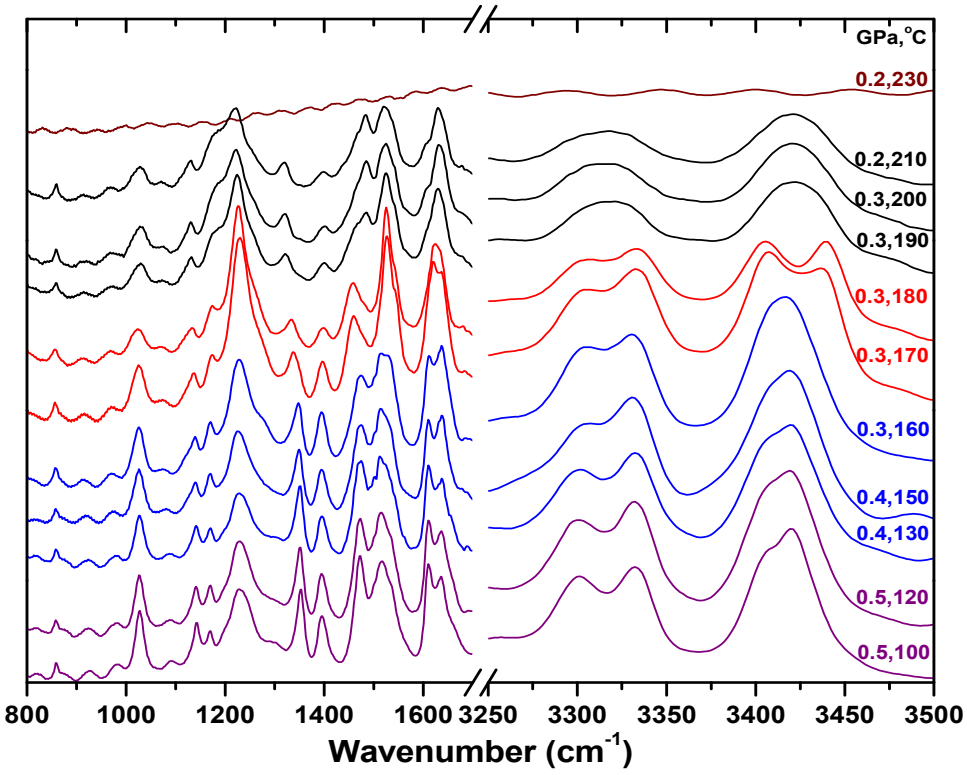

Figure 3.5. MIR spectra taken at increment temperatures along a near 0.4 GPa isobar. The pressure and temperature of each spectrum is indicated on the right side of the figure. Approximate structural phase transitions are indicted with a change in color of the spectra at the respective pressure and temperature: α-phase (purple), β-phase (blue), γ-phase (red), δ-phase (black), and decomposition (wine).

In comparing the ambient temperature frequencies of the 1 atm and 0.4 GPa isobaric experiments, we see a net increase in the hydrogen bonding network. We suspected that the net increase in the hydrogen bonding would make α-phase more resistant to transitioning into β-phase. To further investigate this, initial heating from ~100 – 130°C we again observed characteristic behavior of softening in the $\nu_{as}(NH_2)$ modes at ~3422 and 3405 cm^{-1}. While we observe $\nu_s(NH_2)$ modes at 3302 and 3333 cm^{-1} all harden slightly,

this is opposite of what we observed at 1 atm. The application of 0.4 GPa of pressure with temperature appears to have further stabilized the α-phase with a small but net increase in hydrogen bonding. From 130 – 140°C, we observe the $\nu_{as}(NH_2)$ mode at ~3420 cm^{-1} remain at approximately the same frequency, and hardening by ~5 cm^{-1} in the ~3402 cm^{-1} $\nu_{as}(NH_2)$ mode. While the $\nu_s(NH_2)$ mode at 3302 cm^{-1} hardens slightly, and the $\nu_s(NH_2)$ mode at 3333 cm^{-1} remains approximately the same. This increase in hydrogen bonding made the transition from α → β more resistant, but we do see a noticeable discontinuity in dν/dT (Figure 3.6).

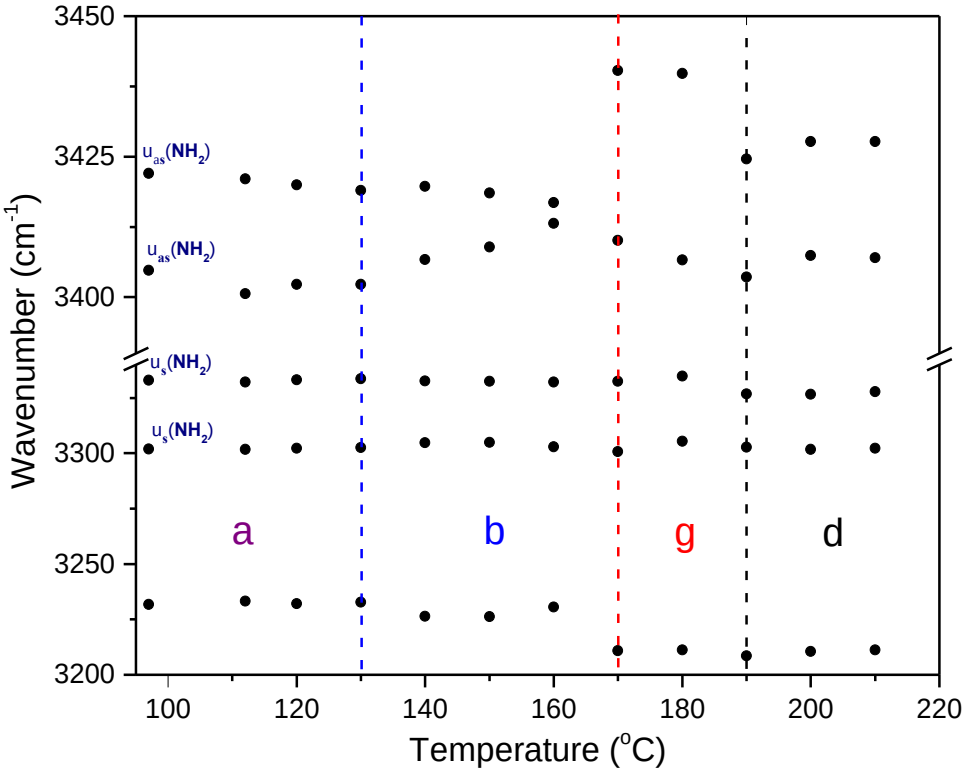

Figure 3.6. Pressure dependence of select modes during a near 0.4 GPa isobaric heating experiment about the range of 3200-3450 cm^{-1}. The dashed lines indicate approximate temperatures for the onset of the indicated structural phase transitions.

These observations indicate an $\alpha \rightarrow \beta$ transition occurring at ~130°C at 0.4 GPa or ~20°C higher than at 1 atm. Additional support comes from the behavior of the $\nu_{as}(C\text{-}NO_2)$ mode at 1143 cm^{-1} and $\nu_s(C\text{-}NO_2)$ mode at 1352 cm^{-1}, which both harden over the 100 – 130°C. Similar behavior is observed in the 1 atm isobaric heating experiment, but the $\nu(C\text{-}NO_2)$ mode at 1141 cm^{-1} softens slightly from 130 – 140°C. This is in contrast to the 1 atm behavior, and is probably an effect of the application of 0.4 GPa creating a more planar layering structure. The β-phase appears to have comparable hydrogen bonding network strength to α-phase, and this is perhaps due to the pressure affect. β-phase has four additional hydrogen bonds in comparison with α-phase; however, at 1 atm β-phase had a slightly weakened net hydrogen bonding network with respect to α-phase. This is because the hydrogen bonds in β-phase are on average longer (weaker) than those found in α-phase. We suspect that the application of pressure has strengthened those weaker bonds to yield a hydrogen bonding network strength similar to that of α-phase at 0.4 GPa.

As temperature is increased further, from 160 – 170°C we observe a strong ~23 cm^{-1} hardening in the $\nu_{as}(NH_2)$ mode at ~3422 cm^{-1}. Additionally, we see strong 20 cm^{-1} softening in the mode at 3230 cm^{-1}: with only minor softening in the $\nu_{as}(NH_2)$ mode at 3333 cm^{-1} and the $\nu_s(NH_2)$ mode at 3302 cm^{-1}. This behavior is identical to what we observed when transitioning from the $\beta \rightarrow \gamma$ phase at 1 atm. In addition to the large discontinuity in $d\nu/dT$, we again see a large visual shift in the IR spectra. These observations indicate that the $\beta \rightarrow \gamma$ phase transition occurs at ~170°C at ~0.3 GPa. Comparing again the magnitude of the hydrogen bonding network of γ-phase with that of α-phase, we observed a similar hydrogen bonding network in high-PT γ-phase with respect

to the high-P α-phase. In addition, we observed the high-PT γ-phase having nearly identical frequencies as that of the 1 atm γ-phase. However, like the 1 atm γ-phase, the ν (C-NO_2) modes at 1137 cm^{-1} and 1345 cm^{-1} soften drastically, but at 0.4 GPa, we observe a less severe softening in these modes. As observed in the 1 atm γ-phase, the ν (C-NO_2) mode at 1345 cm^{-1} softens a greater degree than the ν (C-NO_2) mode. We suspect that the addition of 0.4 GPa of pressure, aided the reconstructive nature of the β → γ-phase transition, but because the layering structure was approaching planar from the pressure effect, the drastic reconstructive nature of γ-phase observed at 1 atm, was tempered.

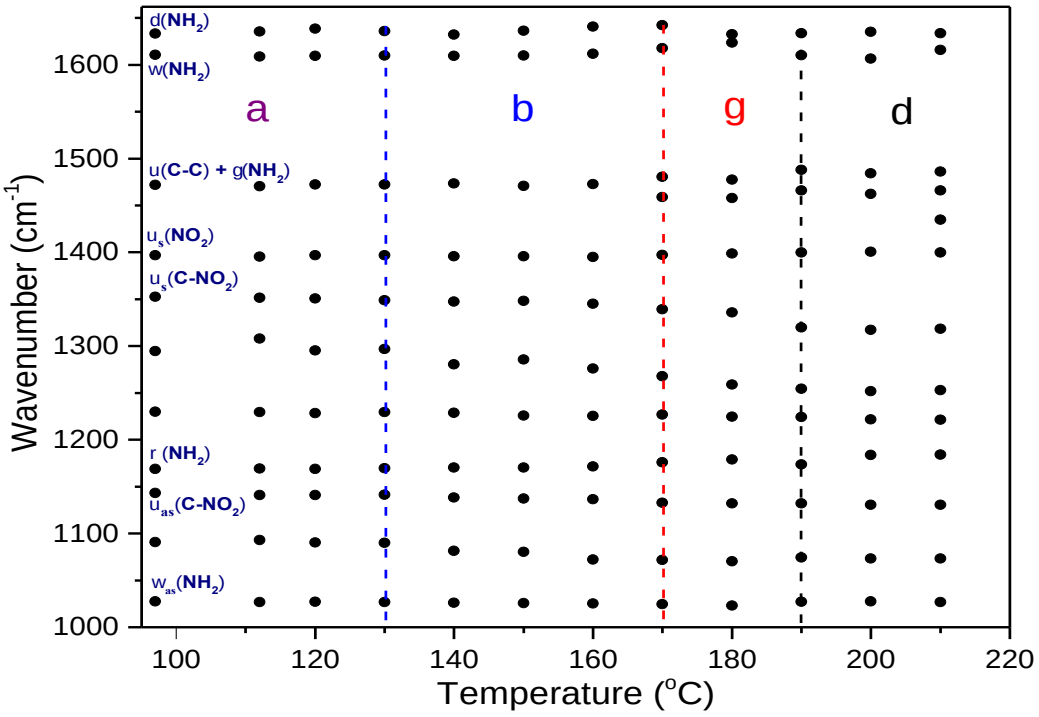

Figure 3.7. Pressure dependence of select modes during a near 0.4 GPa isobaric heating experiment about the range of 1000-1670 cm^{-1}. The dashed lines indicate approximate temperatures for the onset of the indicated structural phase transitions.

Heating from 180 – 190°C, we observe a drastic visual shift in the IR spectra, and extreme softening in the amine vibrational modes (weakening of the hydrogen bonding network). The ν_s (NH_2) modes at 3334 cm^{-1} and 3305 cm^{-1} softened by 8 cm^{-1} and 3 cm^{-1}, respectively. In addition, the ν_{as} (NH_2) modes at 3406 and 3439 cm^{-1} also soften by 3 and 15 cm^{-1}, respectively. We observe the development of a new mode at 1466 cm^{-1} and strong hardening with the ν (C-C) + γ (NH_2) at 1457 cm^{-1} by ~30 cm^{-1}. The drastic visual shift in the IR spectra and extreme softening in the amines is indicative of a $\gamma \rightarrow \delta$ transition, and is the same vibrational behavior we observed during the 1 atm heating experiment. However, we did not observe the loss of the ν (C-NO_2) mode at 1336 cm^{-1} like we did during the 1 atm experiment. Instead, we observe the ν (C-NO_2) mode at 1336 cm^{-1} soften by ~16 cm^{-1}. Overall, we observe a weaker hydrogen bonding network in the high-PT δ-phase with respect to the high-PT γ-phase, but a stronger hydrogen bonding network in high-PT δ-phase with respect to ambient pressure δ-phase. The application of 0.4 GPa of pressure appears to have increased the stability of the hydrogen bonding network of the δ-phase. With further heating to 210°C, we observe slight strengthening of the hydrogen bonding network, but heating slightly above 210°C, we observe loss of the sample spectrum and presence of decomposition products. This observation is slightly counterintuitive because the hydrogen bonding network of high-PT δ-phase is stronger than that of ambient pressure δ-phase, and the ν (C-NO_2) mode is still presence. The stronger hydrogen bonding network and continual presence of ν (C-NO_2) mode, would lead one to believe the decomposition boundary would be higher than that at ambient-P. However, these observations suggest that perhaps with the application of 0.4 GPa of pressure, the first step in decomposition might differ from ambient-P.

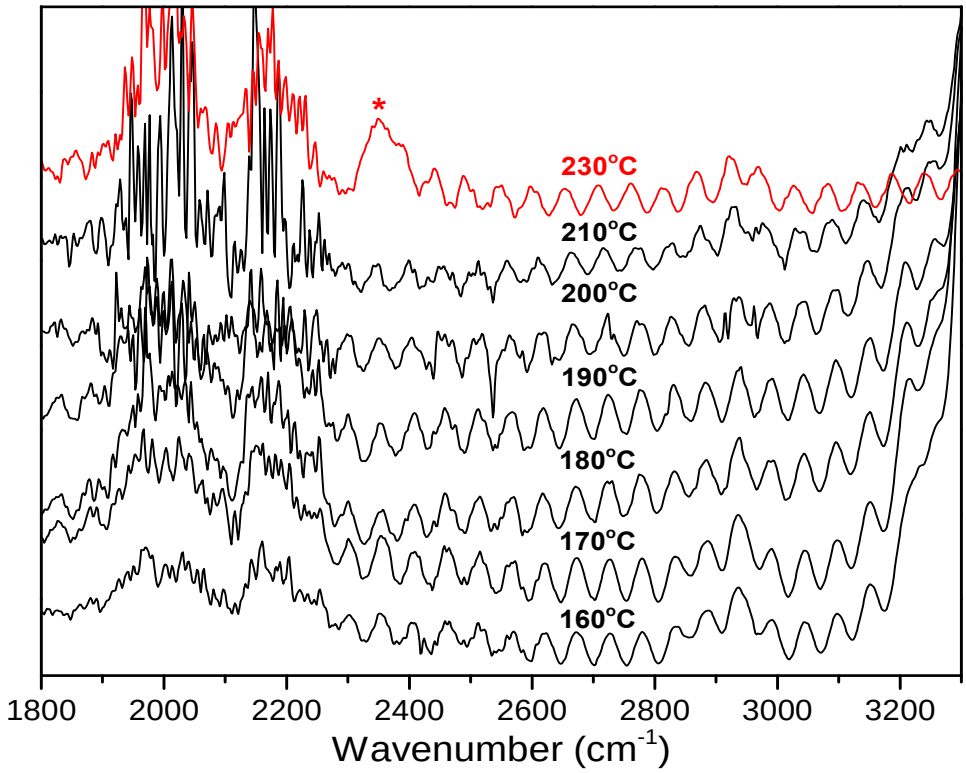

Figure 3.8. Spectrum stacks from a near 0.4 GPa isobaric heating experiment - at indicated temperatures - with characteristic decomposition products shown with red asterisk. The red spectrum indicates decomposition.

3.2.3 A 0.9 GPa isobaric heating experiment

To further explore the high-T phase behavior of FOX-7, a 0.9 GPa isobaric heating experiment was performed. During this experiment, careful attention was given to keeping the 0.9 GPa isobaric pathway and is presented without noticeable variation in pressure (Figure 3.9).

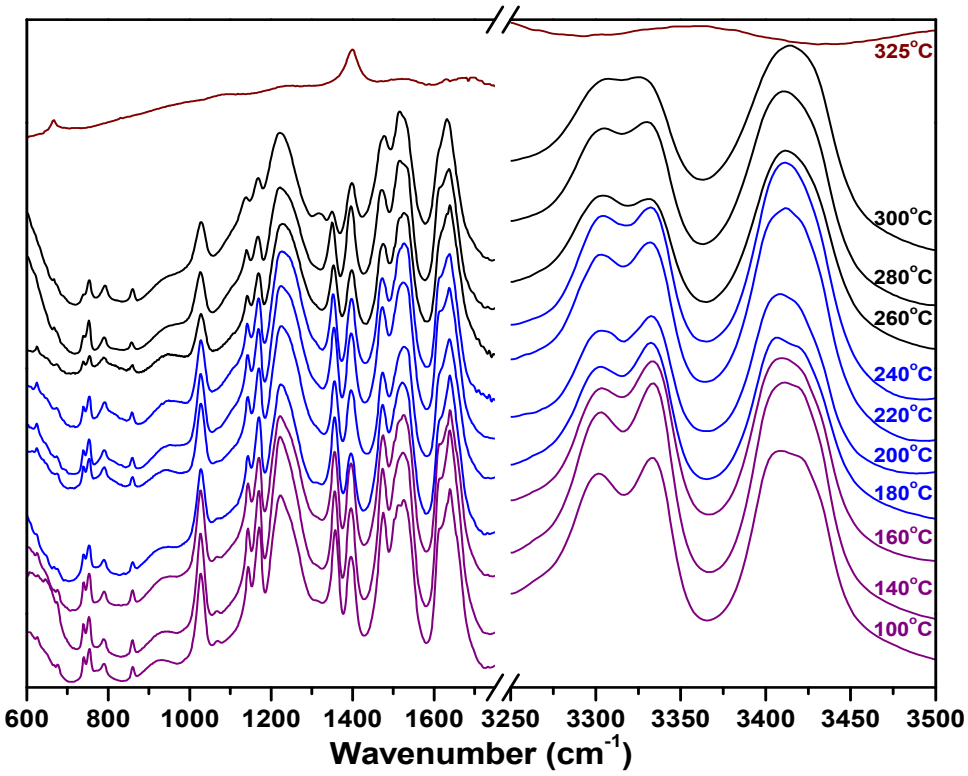

Figure 3.9. MIR spectra taken at increment temperatures along a 0.9 GPa isobar. The temperature of each spectrum is indicated on the right side of the figure. Approximate structural phase transitions are indicted with a change in color of the spectra at the respective pressure and temperature: α-phase (purple), β-phase (blue), δ-phase (black), and decomposition (wine). The γ-phase appears to terminate prior to 0.9 GPa.

Heating from 120 – 160°C revealed strong softening in both $\nu_{as}(NH_2)$ modes found at ~3422 and 3401 cm^{-1}: followed by sharp hardening at 180°C (Figure 3.10). From 180 – 240°C, we observe the 3422 cm^{-1} mode remain at approximately the same frequency, but the 3401 cm^{-1} mode continues to harden up 240°C. Additionally, the mode at ~3234 cm^{-1} remains at approximately the same frequency up to 180°C. We then observe softening at 200°C followed by slight hardening up to 240°C. By applying the characteristic transition criteria identified in the ambient pressure heating experiment, as

well as, the sharp discontinuity in dν/dP, we observe the α → β transition as early as 180°C at 0.9 GPa with a slight increase in the hydrogen bonding network.

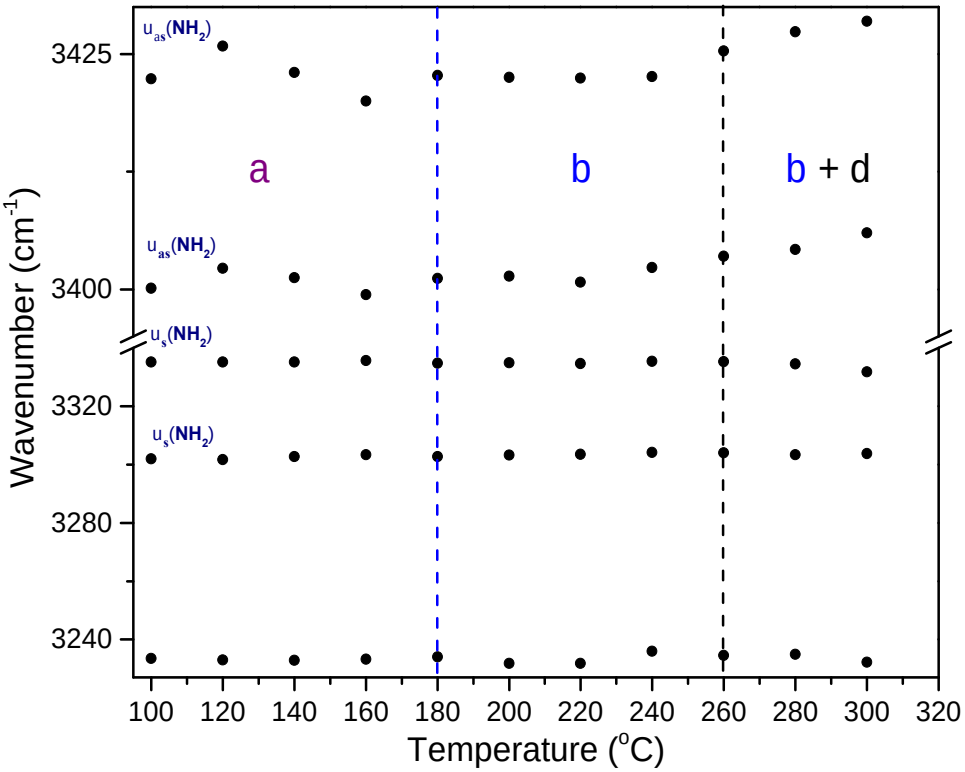

Figure 3.10. Pressure dependence of select modes during a 0.9 GPa isobaric heating experiment about the range of 3230-3430 cm^{-1}. The dashed lines indicate approximate temperatures for the onset of the indicated structural phase transitions.

With further heating from 240 – 260°C, we observe a discontinuity in dν/dP with both $\nu_{as}(NH_2)$ modes hardening up to 300°C. In addition, we observe softening in the mode at ~3234 cm^{-1} from 240 – 260°C which continues to 300°C. The ν (C-NO_2) modes at 1142 and 1353 cm^{-1} remain at approximately the same frequency over this temperature range. Our observations indicate no evidence of the γ-phase, and we believe that at ~260°C, we enter a mixed phase of β + δ that continues up to decomposition at ~325°C. As previously discussed in the 0.4 GPa isobaric heating discussion, we believe that the

layering structure approaches a more planar form with the application of pressure. As shown in 0.4 GPa, the application of pressure hinders the reconstructive nature of the β → γ phase transition; which might suggests that γ-phase becomes energetically unfavorable and terminates between 0.5 – 0.9 GPa and 180 – 260°C in a β–γ–δ triple point.

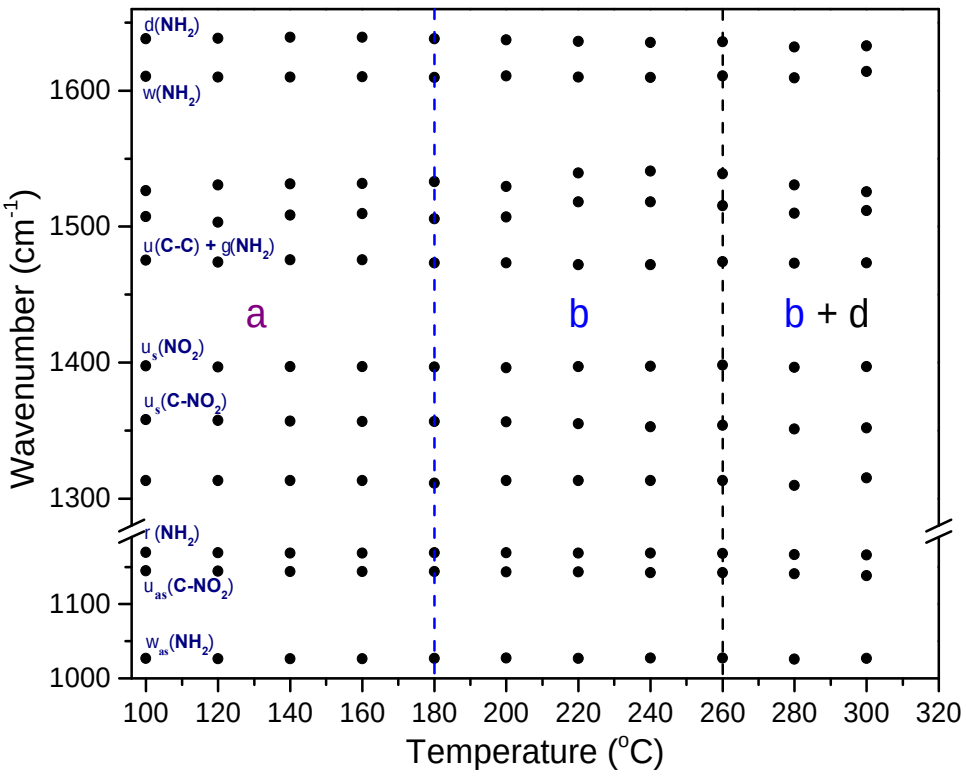

Figure 3.11. Pressure dependence of select modes during a 0.9 GPa isobaric heating experiment about the range of 1000-1670 cm^{-1}. The dashed lines indicate approximate temperatures for the onset of the indicated structural phase transitions.

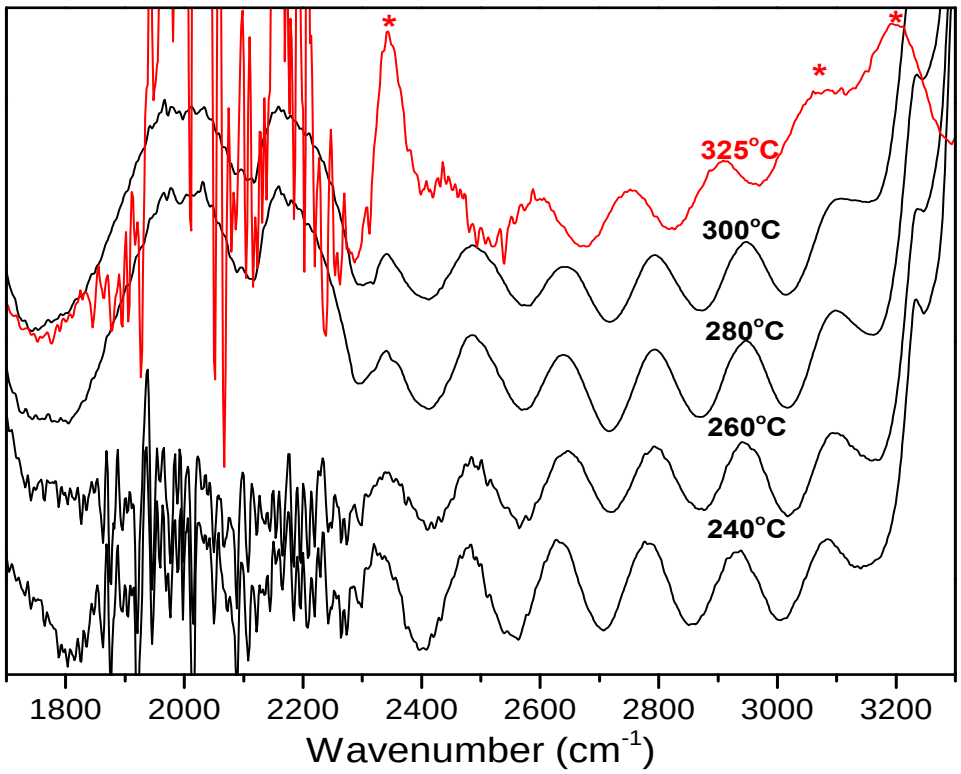

Figure 3.12. Spectrum stacks from a near 0.9 GPa isobaric heating experiment - at indicated temperatures - with characteristic decomposition products shown with red asterisks'. The red spectrum indicates decomposition.

3.2.4 Near 1.1 GPa isobaric heating experiment

During one of our very early experiments, we heated FOX-7 along the 1.07 GPa isobar. It is clear in the mid-IR spectra that the majority of observed frequencies disappear, or are drastically altered, and multiple new frequencies appear from 1900 – 2400 cm^{-1} as the sample undergoes decomposition above 360°C, Figure 3.13. The use of type-Ia diamonds (large nitrogen impurities) masked the majority of the spectrum preventing more detailed analysis: however, as can be seen below, the sample clearly undergoes drastic change above 360°C.

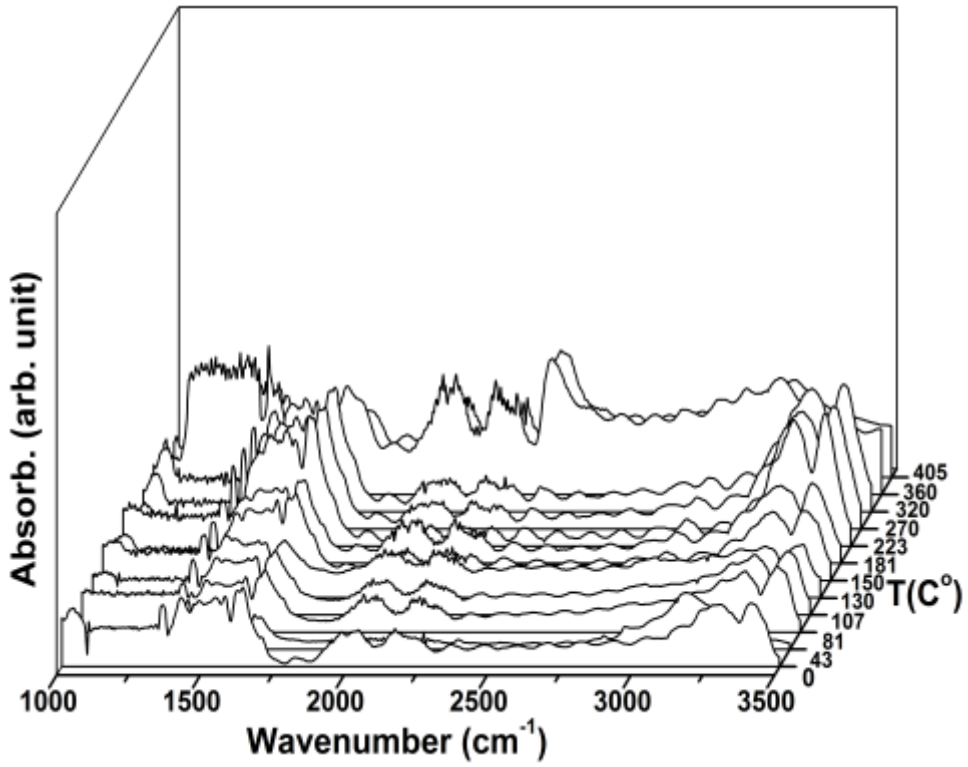

Figure 3.13. The mid-IR spectra, at a 1.07 isobaric heating experiment showing decomposition at 360°C.

After cooling and decompression to ambient conditions, we were unable to detect any evidence of a FOX-7 using either mid-IR micro-spectroscopy or by visual observation of the sample in the DAC sample chamber. Additional experiments are needed to further investigate the onset of FOX-7 decomposition and to determine if the decomposition products at elevated pressures are consistent with the predicted thermal decomposition products of CO_2, N_2O, NO, and HCN detected at ambient pressure and high temperature. [27]

3.2.5 Near 2.0 GPa isobaric heating experiment

The heating experiment commenced at ~2.3 GPa and 52°C. From comparisons to our previous isothermal compression experiments [24], we commenced in phase I of FOX-7. However, isobaric heating is notoriously difficult to control (particularly when commencing from higher pressures) due to thermal expansion of the diamond anvil cell: pressure tends to float as the temperature is increased. We had similar difficulties during this experiment, and in order to compensate for shifts in pressure due to thermal expansion, we lowered the cell pressure slightly to try can keep a near isobaric pathway. In doing so, we passed over the ~2 GPa isobaric phase boundary for phase I back in to alpha phase a few times. While the majority of the spectrum resembles that of phase I, spectra that are below ~2 GPa have some characteristics of α-phase, primarily in the ν_s (C-NO_2) at ~1360 and ν_s (NO_2) at 1400 cm^{-1} , but the amine stretching modes (~3250 – 3450 cm^{-1}) have characteristics of phase I throughout the entirely of the experiment (Figure 3.14).

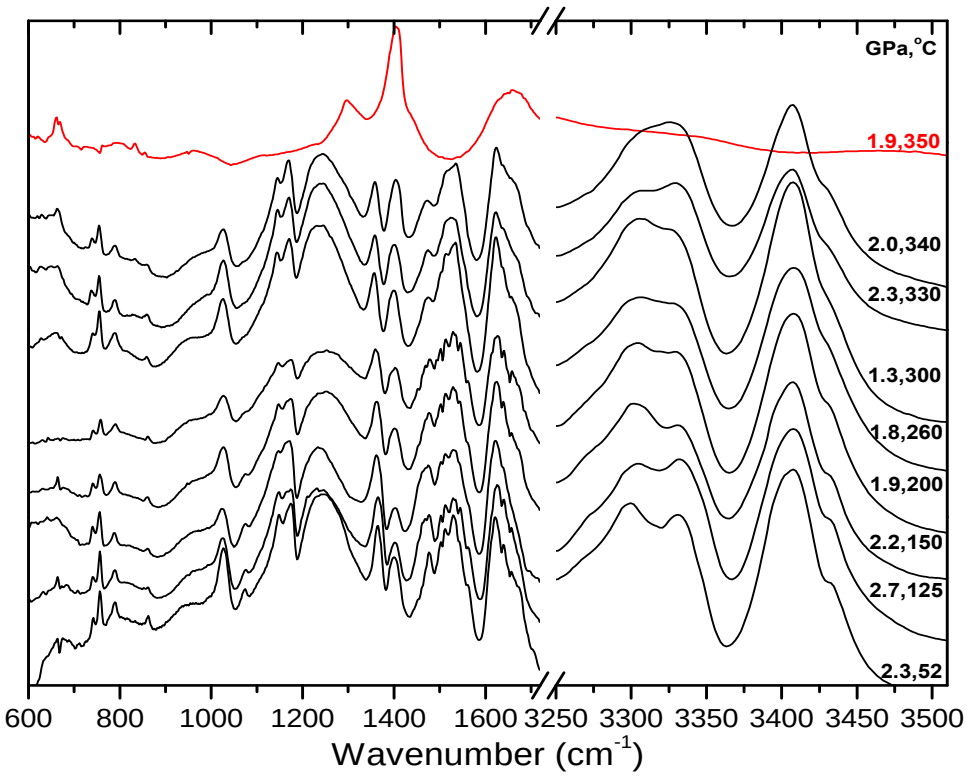

Figure 3.14. MIR spectra taken at increment temperatures along near 2.0 GPa isobar. The pressure and temperature of each spectrum is indicated on the right side of the figure with sample decomposition indicated in red.

We suspect that we retained a mixture of α + phase I through the majority of the experiment. Due to the large variability in pressure and temperature, the data could not be analyzed in the same manner as the previously discussed isobaric heating experiments. However, we did observe the presence of characteristic partial decomposition products of the delta phase form at ~2.3 GPa and 330°C (Figure 3.15); which might suggest an onset of the δ-phase, but do to kinetic reasons, the phase did not fully develop. In addition, we observe sample decomposition at ~1.9 GPa and 350°C. The decomposition phase boundary appears to be trending over as it approaches the isobaric phase boundary for phase I; which

might suggest that transitioning into phase I may play a significant role in the decomposition phase boundary of FOX-7.

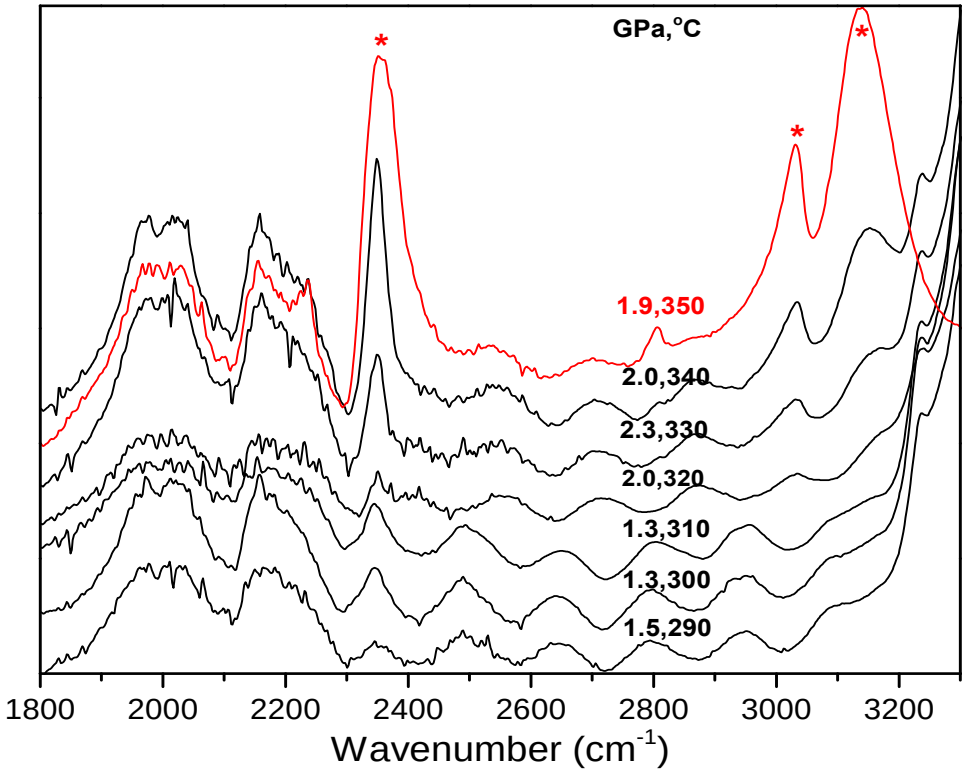

Figure 3.15. Spectrum stacks from a near 2.0 GPa isobaric heating experiment - at indicated pressures and temperatures - with characteristic decomposition products shown with red asterisks'. The red spectrum indicates decomposition.

3.2.6 Near 3.0 GPa isobaric heating experiments

While multiple experiments were performed on this region of phase space, the quality of the spectra for many of the experiments was too poor to discern anything more than a possible decomposition. However, for two experiments, the spectra quality was usable. For the first experiment, larger ~100°C per spectra steps were taken up to 200°C. After 200°C the temperature steps were ~50°C increments up to decomposition (Figure 3.16).

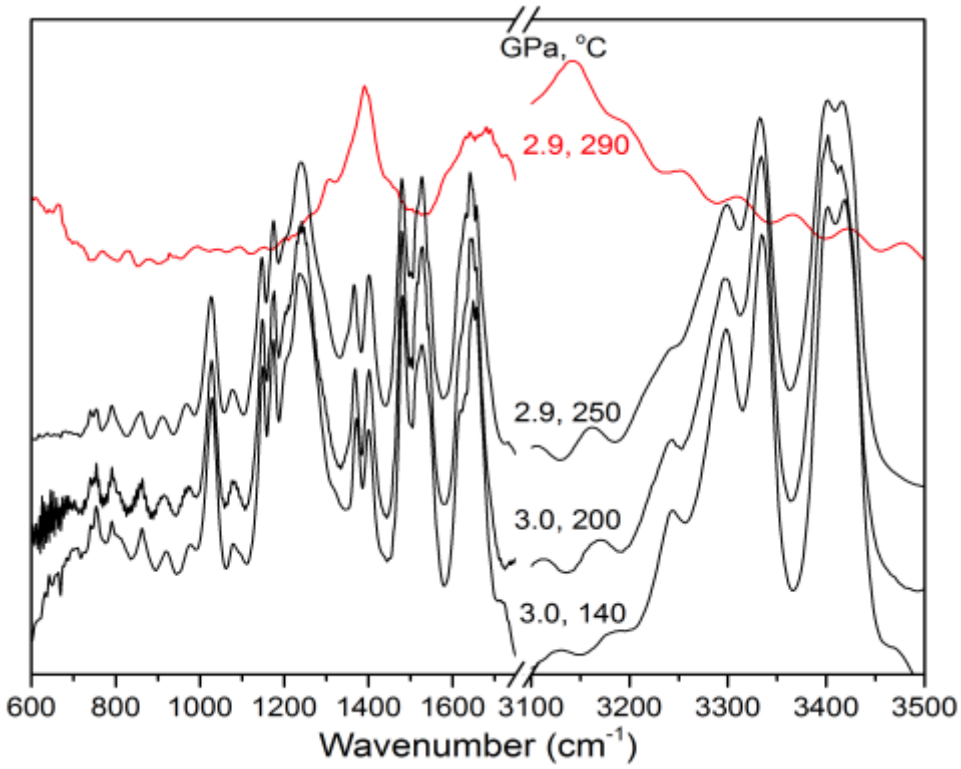

Figure 3.16. Near 3.0 GPa isobaric heating experiment up to decomposition.

While the other experiment had a temperature increase at an incremental rate of ~20°C per spectra up to decomposition; however, for clarity of the figure, only select spectra are shown (figure 3.17). The odd phase behavior and sharp decrease in the decomposition boundary points to evidence of a phase-I structural modification to a potentially higher symmetry than the α-phase ($P2_1/n$) due to the anomalous negative change in slope at a (α + phase I + decomposition) triple or a potential 'island phase'.

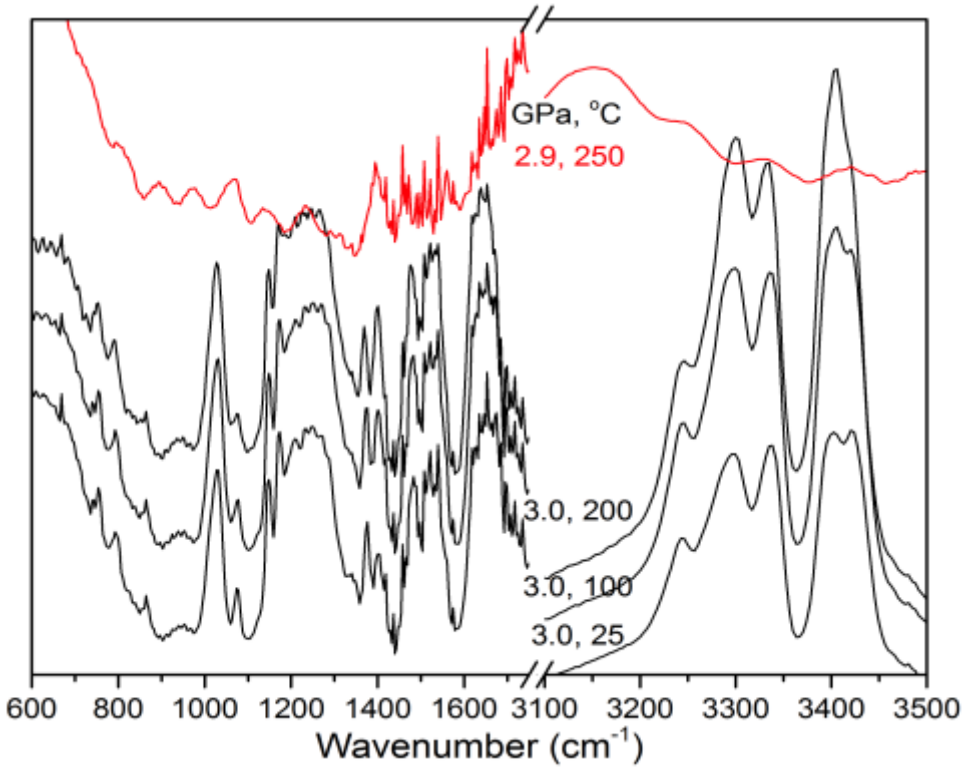

Figure 3.17. Near 3.0 GPa isobaric heating experiment up to decomposition.

3.2.7 Near 6.0 GPa isobaric heating experiment

FOX-7 was heated at a near 6.0 GPa isobar. The ε-phase indicated a rather stable mode behavior up to decomposition at 5.9 GPa and 310°C.

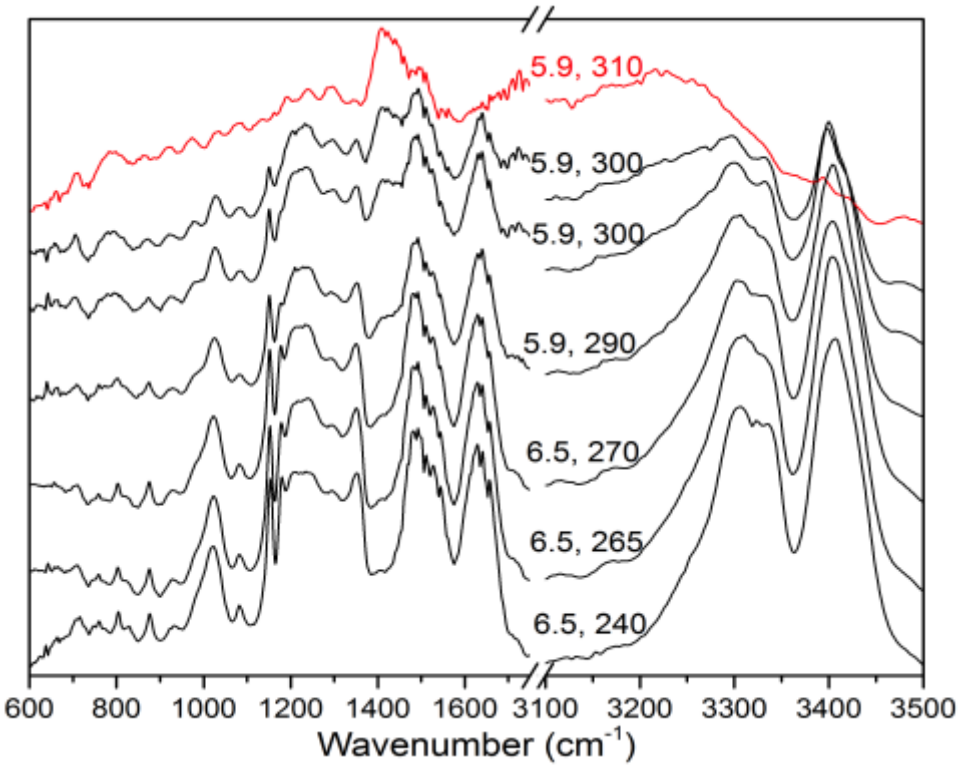

Figure 3.18. MIR spectra of FOX-7 taken at incremental temperatures near 6.0 GPa isobar. The pressure and temperature of each spectrum are indicated on the right side of the figure with the sample decomposition indicated in red.

3.2.8 Near 8.0 GPa isobaric heating experiment

For the 8.0 GPa isobaric heating experiment, we observed an overall decrease in the strength of the hydrogen bonding network from 100 – 375°C. Most notably, the amine stretching modes nearly all softened by ~10 cm^{-1}; while we observed hardening in ω (NH_2) at 1596 cm^{-1} by 11.7 cm^{-1}, ρ (NH_2) at 1183 cm^{-1} by 7.9 cm^{-1}, ω_s (NH_2) at 1082 cm^{-1} by 4.2 cm^{-1}, and ω_{as} (NH_2) at 1005 cm^{-1} by 14.8 cm^{-1}. In addition, we observed strong softening

in the ν_s (C-NO_2) mode at 1367 cm^{-1} by 19.4 cm^{-1} and ν_{as} (C-NO_2) at 1156 cm^{-1} by 6.3 cm^{-1}.

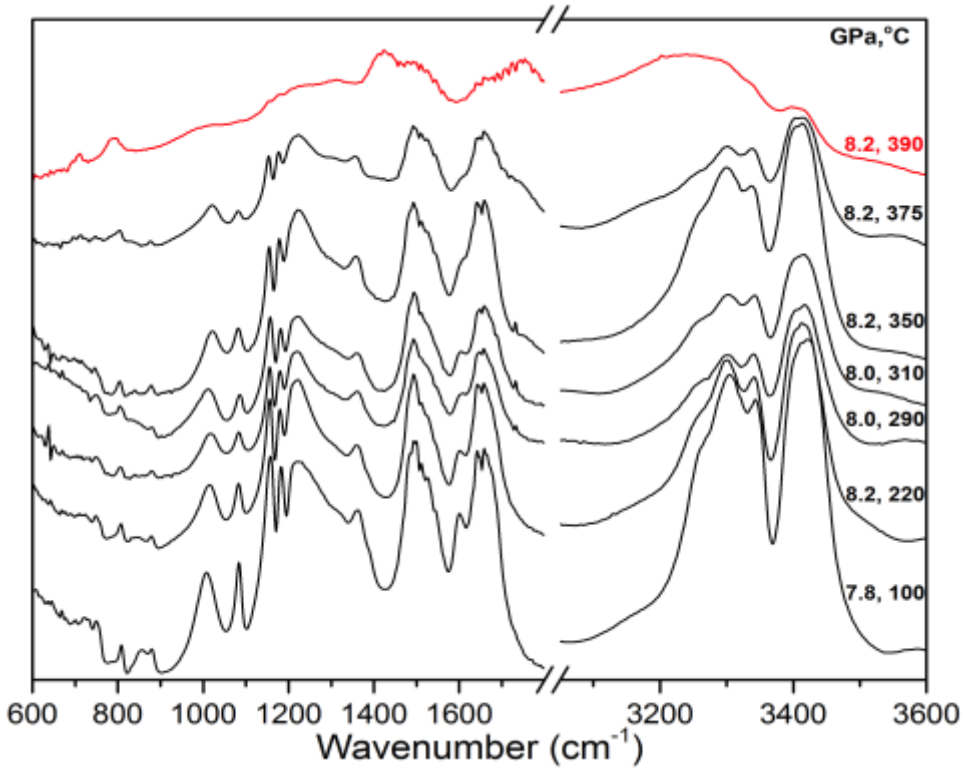

Figure 3.19. MIR spectra of FOX-7 taken at incremental temperatures near 8.0 GPa isobar. The pressure and temperature of each spectrum are indicated on the right side of the figure with the sample decomposition indicated in red.

Interestingly, while the hydrogen bonding network appears to have weakened as a whole with respect to an unheated FOX-7 at 8.0 GPa, the majority of the modes appear to have almost the same frequencies as the ambient-PT α-phase of FOX-7. This might indicate the ε-phase has a similar strength in the hydrogen bonding network to α-phase just prior to decomposition. Upon further heating, we observed full sample decomposition at 390°C with the formation of prominent CO_2 and H_2O signatures among other

decomposition products. It has been reported that the C-NO_2 bonds are more unstable than any other bonds under compression [54], and in fact, one C-NO_2 bond elongates and while the other shortens in the ε-phase[42]. The mode behavior and decomposition products seem to support a common theory behind the decomposition of FOX-7, which is C-NO_2 bond homolysis [37, 54, 55].

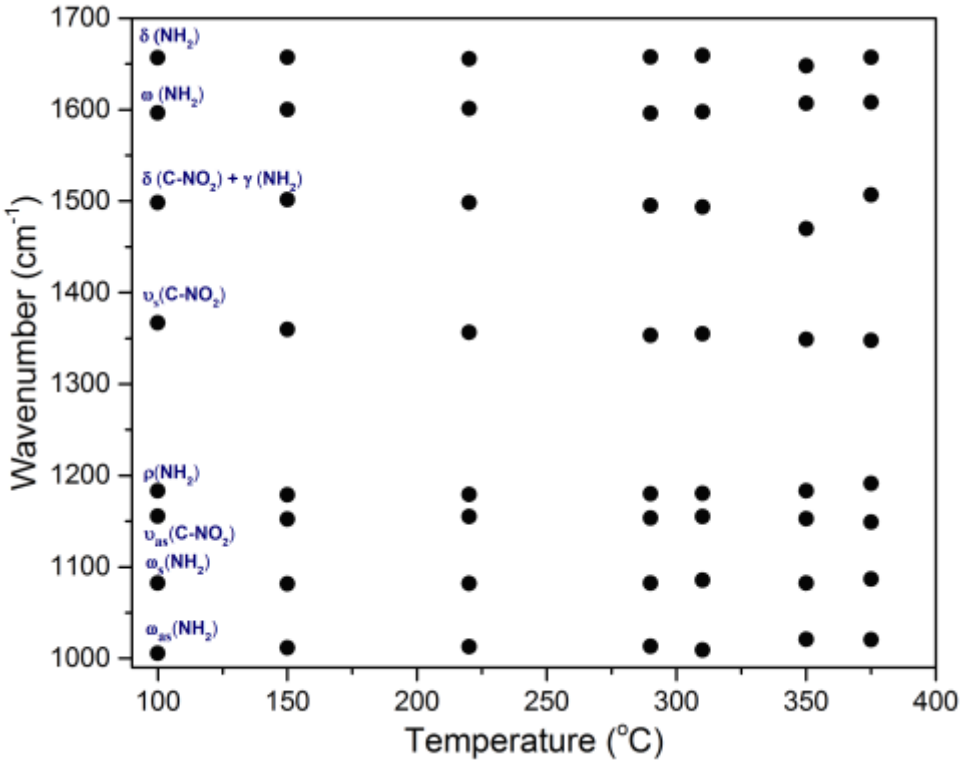

Figure 3.20. Pressure-temperature dependence of select modes of FOX-7 during a near 8.0 GPa isobaric heating experiment in the range of 1000 – 1700 cm^{-1}.

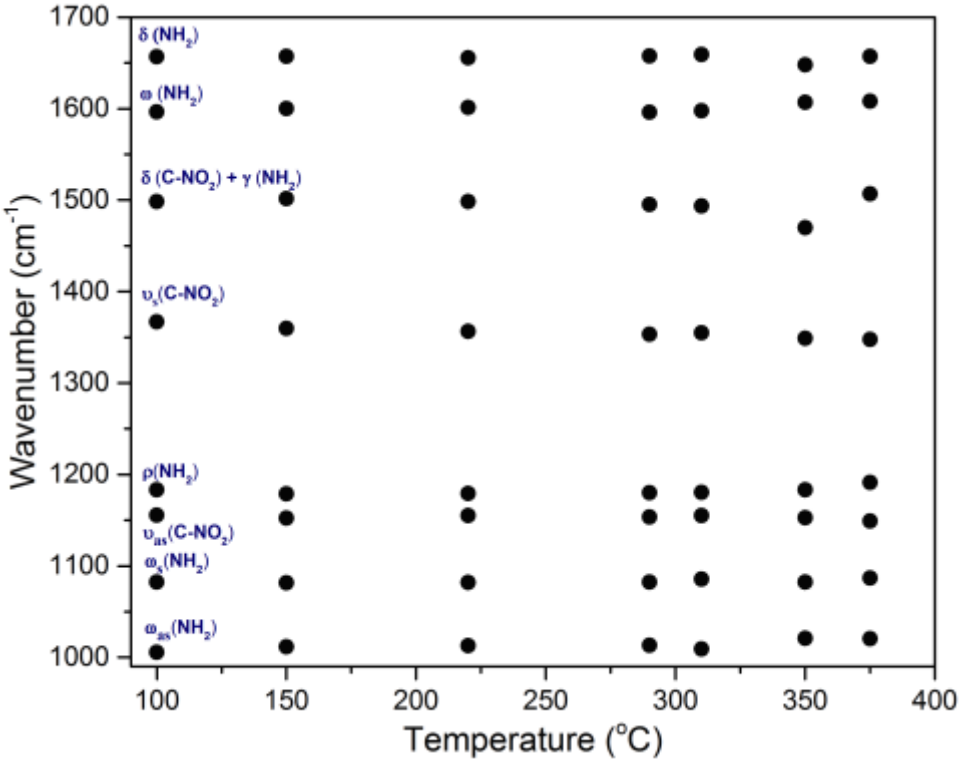

Figure 3.21. Pressure-temperature dependence of select modes of FOX-7 during a near 8.0 GPa isobaric heating experiment in the range of 1000 – 1700 cm^{-1}.

3.3 Infrared Synchrotron Radiation Isothermal Compression Experiments on FOX-7

3.3.1 Ambient temperature isothermal compression experiment

Pravica *et al.*[34] high pressure IR experiments on FOX-7 indicated possible phase transitions near 2, 5, and 10 GPa. In addition, they reported that FOX-7 survived pressure cycling up to 28 GPa without pressure induced decomposition or irreversible phase transitions.

3.3.2 A 100°C isothermal compression experiment

We observed two regions in the 100°C mid-IR isothermal compression where new vibrations developed Figures 3.22 and 3.33. The change of the molecular orientation (and therefore, interaction between molecules) is likely to be reflected in the vibrational spectra, which may manifest in unusual frequency shifts, loss of intensity, or broadening (narrowing) of lines in the spectra. [25] The presence of new vibrations and/or discontinuities in dν/dP slopes are strong indicators of a shift in the structural phase composition to a new form of FOX-7 (Table I).

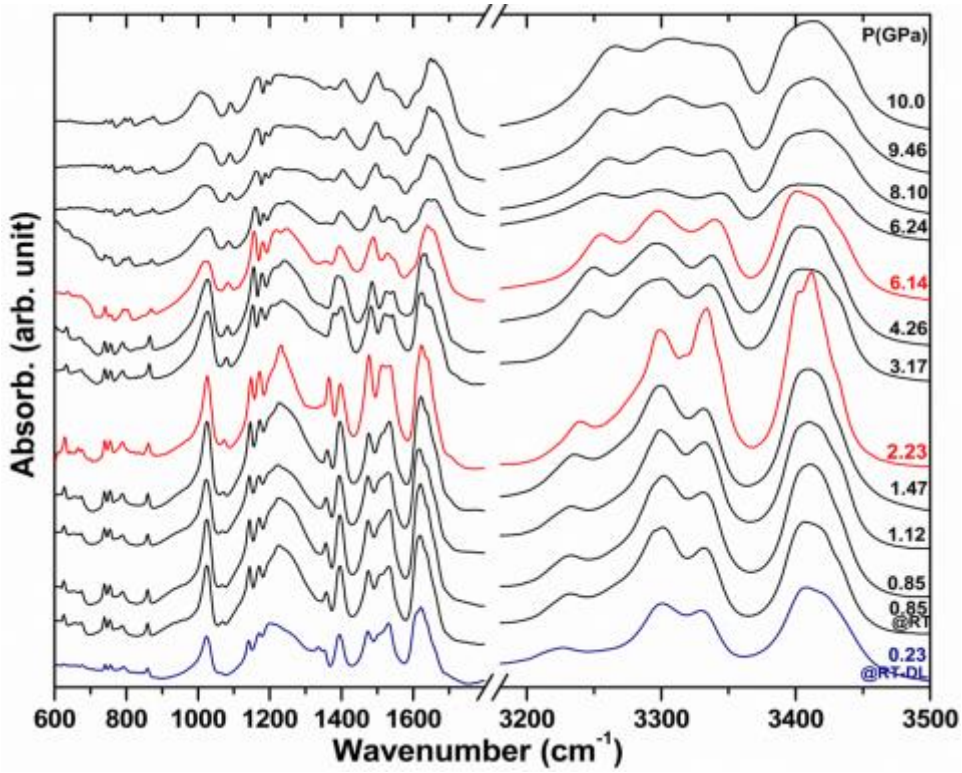

Figure 3.22. Mid-IR spectra, taken at incremented pressures along the 100°C isotherm, reveal new band formations at 1356 and 1597 cm^{-1}. The vibrational data points to the possibility of two solid-solid phase transitions at 2.23 and 6.14 GPa.

With application of pressure up to 2.23 GPa, we observed large shifts in the dν/dP slopes for symmetric NH_2-wagging [$\omega_s(NH_2)$] commencing at 1068 cm^{-1} (4.47 cm^{-1}/GPa), symmetric C-NO_2 stretching [ν_s(C-NO_2)] at 1356 cm^{-1} (7.50 cm^{-1}/GPa), $\omega(NH_2)$ at 1616 cm^{-1} (4.18 cm^{-1}/GPa), and antisymmetric NH_2 stretching [$\nu_{as}(NH_2)$] at 3408 cm^{-1} (-3.27 cm^{-1}/GPa) from 0.85 – 2.23 GPa. With further application of pressure beyond 2.23 GPa, we observed a small but noticeable discontinuity in the dν/dP slope (Figure 3.23) suggesting a potential $\alpha \rightarrow \alpha'$ phase transition. The shift in vibrational spectra with pressure increase may have resemblance to the changes observed in the temperature induced $\alpha \rightarrow \beta$ phase transition. This observed shift, based on ambient pressure and elevated temperature Raman vibrational measurements [26], is marked by large shifts in the amine vibrational modes in the region (~3250 cm^{-1} – 3450 cm^{-1}) which are coupled with an observed $\alpha \rightarrow \beta$ phase transition. Welch et al. [7] suggests that the $\alpha \rightarrow \beta$ phase transition is largely displacive in nature with the molecular layers "top" shifting to the right, "bottom" shifting to the left, and "middle" rotates as a result of intermolecular hydrogen bonding and a "shearing" action. The action corresponds to an interchange between the NO_2 and NH_2 groups, which appear to result in a "reversed-orientation" molecule where one of the molecules is rotated about an axis perpendicular to the C-C axis. [56] As discussed earlier, shear effects can drastically reduce the barrier of C-NO_2 dissociation, suggesting that an $\alpha \rightarrow \beta$-like phase transition should be accompanied with strong shifts in the vibrational behavior of C-NO_2 modes and the interplay with constituent NH_2 modes. We observe this dynamic behavior with the large shifts in dν/dP slopes in both ν_s(C-NO_2) and amine vibrational modes, as well as a noticeable discontinuity in the dν/dP slopes as further indication of an $\alpha \rightarrow \beta$-like structural phase transition. An elevated temperature, ambient pressure single crystal

structural investigation has been performed by Evers et al. [30] who showed the α-phase of FOX-7 to be ($P2_1/n$) monoclinic [a = 6.9340(7), b = 6.6228(8), c = 11.3119(13) Å, and β = 90.065(13)° at 25°C], and the β-phase to be ($P2_12_12_1$) orthorhombic [a = 6.9738(7), b = 6.6350(10), c = 11.6475(16) Å, and β = 90° at 120°C]. While we observe strong evidence of an α → β-like structural phase transition, additional elevated pressure structural measurements are required to draw further correlations between our observed lower pressure (2.23 GPa) α'-phase to the characterized elevated temperature β-phase.

Application of pressure from 2.23 – 6.14 GPa induced shifts in $\omega_s(NH_2)$ commencing at 1068 cm^{-1} (2.25 cm^{-1}/GPa), $\nu_{as}(C\text{-}NO_2)$ at 1140 cm^{-1} (2.25 cm^{-1}/GPa), $\nu_s(C\text{-}NO_2)$ at 1356 cm^{-1} (7.10 cm^{-1}/GPa), C-C stretching + NH_2 scissoring [$\upsilon(C\text{-}C) + \gamma(NH_2)$] at 1471 cm^{-1} (3.72 cm^{-1}/GPa), $\omega(NH_2)$ at 1616 cm^{-1} (4.70 cm^{-1}/GPa), and NH_2 bending [$\delta(NH_2)$] at 1635 cm^{-1} (4.56 cm^{-1}/GPa). At 6.14 GPa we see the development of two new vibrational modes at 1355.7 cm-1 and 1594.8 cm^{-1}; paired a large discontinuity in the $d\nu/dP$ slopes for the above vibrational modes for this pressure region, which is indicative of an additional high pressure structural phase transition to α". While further crystallographic information is required to compare the high pressure α" phase with the high temperature γ phase, we can draw some corollaries. We observe softening in the higher frequency amine modes, which might be attributed to a weakening in the hydrogen-bonding network, Table 1. We suspect that this has to do with a partial or total flattening of the "zigzag" structure in α–FOX-7 into γ-FOX-7. [34] Crawford et al. [31] studied γ-FOX-7 that was quenched to 200 K using XRD and concluded that the wave angle diminished to nearly 180 °C in the γ phase. [31, 57] As the effect of pressure is similar to cooling by increasing molecular densities,

we suspect that we have driven the sample into a phase that is similar in some respect to the low temperature quenched form of the γ phase. [34] Pravica et al. [34] suggest that as the interplanar distances between decrease with this proposed flattening, the weakening in hydrogen bonding would strengthen the C-N bonds from the nitro groups. We observe this strengthening in ν(C-NO_2) given further indication that there was a weakening in the hydrogen bond network when transitioning into the α" phase. With further compression beyond 6.14 GPa, we observe strong hardening in the majority of the above vibrational modes with no additional discontinuities or vibrational mode developing: suggesting a strong α" phase stability up to 10.1 GPa with no observed pressure induced decomposition.

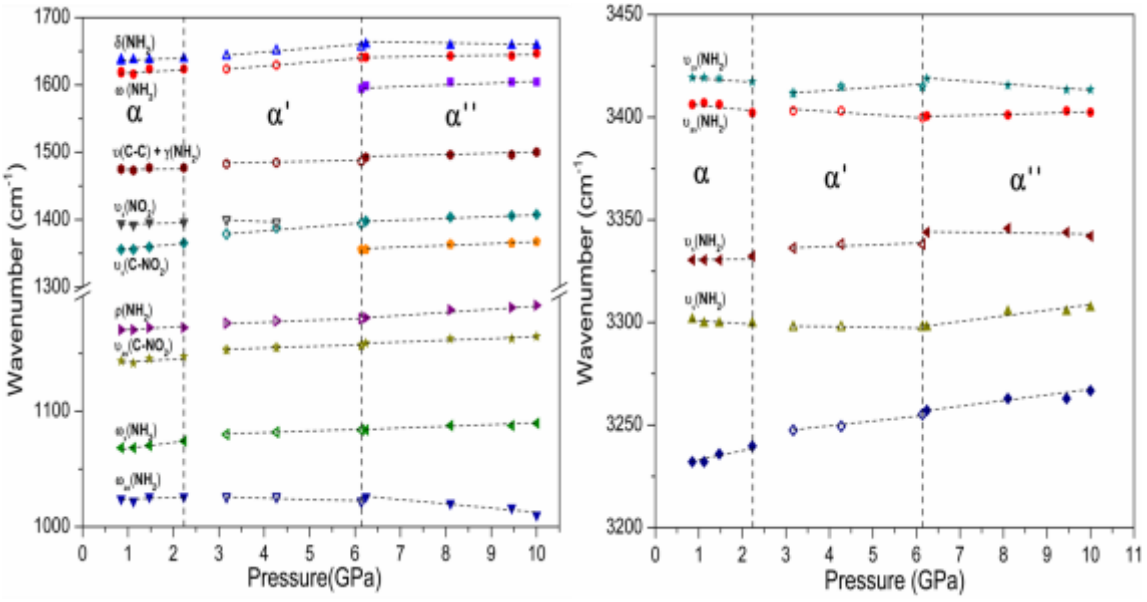

Figure 3.23. Pressure dependence of selected modes at 100°C are shown with phase transitions marked at 2.2 GPa and 6.1 GPa.

Based on the changes described above, two pressure-induced phase transitions are proposed at 2.1 GPa (α' phase) and 6.1 GPa (α" phase) along a 100°C isotherm. Pravica et

al. [34] has reported similar phase transitions at 2.0 and 5.0 GPa in both the mid- and far-IR regimes. The phase transition to α" phase could possibly have a lower onset pressure as a large pressure step was taken during our measurements (4.3 to 6.1 GPa). Upon decompression to 0.23 GPa at room temperature, remnants of the high pressure α" phase were observed, in particular the vibrational mode at ~1335 cm^{-1}, but the majority of the spectrum is primarily associated with the commenced α phase.

3.3.3 A 200°C isothermal compression experiment

A second isothermal compression was carried out on the same sample at 200°C with mid-IR spectra collected at increments of pressure up to 10.4 GPa, figure 3.23. Our investigation revealed two distinct regions where new vibrational modes appear and large discontinuities in *dv/dP* were present. With application of pressure up to 2.02 GPa, we observed shifts in $\omega_{as}(NH_2)$ commencing at 1022 cm^{-1} (1.37 cm^{-1}/GPa), $\omega_s(NH_2)$ at 1068 cm^{-1} (-3.02 cm^{-1}/GPa), $\nu_s(C\text{-}NO_2)$ at 1356 cm^{-1} (-1.67 cm^{-1}/GPa), and $\nu_{as}(NH_2)$ at 3408 cm^{-1} (1.17 cm^{-1}/GPa), Figure 3.24.

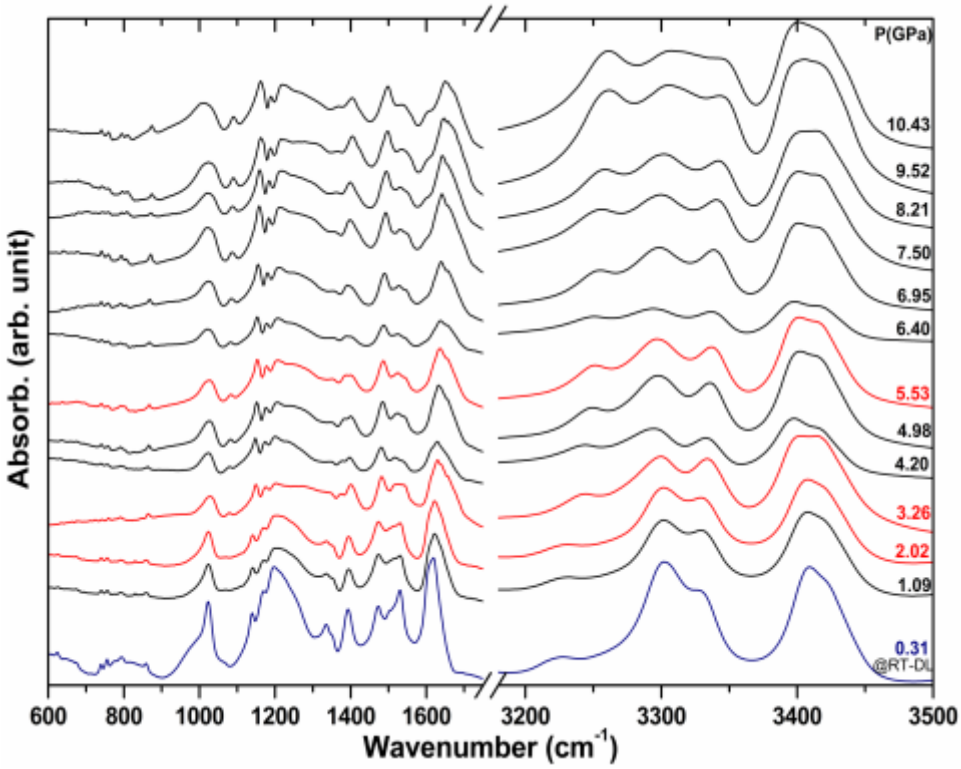

Figure 3.24. Mid-IR spectra, taken at incremented pressures along the 200°C isotherm. The vibrational data points to the possibility of two solid-solid phase transitions at 2.02 to 3.26 GPa and 5.53 GPa.

Further compression to 3.26 revealed a discontinuity in dv/dP paired with the loss of ν_s(C-NO_2) and the development of a new vibrational mode at 1373 cm^{-1}. These observations imply that the $\alpha \rightarrow \alpha'$ phase transition potentially could have commenced as early as 2.02 GPa and fully developed by 3.26 GPa. The history of the sample has potentially weakened the hydrogen bonding network; which promoted a greater decoupling of the between the nitro and amine interactions. The decoupling is seen with the weakening and eventual loss of ν_s(C-NO_2) at 1356 cm^{-1}.

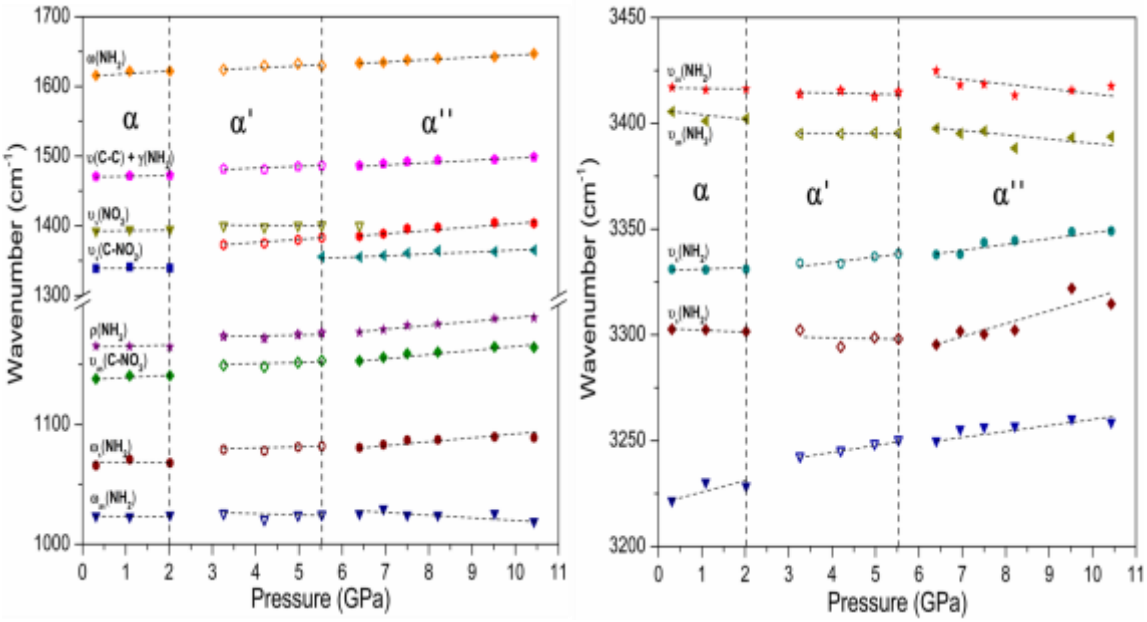

Figure 3.25. Pressure dependence of selected modes at 200°C are shown with phase transitions marked at 2.2 GPa and 5.53 GPa.

While there are differences in the transition characteristics between the 100°C α → α' phase transition and the 200°C, we suspect that we are observing the same α' phase, but perhaps the mechanism (molecular reorientation described by Welch et al. [7]) is more sluggish due to a weakened nitro and amine interaction from the pressure cycling of the sample. Moving from 3.26 – 5.53 GPa, shifts are observed in $\omega_s(NH_2)$ at 1065 cm^{-1} (3.58 cm^{-1}/GPa), $\nu_{as}(C\text{-}NO_2)$ at 1140 cm^{-1} (3.20 cm^{-1}/GPa), $\rho(NH_2)$ at 1165 cm^{-1} (2.95 cm^{-1}/GPa), new mode at 1373 cm^{-1} (4.64 cm^{-1}/GPa), $\upsilon(C\text{-}C) + \gamma(NH_2)$ at 1471 cm^{-1} (3.70 cm^{-1}/GPa), and $\omega(NH_2)$ at 1616 cm^{-1} (2.93 cm^{-1}/GPa). At 5.53 GPa we observe the development of a new vibrational mode at 1355 cm^{-1} and a large discontinuity with respect to observed vibrational behavior at 6.40 GPa; which is indicative of a potential α' → α" transition. The new vibrational mode at 1355 cm^{-1} appears to be characteristic of the α"

phase due to its development in both the 100°C and 200°C α' → α" transition. We suspect that we are seeing the same weakening of the hydrogen bonding network as described in the 100°C isotherm discussion. Due to the history of the sample however, we suspect we are seeing weakening of the hydrogen bonding network to a greater extent due to less dynamic: strengthening of C-NO_2 modes and amine modes. With further compression beyond 6.40 GPa, we observe strong hardening in the majority of the above vibrational modes with no additional discontinuities or vibrational mode developing: suggesting a strong α" phase stability up to 10.43 GPa with no observed pressure induced decomposition. Whereas upon full decompression to 0.31 GPa, only slight remnants of the high pressure α" phase remained with the majority of the downloaded spectrum containing the commenced α phase signature vibrational modes.

3.3.4 A 200°C isothermal far-IR compression experiment

In order to confirm the phase transition pressures, far-IR spectra were collected during isothermal compression at 200°C on a new sample, Figure 3.25. Initial compression from 0.39 – 2.09 GPa revealed strong shifts in *dv/dP* with C-NO_2 deformation [δ(C-NO_2)] commencing at 322 cm^{-1} (4.96 cm-1/GPa), $\omega_{as}(NH_2)$ at 461 cm^{-1} (4.74 cm^{-1}/GPa), $\omega_s(NH_2)$ at 486 cm^{-1} (9.50 cm^{-1}/GPa), δ(C-NH_2) at 523 cm^{-1} (4.33 cm^{-1}/GPa), and skeletal deformation at 577 cm^{-1} (4.29 cm^{-1}/GPa). At 2.09 GPa, we see the development of a new vibrational mode at 488 cm^{-1}, paired with a discontinuity in *dv/dP* with respect to the 2.72 GPa vibrational behavior. We show good agreement with our mid-IR transition pressures for the α → α' phase boundary, nearly isobaric in nature at ~2.0 GPa. Further application of pressure from 2.72 – 5.30 GPa showed large shifts in δ(C-NO_2) at 322 cm^{-1} (4.73 cm-

1/GPa), δ(C-NH) at 399 cm^{-1} (4.23 cm^{-1}/GPa), $\omega_{as}(NH_2)$ at 461 cm^{-1} (4.02 cm^{-1}/GPa), new mode at 488 cm^{-1} (4.23 cm^{-1}/GPa), $\omega_s(NH_2)$ at 486 cm^{-1} (8.84 cm^{-1}/GPa), $\delta(C\text{-}NH_2)$ at 523 cm^{-1} (5.25 cm^{-1}/GPa), and skeletal deformation at 577 cm^{-1} (4.99 cm^{-1}/GPa). Where at 5.53 GPa, we observed the development of a new vibrational mode at 393 cm^{-1}, which combined with the discontinuity in *dv/dP* with respect to the 6.24 GPa vibrational behavior, shows an α' → α" phase boundary at 5.53 GPa. Additional compression up to 10.12 GPa was performed with the majority of the above vibrational modes exhibiting hardening behavior, with no observed decomposition.

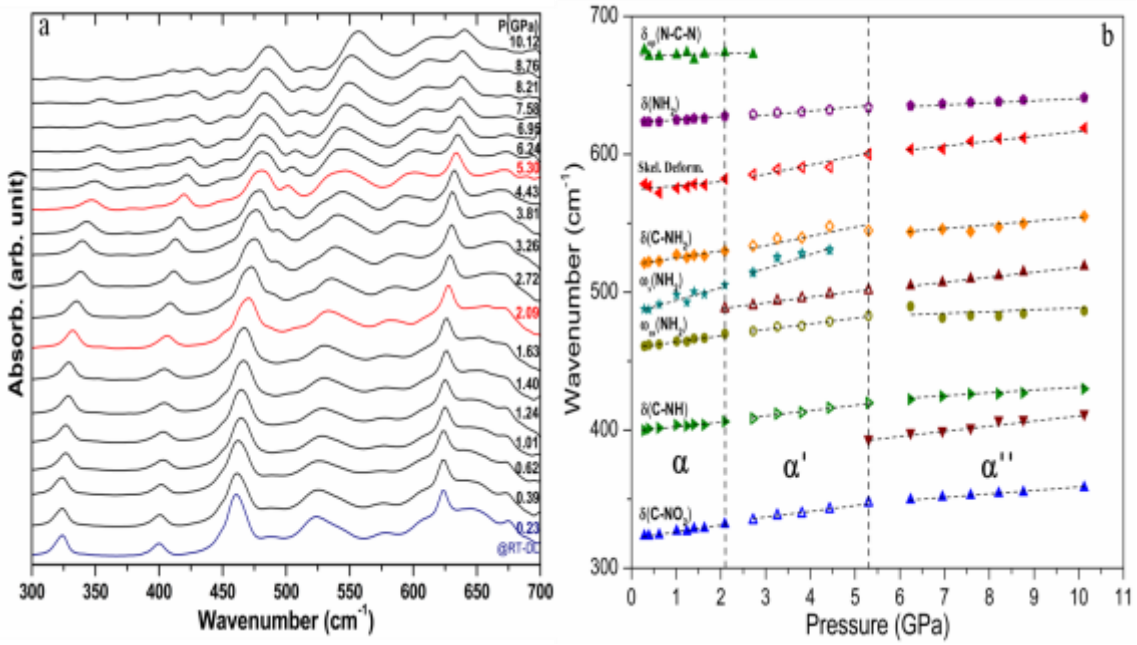

Figure 3.26. A compilation of far-IR spectra at 200°C (a); as well as, the pressure dependence of selected vibrational modes (b).

Table 1. Mode assignments for the spectrum; as well as, the slopes of the frequency shift as a function of pressure for each phase at the highlighted PT regions.

Wavenumber (cm^{-1})	dv/dP (cm^{-1}/GPa)						Assignment[b]
			α'		α''		
	100°C	200°C	100 °C	200 °C	100 °C	200 °C	
	0–2.2 GPa	0 – 2 GPa	2.2 – 6.1 GPa	2 – 5.5 GPa	6.1 – 10 GPa	5.5 – 10.4 GPa	
322[a]		4.96		4.73		2.25	δ (C-NO_2)
						3.80 (393)[c]	
399[a]		2.8		4.23		1.80	δ (C-NH)
461[a]		4.74		4.02		-0.19	ω_{as} (NH_2)
486[a]		9.50		8.84			ω_s (NH_2)
				4.23 (488)[c]		3.77 (488)[c]	
523[a]		4.33		5.25		2.91	δ (C-NH_2)
577[a]		4.29		4.99		4.10	Skeletal def.
625[a]		2.44	2.35	1.93	0.51	1.48	δ (NH_2)
675[a]			0.50	0.04		1.19	δ_{oop} (N-C-N)
858			1.46	1.98	1.37	1.66	
1022	2.09	1.37	-0.10	-0.12	-3.85	-1.54	ω_{as} (NH_2)
1068	4.47	-3.02	2.25	3.58	1.37	2.00	ω_s (NH_2)
1140	3.55	0.05	2.25	3.20	1.37	2.83	ν_{as} (C-NO_2)
1165	1.55	−0.44	1.85	2.95	2.72	3.03	ρ (NH_2)
1356	7.50	−1.67	7.10		2.46		ν_s (C-NO_2)
					3.00 (1356)[c]	2.24 (1355)[c]	
1392	2.10	0.20	-0.10	1.48			ν_s (NO_2)
				4.64 (1373)[c]		4.81 (1373)[c]	
1471	2.09	0.58	3.72	3.70	1.72	2.75	ν (C-C) + γ (NH_2)
1504			3.14	3.86	6.62	2.25	γ (NH_2) + δ (C-NO_2)
1529			2.81	4.43			ν_{as} (NO_2)
					1.52 (1594)[c]		
1616	4.18	0	4.70	2.93	1.22	3.24	ω (NH_2)
1635	1.07		4.56		-0.51	0.52 (1654)[c]	δ (NH_2)
3221	6.02	-1.99	3.64	5.94	2.23	2.36	
3300	-1.02	-0.88	-0.39	1.30	2.38	2.48	$\nu_s(NH_2)$
3330	1.46	0.32	1.36	2.00	-0.44	1.12	$\nu_s(NH_2)$
3408	-3.27	1.17	-0.65	-1.70	0.60	-0.94	$\nu_{as}(NH_2)$
3419	-1.55	0.41	-0.17	-0.44	-1.52	-2.19	$\nu_{as}(NH_2)$

[a]The mode assignments come from the following: far-IR spectra (300-700 cm^{-1}) is at 0.2 GPa and mid-IR spectra from 800-3500 cm^{-1} is at 0.3 GPa. See figure 1 for more details.
[b]Abbreviations for assignments: ω = wagging, δ = deformation/bending, ρ = rocking, τ = torsion/twisting, γ = scissor, ν = stretching, ip = in-plane, oop = out-of-plane, as = asymmetric, s = symmetric
[c]Development of a new vibrational mode. See text for further details.

3.3.5 A 300°C isothermal compression experiment

In order to further investigate the slopes of the isobaric phase I and II boundaries; as well as, the curvature of the decomposition boundary, an additional isothermal compression experiment was conducted. The sample of FOX-7 was initially compressed to 1.1 GPa at 25°C and then heated to 300°C (Figure 3.26). Using the structural distortion

and phase transition criterion regarding phase I and II from our previous publication[4] we were able to discern the phase boundaries through the characteristic vibrational behavior of FOX-7 during a 300°C isothermal compression.

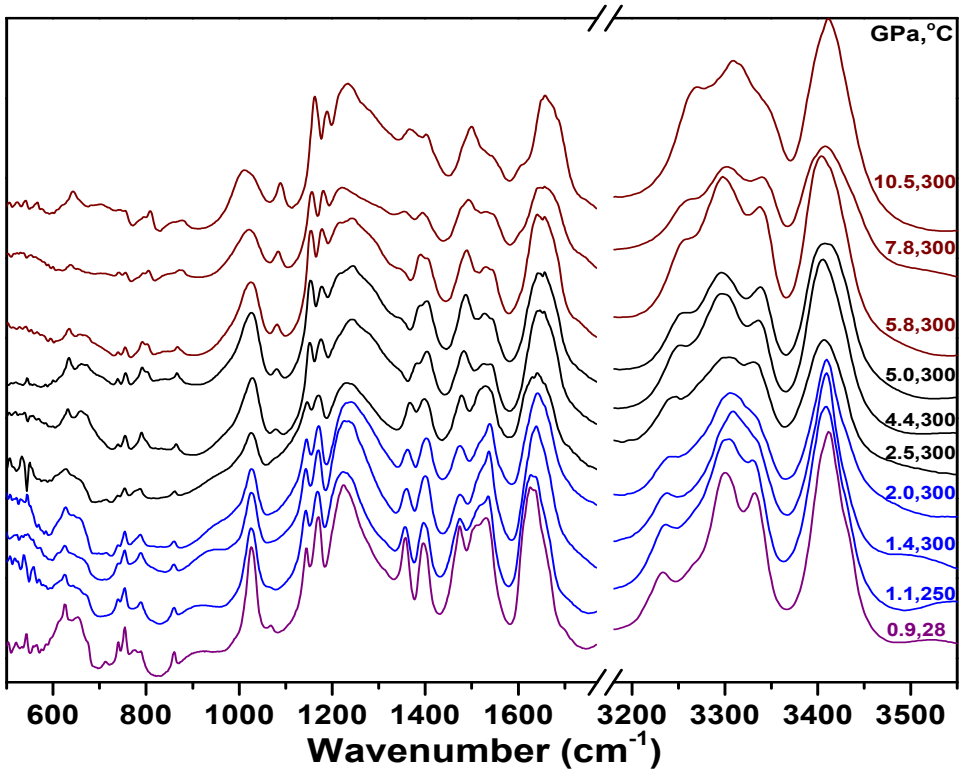

Figure 3.27. MIR spectra taken at increment temperatures along a 300°C isotherm. The pressure and temperature of each spectrum is indicated on the right side of the figure. Approximate structural phase transitions are indicted with a change in color of the spectra at the respective pressure and temperature: α-phase (purple), β-phase (blue), phase-I (black), and phase-II (wine).

Further compression from 1.1 – 2.5 GPa at 300°C, we observe the $\nu(NH_2)$ modes in the 3200 – 3400 cm^{-1} region nearly all uniformly harden, and the $\nu_s(C\text{-}NO_2)$ at 1358 cm^{-1} and $\omega_s(NH_2)$ at 1066 cm^{-1} harden by 9 and 14 cm^{-1}, respectively (Figure 3.28). We

observed a large discontinuity in dν/dP in the amine stretching modes with the application of pressure to 3.2 GPa. The majority of the amine stretching modes shift to higher frequency with the additional compression. We observe the ν_s (C-NO_2) at 1366 cm^{-1} harden by 11 cm^{-1}, and ω_s (NH_2) at 1080 cm^{-1} soften by 4 cm^{-1}. These observations are in agreement with our previous publication transition criterion for an α → phase I transition between 2.5 - 3.2 GPa, 300°C.

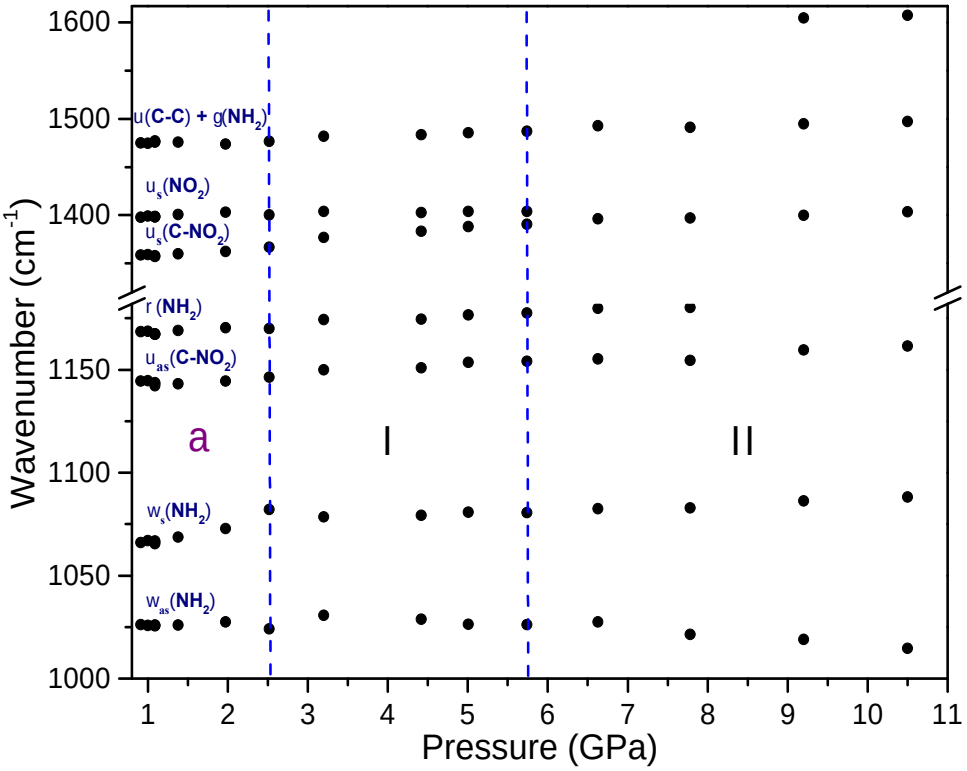

Figure 3.28. Pressure dependence of select modes during a 300°C isothermal compression experiment about the range of 1000-1610 cm^{-1}. The dashed lines indicate approximate pressures for the onset of the indicated structural phase transitions.

Additional compression from 3.2 - 5.7 GPa revealed the hydrogen bonding network within the amines remained approximately the same. However, we did observe the ν_s (C-NO_2) at 1377 cm^{-1} and ω_s (NH_2) at 1076 cm^{-1} harden by 14 and 2 cm^{-1}, respectively. The

strong hardening observed in the ν_s (C-NO_2) mode is the product of the intermolecular layering becoming more planar with the increase in pressure. The nitro groups, which are out-of-plane in the commencing structure, are forced in-plane with the carbon-carbon backbone with increasing pressure. That is why when the pressure was increased to 6.6 GPa, we observed a restructuring of the hydrogen bonding network. The amine stretching modes within 3200 – 3400 uniformly harden, and the ν_s (C-NO_2) at 1391 cm^{-1} and ω_s (NH_2) at 1078 cm^{-1} harden by 6 and 2 cm^{-1}, respectively. In addition, we observed the loss of a ν_{as} (C-NO_2) at 1140 cm^{-1}; which is likely the product of the nitro groups adopting a more stable planar state within the layering structure of FOX-7. These observations are in strong agreement with our criterion for phase II; therefore, we suspect the sample transitioned from phase I → II between 5.7 - 6.6 GPa at 300°C.

Further compression to 10.5 GPa we observed all modes shift to higher frequency expect ω_{as} (NH_2) at 1027 cm^{-1} which softened by 13 cm^{-1}. No additional structural distortions or phase transitions were observed. However, it is important to note that we suspect a change in slope in the decomposition phase boundary near 2 GPa and 300°C because CO_2, a characteristic decomposition product, began to form when transitioning from α → phase-I, but perhaps it did not fully decompose for kinetic reasons (Figure 3.29). In addition, we observe not only CO_2 but additional characteristic decomposition products form just prior to the phase I → II boundary near 4.4 GPa.

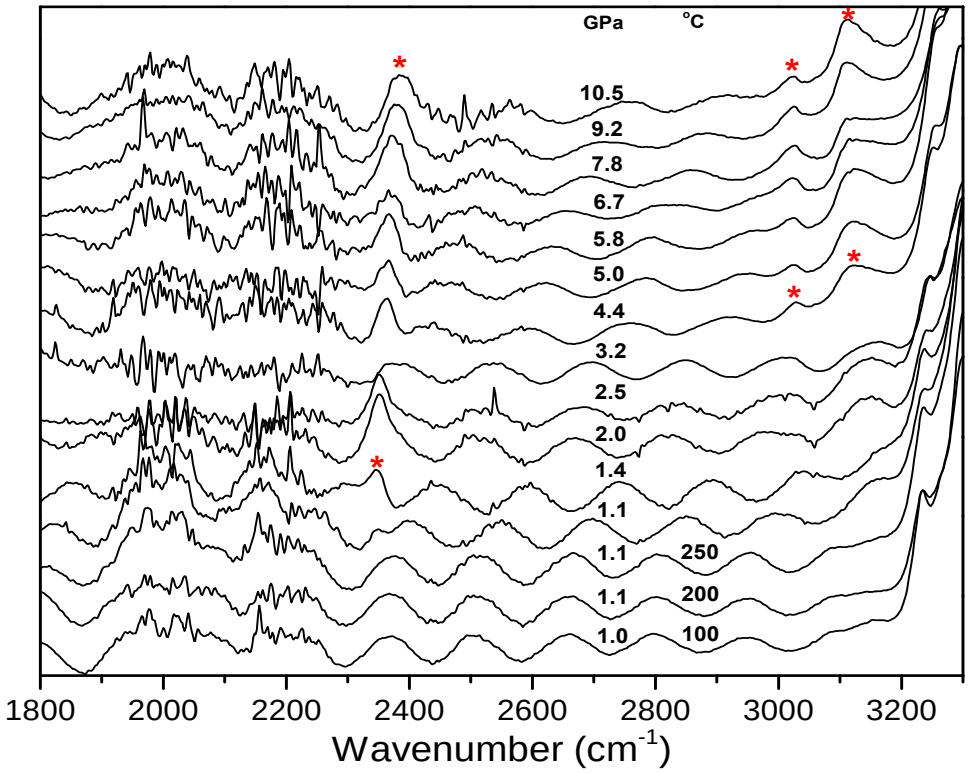

Figure 3.29. Spectrum stacks from a near 300°C isothermal compression experiment - at indicated pressures and temperatures - with characteristic decomposition products shown with red asterisks'. Temperature is 300°C unless otherwise indicated. Note that we observe only partial decomposition of the sample as indicated by the development of characteristic decomposition products.

While kinetics plays a large role in the decomposition of HE, we suspect that the FOX-7 decomposition phase boundary to: 1) have a change in slope near the α → phase-I boundary and 2) remain relatively close to 300°C over the investigated PT-space.

3.4 Infrared Synchrotron Radiation Isobaric Heating Experiments on TATB

3.4.1 Near 4.0 GPa isobaric heating experiment

TATB was initially compressed to 4.6 GPa and heated to decomposition near 4.4 GPa and 360°C.

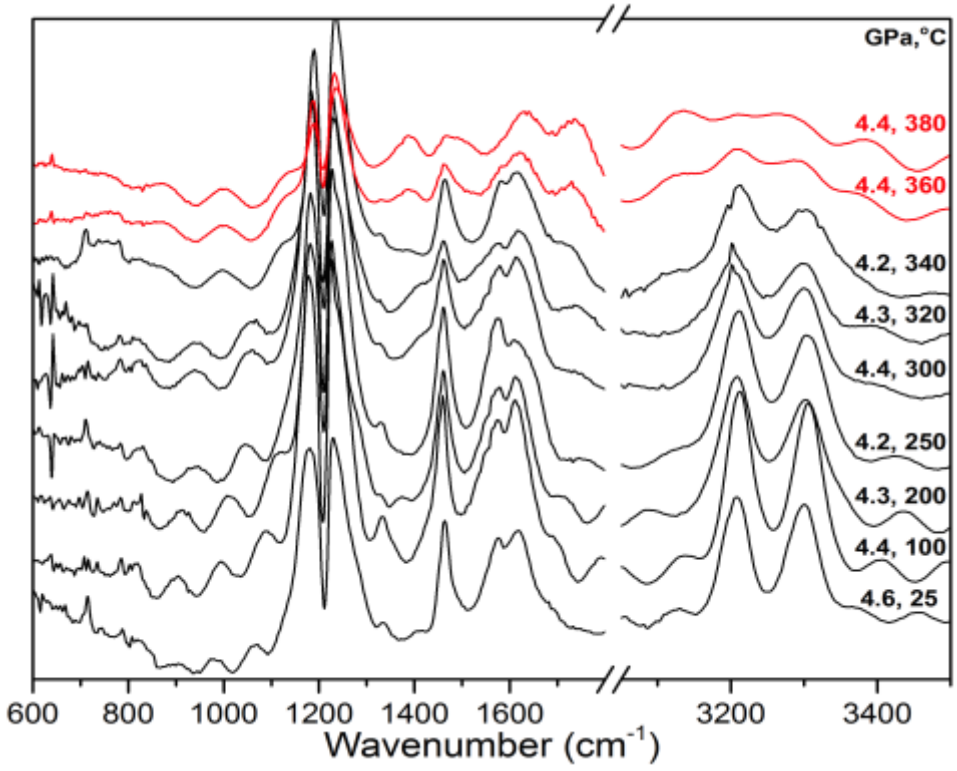

Figure 3.30. MIR spectra of TATB taken at incremental temperatures near 4.4 GPa isobar. The pressure and temperature of each spectrum are indicated on the right side of the figure with the sample decomposition indicated in red.

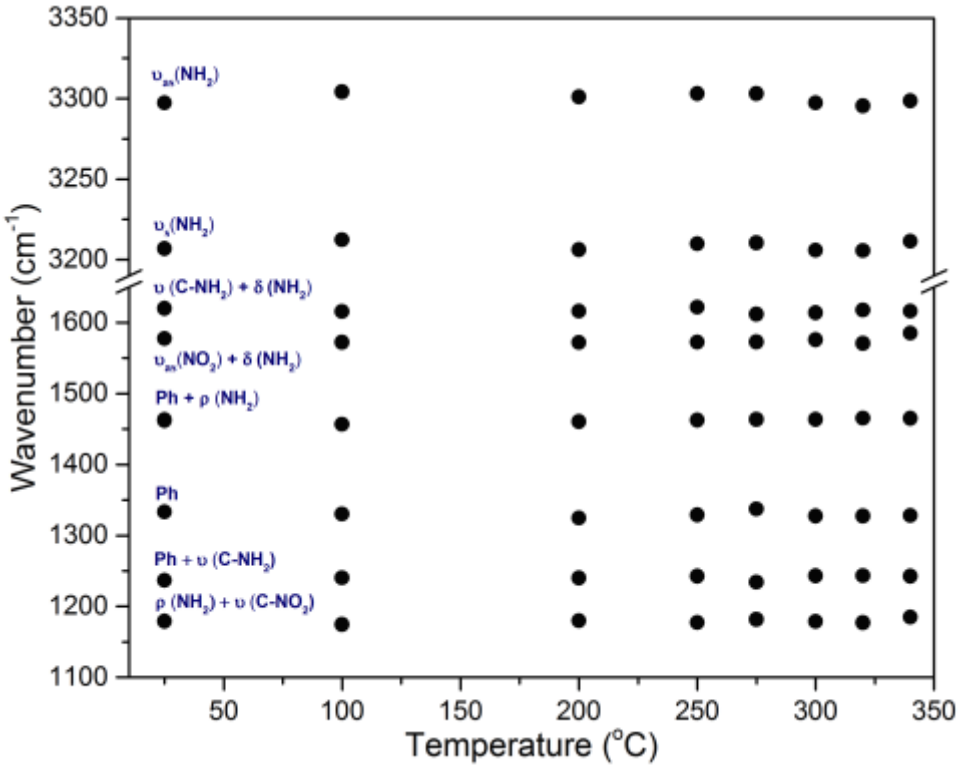

Figure 3.31. Pressure-temperature dependence of select modes of TATB during a near 4.4 GPa isobaric heating experiment in the range of 1100 – 3350 cm^{-1}.

3.4.2 Near 9.0 GPa isobaric heating experiment

For the 9.0 GPa heating experiment, we observe an overall drastic decrease in the strength of the hydrogen bonding network from 25 – 360°C. The amine stretching modes both soften by ~10 cm^{-1}; while we observe strong softening in the Ph + ρ (NH_2) mode at 1455 cm^{-1} by 12.5 cm^{-1}, Ph mode at 1330 cm^{-1} by 20.4 cm^{-1}, and Ph + ν (C-NH_2) mode at 1177 cm^{-1} by 12.4 cm^{-1}. However, the ν (C-NO_2) mode at 1177 cm^{-1} drastically hardened by 17.8 cm^{-1}. Upon further heating to 380°C, we observed complete sample decomposition with the formation of prominent CO_2 and H_2O signatures among other decomposition products.

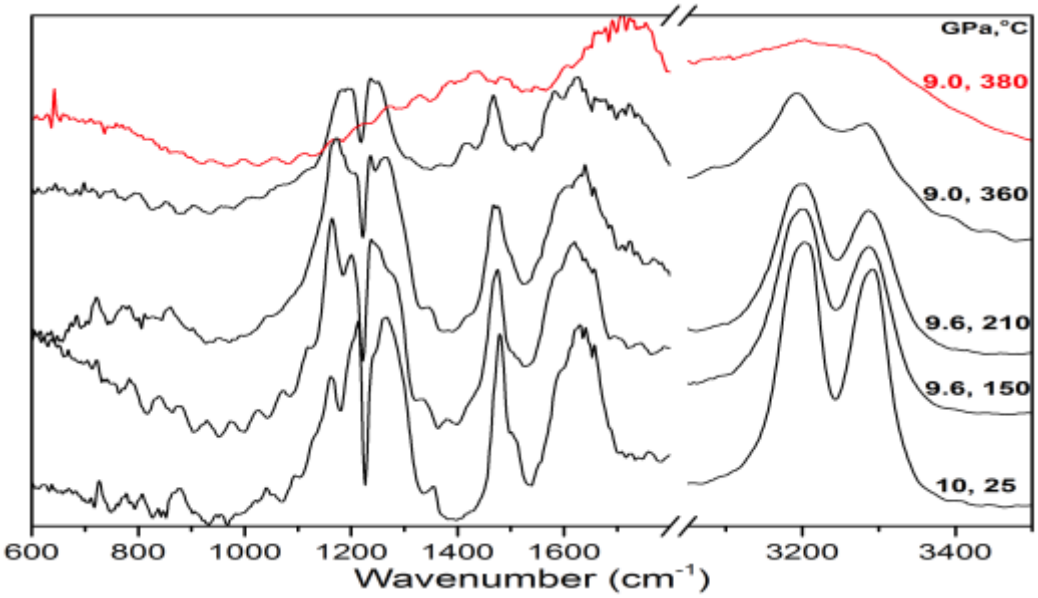

Figure 3.32. MIR spectra of TATB taken at incremental temperatures near 9.0 GPa isobar. The pressure and temperature of each spectrum are indicated on the right side of the figure with the sample decomposition indicated in red.

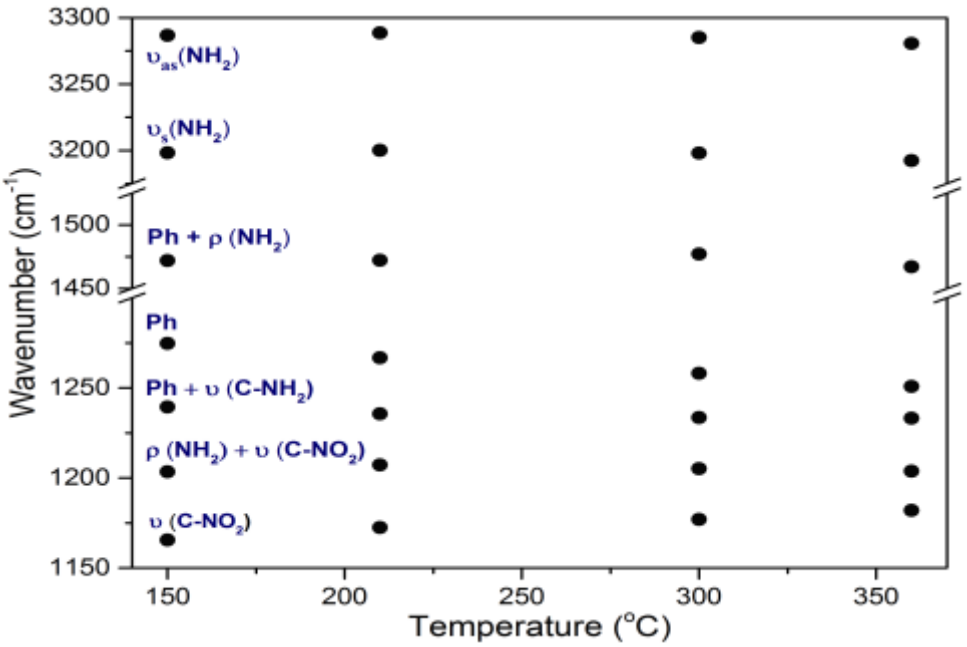

Figure 3.33. Pressure-temperature dependence of select modes of TATB during a near 9.0 GPa isobaric heating experiment in the range of 1150 – 3300 cm^{-1}.

The presence of water in the decomposition products of TATB provides a clue to the mechanisms of decomposition; which is expected to involve either inter/intramolecular hydrogen atom transfer and subsequent formation of H_2O or C-NO_2 bond homolysis and limited H_2O formation.[17] An excellent high pressure photoexcitation experiment by Glascoe, *et al.* [17] indicated the production of H_2O and CO_2 suggesting that pressure might facilitate the hydrogen atom abstraction or that pressure may inhibit the C-NO_2 bond homolysis from occurring. The drastic decrease in the hydrogen bonding network and the hardening of the C-NO_2 mode supports the theory that TATB undergoes either inter/intramolecular hydrogen atom transfer.

3.4.3 Near 10 GPa isobaric heating experiment

TATB was initially compressed to 10.5 GPa and heated to decomposition near 10.9 GPa and 400°C. Due to the large shifts in pressure, the majority of the conventional spectral analysis was rendered mute; however, this is the highest pressure decomposition point ever achieved on TATB, and indicated a very low decomposition boundary slope.

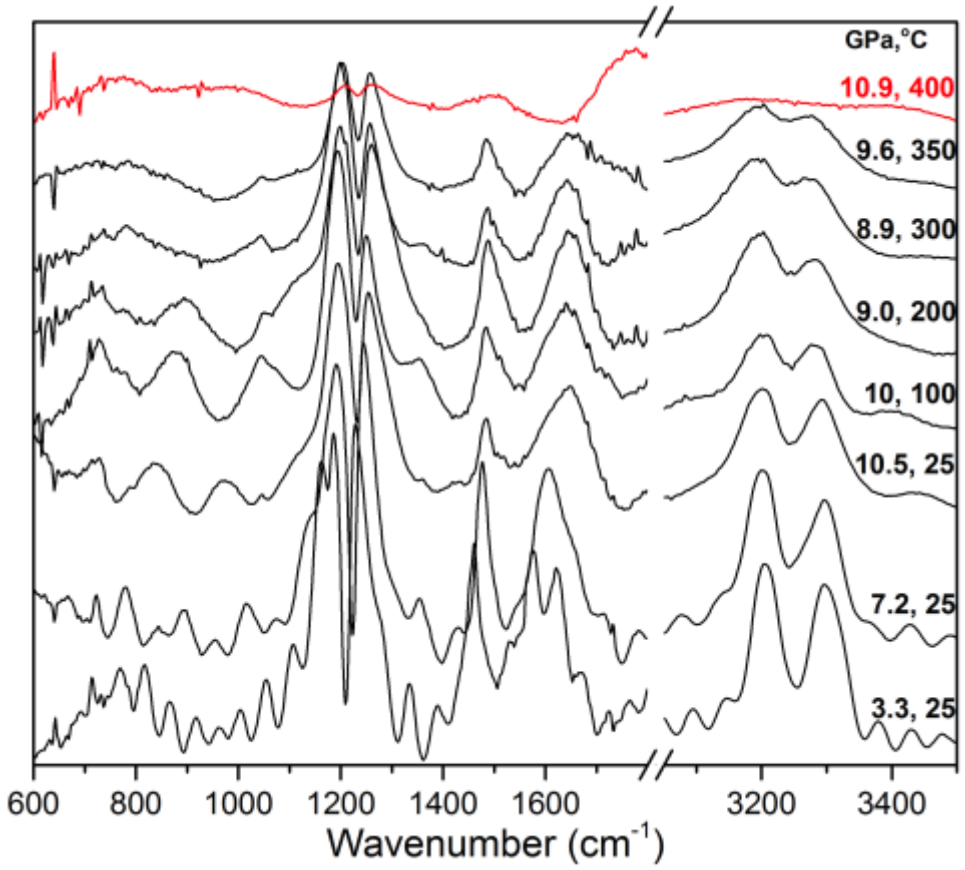

Figure 3.34. MIR spectra of TATB taken at incremental temperatures near 10.0 GPa isobar. The pressure and temperature of each spectrum are indicated on the right side of the figure with the sample decomposition indicated in red.

3.5 Infrared Synchrotron Radiation Isothermal Compression Experiments on TATB

3.5.1 Ambient-temperature isothermal compression experiment

Pravica *et al.*[15] indicated no structural phase transitions or modifications in both the mid- and far-IR up to ~10 GPa. In general, the stability of TATB was indicated to be remarkable with only a slight strengthening of the internmolecular hydrogen bonding with

pressure. In contrast, a single crystal Raman spectroscopy high pressure investigation by Davidson *et al.*[8] indicated that TATB remains both chemically stable and an insulator to 150 GPa with two possibly subtle phase transitions near 28 and 56 GPa. The 'phase transitions' were accompanied by remarkable color changes from yellow to orange and to dark red with increasing pressure; which are suggested to arise from its hydrogen-bonded aromatic two-dimensional layered structure and highly repulsive interlayer interactions hindering the formation of a three dimensional network or metallic states.[8]

3.5.2 A 50°C isothermal compression experiment

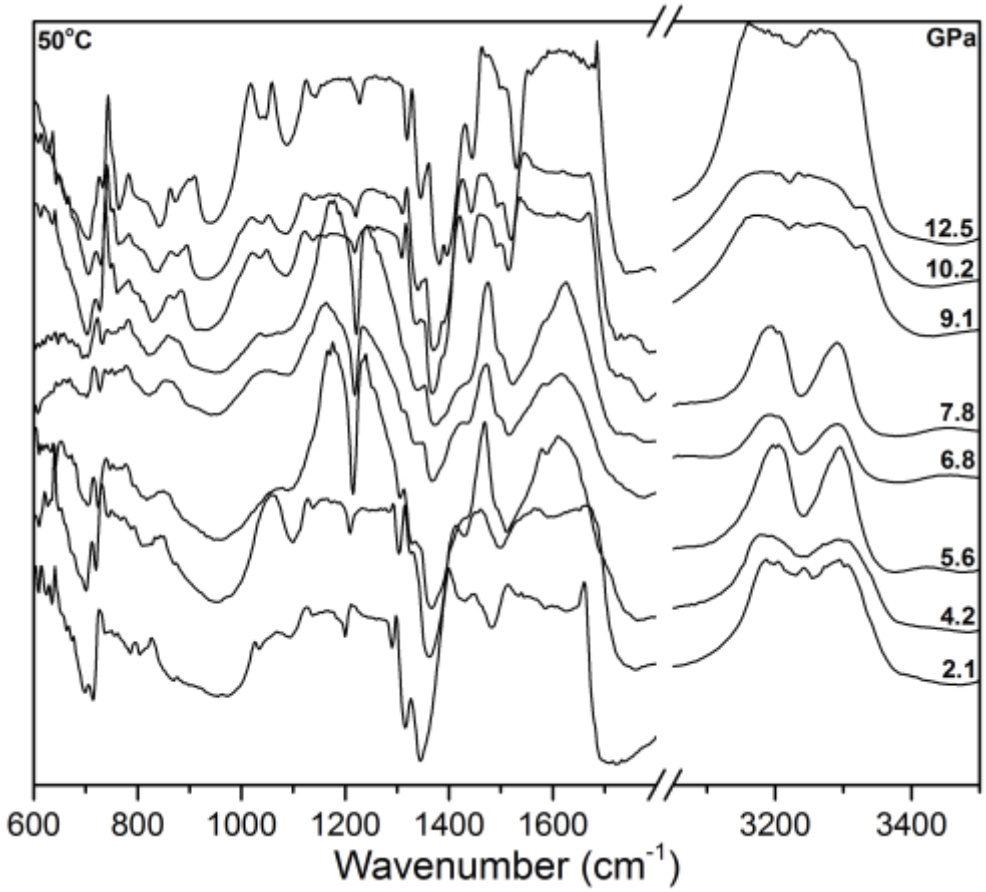

Figure 3.35. MIR spectra of TATB taken at incremental pressures along a 50°C isothermal compression. The pressure of each spectrum is indicated on the right side of the figure.

3.5.3 A 100°C isothermal compression experiment

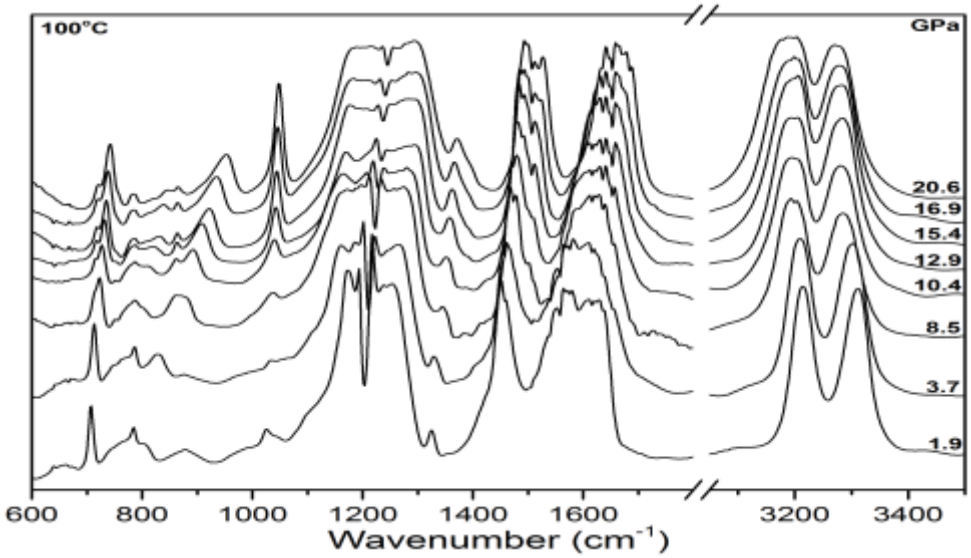

Figure 3.36. MIR spectra of TATB taken at incremental pressures along a 100°C isothermal compression. The pressure of each spectrum is indicated on the right side of the figure.

3.5.4 A 150°C isothermal compression experiment

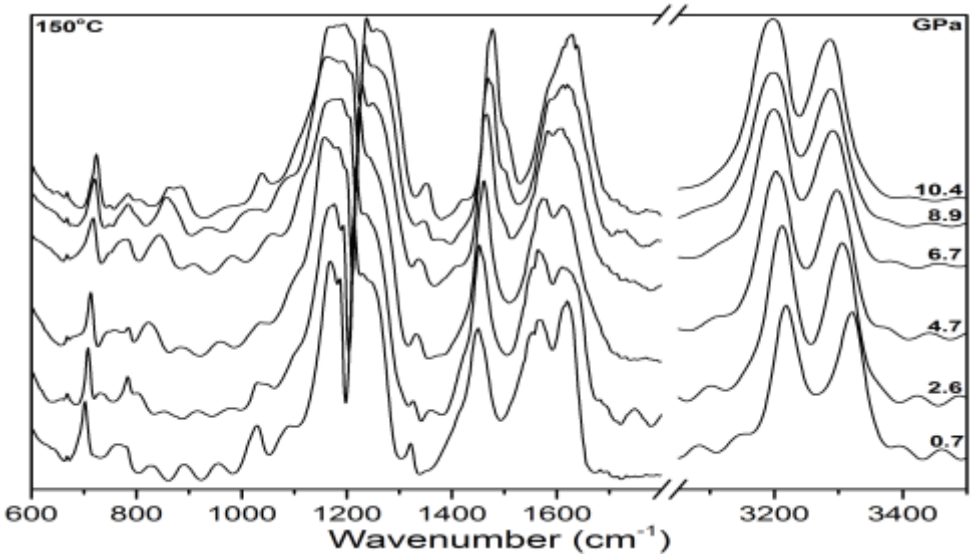

Figure 3.37. MIR spectra of TATB taken at incremental pressures along a 150°C isothermal compression. The pressure of each spectrum is indicated on the right side of the figure.

CHAPTER 4

CONCLUSIONS AND FUTURE WORK

4.1 High Pressure-Temperature Phase Diagram of FOX-7

The P-T diagram of FOX-7 indicates a rich phase behavior below 2 GPa with steep slopes of each high-T phase. Similar phase behavior has been shown in ammonium nitrate (AN) with multiple phases existing below 3 GPa.[58, 59] In comparing the melt-decomposition slope of AN to FOX-7's, decomposition boundary of ~50 ^{o}C/GPa (up to 3 GPa) was reported[58] for AN, while we observe a ~55 ^{o}C/GPa increase (up to 2 GPa) for FOX-7. Much like AN, FOX-7 has multiple triple points at low pressures: ($\beta + \gamma + \delta$) at ~180 – 260^{o}C and 0.5 – 0.9 GPa and another ($\alpha + \beta + \delta$) at ~300^{o}C and 1 GPa. In further comparison to AN, it has been shown that there exists an isobaric IV - IV' phase boundary at ~18 GPa: which terminates isobarically into a change in slope of the melt-decomposition boundary.[58] We see similar behavior in reports on RDX with a change in slope in the melt-decomposition boundary when transitioning into the high-PT phase ε.[60] In addition, RDX also has an isobaric phase boundary between the α- and γ-phase at ~ 4 GPa; which also terminates isobarically into a change in slope of the 'island' phase-ε.[20] In FOX-7, we observe evidence of similar phase behavior with the decomposition phase boundary appearing to change slope as it approaches the near isobaric phase boundary between α and phase-I (Figure 4.1). Our 300^{o}C isothermal compression experiment also showed evidence of the start of decomposition: where the phase I → II isobaric boundary terminates into the 'decomposition phase boundary'.

From our experiments, we were able to determine an anomalous change of slope at (α + Phase I + decomposition) triple point, decomposition boundary of the ε-phase having a slope of ~29°C / GPa, and provide strong evidence supporting the C-NO_2 bond homolysis decomposition mechanism theory. Additionally, the near planar molecular and layering structure, the low symmetry of the ε-phase, and the surprisingly strong cooperative hydrogen bonding network appear to create a very stable form of FOX-7 that potential has comparable or greater stability than TATB.

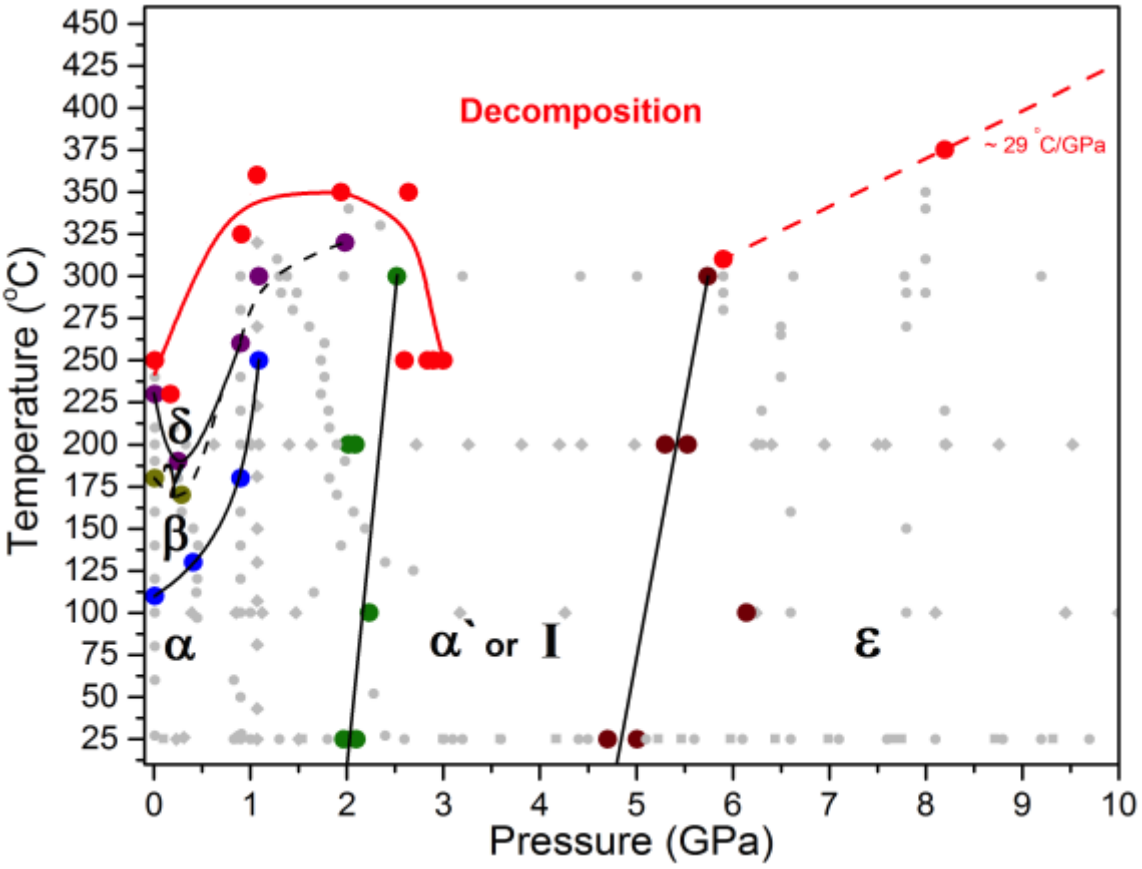

Figure 4.1. The high pressure-temperature phase diagram of FOX-7 with colored symbols indicating the presence of the respective phase along a particular PT pathway represented by grey symbols, and the decomposition boundary is indicated in red symbols (lines).

4.2 High Pressure-Temperature Phase Diagram of TATB

From our data, we were able to determine the slope of the decomposition boundary of TATB to be ~4 ^{o}C / GPa. The very shallow slope might be due to the relatively weak hydrogen bonding network that develops when heating TATB at elevated pressures; however additional experiments are needed to provide further insights.

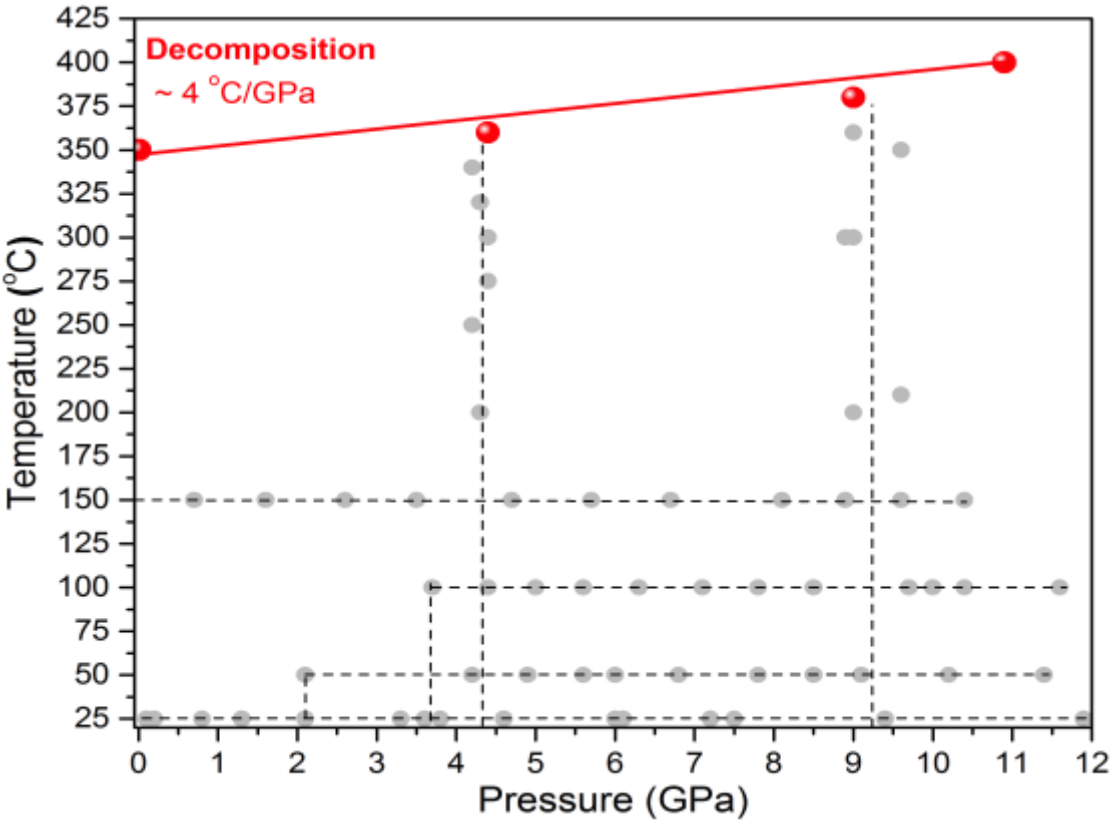

Figure 4.2. The high pressure-temperature phase diagram of TATB with grey symbols (lines) indicating PT pathways, and the decomposition boundary is indicated in red symbols (lines).

4.3 Similarities and Differences in the Phase Behavior of TATB and FOX-7

The ε-phase of FOX-7 and TATB are remarkably similar with both presenting in near planar molecular/layering structures, triclinic symmetry, and nearly identical decomposition products. The differences provide interesting insights into the mechanisms behind sensitivity and performance. In particular, the decomposition boundary of the ε-phase of FOX-7 is much steeper with an ~29°C / GPa slope; while TATB has a very shallow ~4°C / GPa slope. This demonstrates the importance of a cooperative hydrogen bonding network at elevated pressures, and provides evidence for how hydrogen bonding plays such an important role in the decomposition mechanisms of high explosives. The proposed C-NO_2 bond homolysis for FOX-7 appears to be supported by the strong softening of C-NO_2 stretching modes; however, the hardening of C-NO_2 stretching modes in TATB and overall weakening of the hydrogen bonding environment suggest hydrogen atom transfer might be the dominate decomposition mechanism. The differences in mechanisms and hydrogen bonding environments may be responsible for difference in decomposition boundary slopes. The hydrogen bonding environment in FOX-7 appears to be more resilient to heating at pressure than TATB and creates a very stable form of FOX-7 that potentially has comparable or greater stability than TATB. In moving forward with future insensitive high explosive development, compounds with low symmetry, that present in near graphitic like layering structures, near planar molecular symmetry, CHNO ratios similar to TATB or FOX-7, and a strong cooperative hydrogen bonding network, maybe desirable. Finally, it is important to note that the effect of pressure and heating rates can induce different decomposition pathways; while our work provides excellent insights into the sensitivity and performance characteristics of high explosives, more work is needed and ongoing.

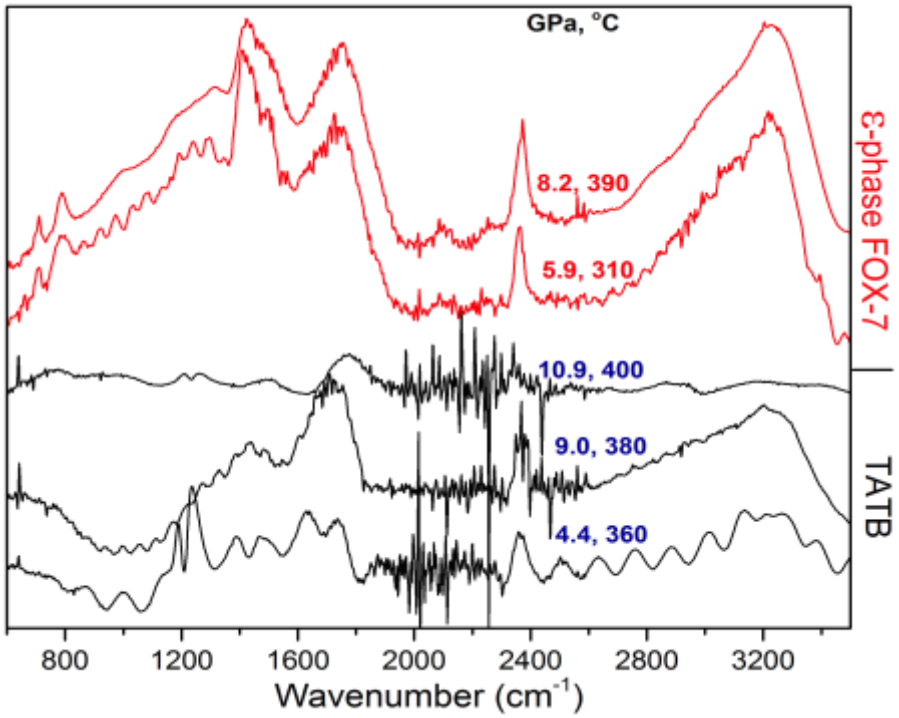

Figure 4.3. MIR spectra of FOX-7 decomposition products from the e-phase indicated in red compared to TATB decomposition products indicated in black.

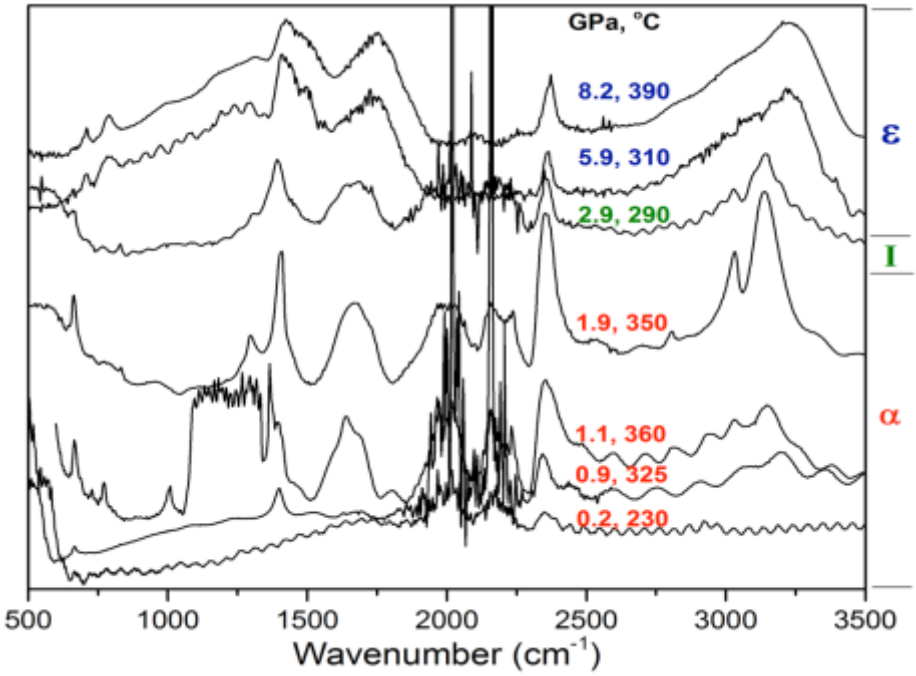

Figure 4.4. The decomposition products of FOX-7 for each high pressure phase.

4.4 Future Direction

As the work has shown, polymorphism plays a large role in the performance and sensitivity of high explosives; to further elucidate this, the commonly used secondary explosive 1,3,5,7-tetranitro-1,3,5,7-tetrazacyclooctane (HMX) has four stable polymorphs under ambient conditions with the β-form being the most stable, and the shock sensitivity of the four forms follows the order $\delta > \gamma > \alpha > \beta$.[61] Consequently, the risk of accidental detonation of δ-, γ-, and α-forms means that only β-HMX is permitted in munitions.[62] However, polymorphism is only one component behind the performance and sensitivity of high explosives. During a detonation event, energetic materials are exposed to immense changes in pressure (P), temperature (T), and strain (ε). While there has been great progress towards understanding the mechanisms behind sensitivity and performance, due to experimental difficulty, it is difficult to discern the magnitude of the contribution from each external stimuli variable (P, T, ε). In order to better understand the mechanisms behind performance and sensitivity, it is important to investigate high explosives under these various conditions, and over the years, many studies have investigated the static compression (high P-T, extremely low-ε, and long time periods - hours)[9, 40, 58, 59, 63-68] and dynamic compression (high P-T-ε, and very short time periods – μs)[69-72] of high explosives.

However there still remains an unexplored strain rate gap between static ($<10^{-3}$ s^{-1}) and dynamic ($>10^{5}$ s^{-1}) compression.[73] Exploring the strain rate gap region is crucial for measuring the kinetics of phase transitions, investigating structural stability/transformations as a function of compression rate, determining structural evolution and transition pathways.[73] To our knowledge, no high P-T moderate strain rate

(10^{-1} - 10^{2} s^{-1}) experiments have been conducted on high explosives. Additionally, there also remain a heating rate gap between static (hours long experiments) and dynamic (unknown/unmeasurable heating rate). To our knowledge, only three investigations[17, 74, 75] have been conducted on the pressure-dependency of decomposition kinetics of high explosives. The pressure-dependent kinetics of thermal decomposition is of great importance to the assessment and prediction of thermal safety of high explosives because pressure is a dynamic variable in any sealed container that is heated.[17] In addition, the complexity of the reactions involved and the observed temperature-dependent effects, an understanding of pressure effects is necessary for modeling combustion and explosion behavior.[75]

The project has identified multiple areas of future exploration for identifying the role strain and thermal kinetics plays in the decomposition behavior of FOX-7: in particular, the role of kinetics in the near 3.0 GPa, and the unique decomposition behavior identified in the ε-phase. The development of a new designer diamond anvil that is doped with boron that creates an electrical conductive surface that acts as a highly localized and fast response heater[76, 77] will allow for the most accurate thermal kinetics investigations to-date. In addition, the heating anvils operate with very little pressure drift upon heating which will allow us to conduct various isobaric heating experiments with greater efficiency and over a broader range of heating rates than Glascoe *et al.*[17] who's studies were drastically hindered from thermal expansion based pressure drift that rendered a large majority of their data unanalyzable. Our ability to conduct repeatable initial isobaric pressure conditions over a broad range of heating rates allows us to develop a highly accurate image of the pressure dependency of thermal decomposition kinetics. With the use of our heating anvils

and the IR-beamline at NSLS II, we will conduct various kinetics experiments on FOX-7 over the appropriate regions of phase-space.

Furthermore, DAC strain rate experiments will be performed at APS Sector 16 (HPCAT, ID-B beamline); which specializes in high-pressure angle dispersive X-ray diffraction with a wavelength of ~0.4 Å, a spot size of 5 x 3 μm^2, and employees a CMOS Pilatus 100k area detector. Diamond anvil cells coupled with a piezoelectric module, that is actuated by a coupled power supply and waveform generator that will be used to apply a rapid pressure increase (<0.1s) while collecting X-ray diffraction spectra *in situ* at 0.1 s per pattern[78], will be used to execute the experiments. Our collaborator Nenad Velisavljevic from Los Alamos National Laboratory has successfully applied this technique to elemental zirconium using the described beamline.[73] The results from this experiment yielded high quality data that shows the kinetics of phase transition in the elemental zirconium over a large temporal region. The use of the CMOS Pilatus 100k area detector allowed Velisavljevic *et al.*[9] to collect spectra at 0.1s per pattern yielding a statistically sound volume of data from which to fit kinetic models.[78] We propose using the same proven technique to conduct the first high P-T moderate strain rate experiment on high explosives. The information collected will aid in our computational studies and enhance overall models of detonation. Additionally, this study will aid in our fundamental understanding of how organic materials behave under high P-T moderate strain conditions: information that is highly valuable to geophysical research (high P-T minerals synthesis, strain from tectonic plate shifts), pharmaceutical development (high P-T tabulating strain effects on active ingredients), petroleum industry (oil and gas exploration), and has a large

influence on our ability to gain insights into the fundamental mechanisms behind performance and sensitivity of high explosives for national defense.

Our future experiments would help in developing a fundamental understanding of how kinetics and polymorphism influence the performance and sensitivity characteristics of energetic materials. We plan high P-T moderate strain and heating rate experiments at the Advanced Photon Source (APS), and the high P-T thermal kinetics of decomposition experiments at the National Synchrotron Light Source II (NSLS II). These studies will establish the first evidence of the effects of moderate strain rates on low-pressure polymorphism. In addition, these studies will provide the rate constants and activation energies of decomposition for each high-pressure polymorph. The combination of these two, paired with the depth of the study presented here, will allow for highly accurate models of detonation to be developed that will help further elucidate the underlying mechanisms behind performance and sensitivity characteristics in energetic materials.

REFERENCES

1. S. Fordham, *High Explosives and Propellants: Edition 2*. (Elsevier, 2013).
2. T. M. Klapotke, *Chemistry of High-Energy Materials*. (Walter de Gruyter GMbH & Co KG, 2015).
3. T. Andrade, *The Gunpowder Age: China, Military Innovation, and the Rise of the West in World History*. (Princeton University Press, 2016).
4. DiDattica, (2008).
5. J. Y. a. S. Zitrin, *Modern Methods and Applications in Analysis of Explosives*, 1st ed. (Wiley, 1996).
6. A. Beveridge, *Forensic Investigation of Explosions*. (Taylor & Francis, 1998).
7. J. M. Welch, Dissertation, Ludwig-Maximilians-Universitat Munchen, 2008.
8. R. P. D. Alistair J. Davidson, Dana M. Dattelbaum, and Choong-Shik Yoo, Journal of Chemical Physics **135**, 174507-174505 (2011).
9. N. V. Lewis L. Stevens, Daniel E. Hooks, and Dana M. Dattelbaum, Propellants, Explosives, Pyrotechnics **33** (4), 286 - 295 (2008).
10. T. R. G. a. A. Popolato, *LASL Explosive Property Data*. (University of California Press, Berkeley, CA, 1980).
11. M. R. M. a. L. E. Fried, Journal of Physical Chemistry C **116**, 2116 - 2122 (2012).
12. D. S. V. Veera M. Boddu, Tushar K. Ghosh, and R. Damavarapu, Journal of Hazardous Materials **181**, 1 - 8 (2010).
13. F. Z. Heliang Sui, Kemei Cheng, Xueyong Liu, and Xin Ju, Spectrochimica Acta Part A: Molecular and Biomolecular Spectroscopy **114**, 137 - 143 (2013).

14. S. D. M. a. A. P. Shreve, Journal of Chemical Physics **119** (12), 5834 - 5840 (2003).

15. B. Y. Michael Pravica, Zhenxian Liu, and Oliver Tschauner, Physical Review B **76**, 064102-064104 (2007).

16. G. I. P. S.M. Peiris, and T.P. Russell, presented at the Shock Compression of Condensed Matter, 2000 (unpublished).

17. J. M. Z. Elizabeth A. Glascoe, Michael R. Armstrong, Jonathan C. Crowhurst, Christian D. Grant, and Laurence E. Fried, J. Phys. Chem. A **113**, 5881 - 5887 (2009).

18. B. F. Yulga, University of Nevada, 2009.

19. J. Z. Hong Liu, Guangfu Ji, Dongqing Wei, and Zizheng Gong, Physics Letters A **358**, 63 - 69 (2006).

20. X. Z. Weihua Zhu, Tao Wei, and Heming Xiao, Theor. Chem. Acc. **124**, 179 - 186 (2009).

21. D. Mathieu, Journal of Physical Chemistry A **116**, 1794 - 1800 (2012).

22. A. L. H. Ostmark, H. Bergman, N. Wingborg, U. Wellmar, and U. Bemm, presented at the Proceedings of the 11th International Detonation Symposium, Office of Naval Research, Norfolk, 1998 (unpublished).

23. M. B. T. M. Anniyappan, G.M. Gore, S. Venugopalan, and B.R. Gandhe, Journal of Hazardous Materials **137**, 812 - 819 (2006).

24. R. S. C. Matthew M. Bishop, Michael Pravica, Josh Coe, Zhenxian Liu, Dana Dattlebaum, Yogesh Vohra, and Nenad Velisavljevic, Journal of Chemical Physics **137**, 174304-174308 (2012).

25. P. B. K. a. M. Herrmann, Part. Part. Syst. Charact. **22**, 418 - 422 (2005).

26. S. M. Gerardo Majano, Thomas Bein, and Thomas M. Klapotke, Journal of Physical Chemistry C **111**, 6694 - 6699 (2007).

27. J.-z. L. Xue-zhong Fan, and Zi-ru Liu, Journal of Physical Chemistry A **111**, 13291 - 13295 (2007).

28. R. S. C. M. M. Bishop, Z. Liu, D. N. Preston, M. M. Sandstrom, D. M. Dattelbaum, Y. K. Vohra, and N. Velisavljevic, Journal of Physics: Conference Series **500**, 052005 (2014).

29. V. P. F. I.V. Chemagina, B.G. Loboiko, M.B. Kazakova, Yu.A. Shakhtorin, V.M. Lagutina, N.P. Taibinov, N.V. Garmasheva, and A.V. Alekseev, AIP Conf. Proc. **849**, 174 - 178 (2006).

30. T. M. K. Jurgen Evers, Peter Mayer, Gilbert Oehlinger, and Jan Welch, Inorganic Chemistry **45**, 4996 - 5007 (2006).

31. J. E. Margaret-Jane Crawford, Michael Gobel, Thomas M. Klapotke, Peter Mayer, Gilbert Oehlinger, and Jan M. Welch, Propellants, Explosives, Pyrotechnics **32** (6), 478 - 495 (2007).

32. Y. T. Z.A. Dreger, and Y.M. Gupta, Chemical Physics Letters **584**, 83 - 87 (2013).

33. Y. T. Zbigniew A. Dreger, and Yogendra M. Gupta, Journal of Physical Chemistry A **118** (27), 5002 - 5012 (2014).

34. Y. L. Michael Pravica, John Robinson, Nenad Velisavljevic, Zhenxian Liu, and Martin Galley, Journal of Applied Physics **111**, 103534 (2012).

35. Velisavljevic, (Los Alamos National Laboratory, 2015).

36. O. S. Roman V. Tsyshevsky, and Maija M. Kuklja, Molecules **21**, 236 (2016).

37. J. Z. a. H. Liu, Comp. Mat. Sci. **42**, 698 - 703 (2008).

38. P. V. S. Anna V. Kimmel, Alexander L. Shluger, and Maija M. Kuklja, Journal of Physical Chemistry A **112**, 4496 - 4500 (2008).

39. S. N. A. U.R. Nair, A. Subhananda Rao, and B.R. Gandhe, Defense Science Journal **60** (2), 137 - 151 (2010).

40. N. V. Matthew M. Bishop, Raja Chellapa, and Yogesh K. Vohra, Journal of Physical Chemistry A **119**, 9739 - 9747 (2015).

41. P. L. C. Steven Hunter, Alistair J. Davidson, David I. A. Millar, Stewart F. Parker, William G. Marshall, Ronald I. Smith, Carole A. Morrison, and Colin R. Pulham, Journal of Physical Chemistry C **119**, 2322 - 2334 (2015).

42. A. I. S. Zbigniew A. Dreger, Zhi-Gang Yu, Yu-Sheng Chen, Yuchuan Tao, and Yogendra M. Gupta, Journal of Physical Chemistry C **120**, 1218 - 1224 (2016).

43. DiamondAnvils, (2010).

44. Almax-EasyLabs, (2012).

45. M. T. A. Dewaele, P. Loubeyre, and M. Mezouar, Phys. Rev. B **78**, 104102 (2008).

46. J. X. H. K. Mao, and P. M. Bell, J. Geophys. Res. **91**, 4673 (1986).

47. L. S. D. S. Rekhi, and S. K. Saxena, High Temp. - High Pres. **31**, 299 (1999).

48. B. D. Mistry, *A Handbook of Spectroscopic Data Chemistry*. (Oxford Book Company, 2009).

49. P. B. E. Pretsch, and M. Badertscher, *Structure Determination of Organic Compounds: Tables of Spectral Data*. (Springer, 2009).

50. H. F. S. J. B. Lambert, D. Lightner, and R. G. Cooks, *Organic Structural Spectroscopy*. (Prentice-Hall, 1998).

51. L. H. D. N. B. Colthup, and S. E. Wiberley, *Introduction to Infrared and Raman Spectroscopy*. (Academic, 1990).

52. J. A. B. Dan C. Sorescu, and Donald L. Thompson, Journal of Physical Chemistry A **105**, 5010 - 5021 (2001).

53. H.-M. X. Xue-Hai Ju, and Qi-Ying Xia, Journal of Chemical Physics **119**, 10247 (2003).

54. W. Z. Qiong Wu, and Heming Xiao, J. Mol. Model **19**, 4039 - 4047 (2013).

55. M. M. K. a. S. N. Rashkeev, Journal of Energetic Materials **28**, 66 - 77 (2010).

56. M. M. K. S. N. Rashkeev, and F. J. Zerilli, Applied Physics Letters **82** (9), 1371 - 1373 (2003).

57. C. P. W. S. M. Peiris, M. M. Kuklja, and F. J. Zerilli, presented at the 12th International Detonation Symposium, San Diego, 2002 (unpublished).

58. M. D. a. C.-S. Yoo, Journal of Chemical Physics **139**, 214503 (2013).

59. D. M. D. Raja S. Chellappa, Nenad Velisavljevic, and Stephen Sheffield, Journal of Chemical Physics **137**, 064504 (2012).

60. Z. A. D. a. Y. M. Gupta, Journal of Physical Chemistry A **114**, 8099 - 8105 (2010).

61. S. J. P. P. a. J. E. Field, Proc. Royal Soc. London A: Mathematical, Physical, and Engineering Sciences **383**, 399 - 407 (1982).

62. D. I. Millar, *Energetic Materials at Extreme Conditions*. (Springer Science & Business Media, 2011).

63. P. J. M. T. P. Russell, G. J. Piermarini, and S. Block, J. Phys. Chem. **97**, 1993 - 1997 (1993).

64. R. S. C. D. M. Dattelbaum, P. R. Bowden, J. D. Coe, and M. A. Margevicius, Appl. Phys. Let. **104**, 021911 (2014).

65. M. M. T. a. J. M. Leger, J. Chem. Phys. **89**, 194255-194217 (1988).

66. F. A. G. L. Ciabini, M. Santoro, R. Bini, V. Schettino, and M. Mezouar, Physical Review B **72**, 094108 (2005).

67. J. A. Ciezak and T. A. Jenkins, Propel. Explos. Pyro. **33**, 390 - 395 (2008).

68. J. C. G. a. S. M. Peiris, J. Phys. Chem. **114**, 8099 - 8105 (2010).

69. S. P. Marsh, Univ. of California Press, 5 (1980).

70. C.-S. Y. a. H. Cynn, J. Chem. Phys. **111**, 10229 (1999).

71. Z. A. D. J. E. Patterson, and Y. M. Gupta, j. Phys. Chem. B **111**, 10897 - 10904 (2007).

72. P. A. P. F. W. Sandstrom, and B. Olinger, AIP Conf. Proc. **309**, 1409 (1994).

73. S. S. N. Velisavljevic, R. Saavedra, R. S. Chellappa, A. Rothkirch, D. M. Dattelbaum, Z. Konopkova, H-P. Liermann, M. M. Bishop, G. M. Tsoi, and Y. K. Vohra, J. Phys. Conf. Ser. **500** (500), 032020 (2014).

74. a. S. B. G. J. Piermarini, J. Phys. Chem. **93**, 457 - 462 (1989).

75. S. B. G. J. Piermarini, and P. J. Miller, J. Phys. Chem. **91**, 3872 - 3878 (1987).

76. J. M. Montgomery, University of Alabama at Birmingham, 2015.

77. G. T. G. K. Samudrala, A. V. Stanishevsky, J. M. Montgomery, Y. K. Vohra, and S. Weir, High Pressure Research **31**, 388 - 398 (2011).

78. N. V. M. K. Jacobsen, and S. V. Sinogeikin, J. Appl. Phys. **118**, 025902 (2015).